Optimizing Thermal Performance of Building Envelopes by Mitigation of Thermal Bridging – Experimental and Numerical Investigation

by

Abdalhadi Alhawari

B.Sc., University of Tripoli, Libya, 2006
M.Sc., University of Colorado Boulder, USA, 2012

A Dissertation Submitted in Partial Fulfillment
of the Requirements for the Degree of

DOCTOR OF PHILOSOPHY

in the Department of Mechanical Engineering

University of Victoria

Supervisory Committee

Optimizing Thermal Performance of Building Envelopes by Mitigation of Thermal Bridging – Experimental and Numerical Investigation

by

Abdalhadi Alhawari

B.Sc., University of Tripoli, Libya, 2006
M.Sc., University of Colorado Boulder, USA, 2012

Supervisory Committee

Dr. Phalguni Mukhopadhyaya, Supervisor
Department of Civil Engineering

Dr. Caterina Valeo, Member
Department of Mechanical Engineering

Dr. Fayez Gebali, Outside Member
Department of Electrical and Computer Engineering

Abstract

Due to regulatory requirements and a growing environmental consciousness, improving building energy performance is crucial in today's construction industry. Thermal bridge, which compromises buildings' energy efficiency, durability, and indoor air quality is a pressing concern for building design and performance. This research aims to explore and address the phenomenon of thermal bridge in building envelope construction by offering valuable insights and innovative solutions. Two analysis methodologies have been incorporated in this research. The first method is a finite element simulation tool (HEAT3), which was used to predict the efficacy of the proposed ideas. The second method is a laboratory investigation that was performed using the hot box apparatus.

A crucial aspect of this research initiative involved designing, constructing, and calibrating a unique hot box apparatus. This apparatus was constructed using vacuum insulation panels (VIPs) as core materials for its envelope. The choice of materials and construction details ensured exceptional temperature stability with minimal fluctuations within the chambers, a crucial factor for the performance of the hot box apparatus. Owning such a test facility provides a substantial advantage such as the ability to conduct multiple tests for each sample in significantly shorter timeframes, unlike commercial laboratories.

Laboratory assessment is an important method to evaluate the real-world performance of building components. Besides numerical analysis, this dissertation stands as the first to experimentally assess the efficacy of an available thermal break product, which was highlighted in the literature as the most effective technique to mitigate the impacts of balcony thermal bridges. This dissertation also investigates two novel techniques aimed at reducing heat loss through balcony thermal bridges. Another key focus of this research

was to investigate the impact of a generic aluminum cladding attachment system on the thermal performance of lightweight steel-framed wall systems.

Overall, the outcomes of this research initiative demonstrate a high degree of consistency between results obtained through numerical simulations and experimental measurements. This work serves as a valuable resource for architects, engineers, and policymakers, facilitating the promotion of sustainable and energy-efficient building practices. It not only addresses critical issues related to thermal bridges but also proposes innovative solutions and provides a robust experimental platform to advance our understanding of building performance and energy efficiency.

Table of Contents

Supervisory Committee ii
Abstract iii
Table of Contents v
List of Tables vii
List of Figures viii
Acknowledgments x
Dedication xi
Introduction 1
Chapter 1: Thermal Bridges in Building Envelopes – An Overview of Impacts and Solutions 6
1.1 Abstract 6
1.2 Introduction 6
1.3 Consequences of Thermal Bridges 7
1.4 Types of Building Thermal Bridges 8
1.4.1 Constructional/Structural thermal bridges 9
1.4.2 Geometrical thermal bridges 9
1.4.3 Systematic thermal bridges 10
1.5 Linear and Point Thermal Transmittance 10
1.6 Approaches to Reduce the Impact of Thermal Bridges 13
1.6.1 Wall-to-roof interface 13
1.6.2 Window perimeters 14
1.6.3 Interface between building assemblies 15
1.6.4 Sun-shade structures 15
1.6.5 Exterior wall studs. 15
1.6.6 Balconies extended slab. 16
1.7 Minimizing Impacts of Balcony Thermal Bridges 16
1.8 Conclusions 26
Chapter 2: Construction and Calibration of a Unique Hot Box Apparatus 27
2.1 Abstract 27
2.2 Introduction and Background 28
2.3 Literature Review 31
2.4 Description of the Apparatus 37
2.4.1 Environment Chambers 37
2.4.2 Specimen Frame 38
2.4.3 Heating System 39
2.4.4 Cooling System 40
2.4.5 Radiation Baffles 40
2.4.6 Air Circulation Systems 41
2.4.7 Temperature Sensors 42
2.4.8 Heat Flux Sensors 43
2.5 Calibration Procedure 43
2.5.1 Temperature Stability 44
2.5.2 Experimental, Numerical, and Theoretical Thermal Analyses 45
2.5.3 Energy Balance 48

2.6 Summary of Observations and Conclusions 52
Chapter 3: Mitigating Balcony Thermal Bridging: Experimental and Numerical Investigation of Innovative Solutions for Energy-Efficient Building Envelopes 54
3.1 Abstract 54
3.2 Introduction 55
3.2.1 Literature review 56
3.3 Aim of the work 59
3.4 Materials and Methodologies 59
3.4.1 Description of the tested specimens 62
3.4.2 Numerical simulation 67
3.4.3 Parametric study 69
3.4.4 Laboratory work 71
3.4.5 Brief description of the test facility 71
3.4.6 Estimation of extraordinary losses 74
3.4.7 Measured data. 79
3.5 Results and discussion 81
3.5.1 Heat flow analyses 81
3.5.2 Temperature analysis 86
3.6 Conclusions 89
Chapter 4: Impact of Cladding Attachment Structural Elements on the Thermal Performance of Exterior Insulated Steel-Framed Walls 91
4.1 Abstract 91
4.2 Introduction 92
4.2.1 Lightweight Steel Framing (LSF) 93
4.3 Research Background 94
4.4 Objectives and Scope 97
4.5 Construction of Test Specimens 97
4.6 Methodology 102
4.6.1 Numerical simulations 102
4.6.2 Laboratory work 104
4.6.3 Measured data 109
4.6.4 Computation procedure 111
4.7 Results and discussion 114
4.8 Conclusions 119
Chapter 5: Conclusions and Outlook. 122
5.1 Conclusions 122
5.2 Outlook on future work 124
Bibliography 126

List of Tables

Table 2.1. Detailed description of selected studies utilizing comparable test apparatus. 36
Table 2.2. Materials' properties [89]–[93]. 39
Table 2.3. Comparison between theoretical, numerical, and experimental heat flowrates. 47
Table 2.4. Extraneous loss associated with hot box measurements. 51
Table 3.1. Summary of the analyzed cases. 60
Table 3.2. Properties of conventional concrete and aerogel-concrete. 66
Table 3.3. Properties of incorporated materials 67
Table 3.4. Percentages of reduction in heat flow rate via concrete slab in respect to warm side. 70
Table 3.5. Measurements of estimation of metering box wall loss. 75
Table 3.6. Measurement data collected/calculated to estimate the flanking loss. 77
Table 3.7. Collected measurements of conventional slab. 79
Table 3.8. Collected measurements of thermally interrupted slab. 80
Table 3.9. Collected measurements of thermally interrupted slab with GFRP reinforcement. 80
Table 3.10. Collected measurements of thermally interrupted slab with aerogel-concrete at interior surfaces. 80
Table 3.11. Collected measurements of thermally interrupted slab with aerogel-concrete at the interior and exterior surfaces. 81
Table 3.12. Thermal analysis for conventional slab. 81
Table 3.13. Thermal analysis for thermally interrupted slab. 82
Table 3.14. Thermal analysis for thermally interrupted slab with GFRP. 83
Table 3.15. Thermal analysis for interrupted slab with aerogel-concrete at interior surfaces. 83
Table 3.16. Thermal analysis for thermally interrupted slab with aerogel-concrete at both surfaces. 84
Table 4.1. Materials and properties. 97
Table 4.2. Summary of materials/components incorporated in the studied configurations. 100
Table 4.3. Measured data. 110
Table 4.4. Heat loss amounts associated with numerical simulations and experimental measurements. 112
Table 4.5. Obtained results of tested wall configurations. 115

List of Figures

Figure 1.1. Schematic constructional/structural thermal bridges. 9
Figure 1.2. Schematic of a geometrical thermal bridge. 9
Figure 1.3. Schematic of a systematic thermal bridges 10
Figure 1.4. Sketches of different wall configurations 11
Figure 1.5. Sketch of wall to roof interface 14
Figure 1.6. Sketch of window perimeter 14
Figure 1.7. Sketch of sunshade element 15
Figure 1.8.Commercially available thermal break product 19
Figure 2.1. Schematics of: (a) guarded hot plate; (b) calibrated hot box; (c) guarded hot box. 30
Figure 2.2. (a) Environment chamber; (b) interior view of the chamber; (c) specimen frame 38
Figure 2.3. (a) Ceramic heat bulb; (b) DC power supply regulator. 40
Figure 2.4. (a) Radiation baffle element; (b) fans attached to the baffle. 41
Figure 2.5. Scheme of temperature sensors' layout. 42
Figure 2.6. Air curtain temperature profile of: (a) metering chamber; (b) climate chamber. 45
Figure 2.7. Laboratory temperature profile. 45
Figure 2.8. Comparison between theoretical, numerical, and experimental heat flow rates. 47
Figure 2.9. Scheme of heat flow paths. 49
Figure 2.10. Relation between temperature gradients and extraneous heat loss as: (a) an amount; (b) a percentage. 52
Figure 3.1. (a) Uniform panel; (b) Uniform panel with an aperture; (c) Uniform panel in use to support the concrete board prior testing. 62
Figure 3.2. Conventional slab. 63
Figure 3.3. Thermally interrupted slab: (a) Prior to the pouring of concrete; (b) Tested specimen. 64
Figure 3.4. Thermally interrupted slab with glass fiber reinforcement: 65
Figure 3.5. Thermally interrupted slab with aerogel-concrete layers at warm surfaces: (a) Schematic; (b) Casted specimen. 66
Figure 3.6. Thermally interrupted slab with aerogel-concrete at both surfaces 66
Figure 3.7. The warm side of the tested concrete board 69
Figure 3.8. (a) Placing the specimen into the chamber; (b) Specimen ready for testing. . 72
Figure 3.9. Thermal break product 73
Figure 3.10. GFRP rebars 74
Figure 3.11. Aerogel-concrete ingredients 74

Figure 3.12. Correlation between metering box wall loss and temperature difference... 76
Figure 3.13. Relation between heat flux via uniform panel and temperature difference 77
Figure 3.14. Relation between flanking loss and temperature difference 78
Figure 3.15. Locations of temperature sensors 79
Figure 3.16. Heat flow rate in case benchmark cases 85
Figure 3.17. Heat flow rate for enhanced cases 86
Figure 3.18. Temperature analysis for conventional and thermally interrupted slabs.... 88
Figure 3.19. Temperature analysis for enhanced slabs 88
Figure 4.1. Exterior insulated steel-framed composite wall assembly. [137] 94
Figure 4.2. Schematic diagram of the reference case. 99
Figure 4.3. Sketches of investigated configurations. 102
Figure 4.4. Boundary conditions: (a) Interior side; (b) Exterior side. 104
Figure 4.5. Scheme of hot box apparatus 106
Figure 4.6. Scheme of heat flow paths. 108
Figure 4.7. Sample of measured data. 111
Figure 4.8. Metered sample mounted inside the specimen frame: (a) Sketch; (b) Real. 113
Figure 4.9. Relation between the temperature differences and amount of heat flows. . 116
Figure 4.10. Relation between the mean temperatures and thermal transmittances. 117
Figure 4.11. Thermal transmittance of tested wall configurations obtained numerically and experimentally. 119

Acknowledgments

First, I am grateful to my home country, Libya, for the generous financial assistance provided during these challenging times that the nation is facing. This support alleviated any financial worries I had when deciding to embark on this journey.

I would like to express my honest gratitude and deepest appreciation to my supervisor, Dr. Phalguni Mukhopadhyaya, whose unwavering mentorship has played an instrumental role in my personal and professional growth. His constant encouragement and support have been invaluable throughout this journey.

I want to extend my heartfelt gratitude to my friends, colleagues, and laboratory personnel. I would like to give special thanks to Dr. Armando Tura and Mr. Bastien Lanusse for their assistance in laboratory activities.

Last but certainly not least, I find it nearly impossible to say enough that can express and convey my love and profound gratitude to my family for their unwavering support throughout every stage of my education journey.

Dedication

I dedicate this thesis to the soul of my father.

(*May Allah give him mercy and grant him amongst the highest levels of Jannah*).

Introduction

The building sector has seen a substantial surge in energy consumption over the past decades. This increase can be primarily attributed to various factors such as population growth, increased indoor occupancy, rising expectations for indoor comfort involving temperature, humidity and air quality, and the effects of climate change. According to the International Energy Agency (IEA) [1], the combined energy usage for building operations and construction accounts for 35% of the world's total energy consumption, while also contributing to nearly 38% of both direct and indirect greenhouse gas emissions [2], [3].

The literature further highlights this trend by revealing that the building sector's energy consumption stands at 33% in Canada and 40% in the United States. In the context of Canadian residential buildings, 63% of the consumed energy is utilized for space heating [4], [5]. Given the profound implications of such extensive energy utilization, regulatory frameworks and building energy codes have shifted their focus toward enhancing the energy efficiency of buildings. In addition, building energy codes have introduced new measures to ensure that overall carbon emission limits for the construction, operation, and renewals of buildings are realized. The preliminary step in this regard is the enhancement of the thermal resistivity offered by a building's external envelope. This improvement can be achieved by incorporating materials of high thermal resistance and by mitigating the impacts of thermal bridges. Thermal bridges happen when highly conductive materials penetrate the layers of insulation, leading to higher thermal transmission.

There are various forms of thermal bridges. For example, balconies and slab edges, wall studs and cladding attachment, corners, wall-to-roof and floor transitions, and window-

wall transitions. These thermal bridges collectively or individually undermine the thermal efficiency of the building envelopes. Among all thermal bridges, the balcony thermal bridge causes the highest percentage of heat loss. Thus, given the substantial influence of the balcony thermal bridge on the energy efficiency of buildings and the complexities involved in addressing them, it has been selected as a primary research focus of this dissertation. The following paragraphs outline the overall organization of this dissertation.

Firstly, surveying previous research, the literature review section delves into the existing body of work concerning the consequences and significance of addressing thermal bridging, with a particular emphasis on the balcony thermal bridge. Published research papers have presented diverse solutions, such as insulating exposed slabs or integrating thermal break products within balcony constructions. Notably, the latter approach (i.e., integration of thermal break) has emerged as the most impactful method for mitigating the adverse effects of balcony thermal bridging.

Several studies have been conducted to assess the efficiency of thermal breaks in a balcony slab. However, it is noteworthy that most of these studies have adopted a numerical approach, employing various finite element tools for their analyses. While these numerical simulations offer valuable insights, there exists a significant gap in the experimental validation of these findings through laboratory assessment. Thus, this dissertation seeks to address this gap by conducting laboratory experiments to evaluate the real-world effectiveness of thermal breaks in managing the challenges posed by balcony thermal bridges.

Secondly, after going through the related literature and identifying the knowledge gap, the selection/development of an appropriate testing device to conduct laboratory investigations is the obvious next step. There are various laboratory-based test devices

for evaluating the thermal performance of building materials and components. For example, small-scale insulation specimens (e.g., 300 mm x 300 mm insulation boards) can be assessed using devices like guarded hot plate or heat flow meter. On the other hand, when dealing with multilayer large-scale specimens, hot box apparatus is used to characterize thermal performance. In the context of this research initiative, laboratory work involves the utilization of a hot box apparatus. A comprehensive review of both the available literature and the standards, developed by organizations like ASTM International (formerly known as the American Society for Testing and Materials) and ISO (International Organization for Standardization) which outline the requisites for constructing and operating such equipment, was conducted. A small-scale calibrated hot box test facility was constructed and calibrated in the building science laboratory at the University of Victoria. The construction of this apparatus stands out due to the incorporation of vacuum insulation panels (VIPs) as a main wall component of the climate chamber. This inventive use of VIPs contributes to achieving exceptional temperature stability within the chambers. Consequently, ensures a level of temperature stability that goes beyond the period of stability time prescribed by ASTM C1363 and ISO 8990 standards.

Thirdly, with the credibility of results from the hot box apparatus that established through the calibration process, the next phase involves constructing and testing concrete balcony slab of specific dimensions (750 mm x 350 mm x 200 mm). This concrete slab represents the conventional balcony, which acts as a representation of the most challenging thermal bridge. Following the examination of the conventional balcony, attention shifts to the creation of the thermally broken balcony slab configurations. At first, the commercially available thermal break product was selected as a benchmark against which the potential enhancements proposed for the subsequent improvement scenario would be evaluated. Subsequently, the focus turns to evaluating proposed

modifications against the aforementioned benchmark. Proposed modifications involve replacing thermal break reinforcement with materials of lower conductivity and using low conductivity concrete mixture on slab surfaces. The goal is to furtherly reduce the impact of the balcony thermal bridge in comparison with the benchmark (i.e., commercially available thermal break). The reduction in heat flow via the slab and the slab surface temperature have been investigated under a wide range of temperature gradients. The proposed configurations have demonstrated enhancements in reducing heat transfer through balcony slabs and elevating the temperature of the inner surfaces of the slab.

Finally, this dissertation examines another type of thermal bridge, the one formed by attachment elements of the cladding layer of the lightweight steel framed (LSF) wall. The attachment system comprises various components that compromise the thermal resistance of the insulation layer in the building envelope. Often, the impact of these elements is overlooked when estimating the overall thermal resistance of the building envelope. Therefore, this dissertation aims to quantify the impact of cladding attachment elements on the thermal performance of building envelopes through laboratory experiments using a hot box apparatus and numerical simulations. The observations demonstrate strong consistency between experimental and numerical results, the differences were always below 5%. Initially, the influence of each component of the cladding attachment is investigated independently. Thereafter, the remaining components are gradually introduced, with each step assessing the increase in heat flow. This increment in heat flow is compared with the baseline case, representing a wall section devoid of any cladding attachment elements. Finally, the influence of adding neoprene spacers at the interfaces of the cladding attachment elements is evaluated. Introducing the neoprene spacers help reducing the heat transfer through LSF walls. This

investigation seeks to emphasize the impact of secondary building envelope elements and highlight the importance of considering them in energy modelling.

In summary, the objectives and contributions of this dissertation can be outlined as follows:

1. *Establishing a unique hot box test facility*: The objective is to establish a hot box test apparatus that adheres to recognized standards. Particular emphasis is placed on integrating vacuum insulation panels (VIPs) to ensure exceptional temperature stability within the climate chambers. This facility will provide convenient access for conducting experiments, eliminating the need for expensive and time-consuming investigations in commercial laboratories.

2. *Laboratory investigations on balcony thermal bridge*: The objective involves conducting experimental studies to assess the actual efficacy of various mitigation strategies aimed at addressing thermal bridges in concrete balconies. This initiative aims to validate existing numerical simulations and enhance comprehension by leveraging real-world experimental data.

3. *Emphasizing the impact of cladding attachment elements:* The objective is to underscore the substantial impact of cladding attachment elements on the thermal performance of the building envelope. This objective also involves evaluating the effectiveness of a mitigation strategy in addressing the impact.

4. *Validation* of *experimental and numerical approaches:* The objective is to demonstrate the consistency and reliability of both experimental and numerical observations of various thermal bridging scenarios.

Chapter 1: Thermal Bridges in Building Envelopes – An Overview of Impacts and Solutions

The content of this chapter was published in the following journal:

A. Alhawari and P. Mukhopadhyaya, "Thermal bridges in building envelopes – An overview of impacts and solutions," International Review of Applied Sciences and Engineering, vol. 9, no. 1, pp. 31–40, Jun. 2018, doi: 10.1556/1848.2018.9.1.5.

1.1 Abstract

Increasing building energy performance has become an obligatory objective in many countries. Thermal bridge is a major cause of poor energy performance, durability, and indoor air quality of buildings. This paper starts with a review of thermal bridges and their negative impacts on building energy efficiency. Based on published literatures, various types of building thermal bridges are discussed in this paper, including the most effective solutions to diminish their impacts. In addition, various numerical and experimental studies on the balcony thermal bridge are explored. Results show that among all types of thermal bridges, the exposed balcony slab produces the most challenging thermal bridging problem where an integrated thermal and structural design is required. Using low thermal conductivity materials in building construction could help in reducing the impact of thermal bridges. Finally, further investigations are needed to develop more innovative and effective solutions for the balcony thermal bridge.

1.2 Introduction

Globally, over the past decades, demand for energy is increasing rapidly every year and a significant portion of this demand is consumed by residential buildings sector. After the energy crisis in the 1970s and the desire to diminish the environmental pollution problem, search for alternative resources to crude oil, such as solar and wind energy, had

become a priority of many nations. Simultaneously, number of regulations have been adapted to minimize the energy consumption in different sectors [6]. Because of the extremely cold climate in Canada, residential buildings sector consume about 17% of total energy usage and space heating consumes about 63% of the total energy consumed in residential buildings sector [4]. The building envelope has some areas with low thermal resistance through which the heat can transfer easily, for example, windows, doors, skylights, and thermal bridges. Thermal bridges are defined as areas of building envelope with very low thermal resistance, usually as a result of a penetration through building insulation layers. According to Passive House standards, the total heat transfer coefficient of opaque wall components in cool climate zone must not exceed 0.15 W/(m^2 K) [7].Various types of high energy efficient walls, roofs, and windows have been developed to reduce the buildings energy consumption. In addition, different advanced thermal insulation materials have been integrated in building envelope constructions such as phase change material (PCM), aerogel blanket insulation, vacuum insulation panel (VIP) etc. to reduce heat transfer through exterior building envelopes [8].

1.3 Consequences of Thermal Bridges

After windows and exterior doors, the second essential cause of heat loss in the high-rise buildings is non-insulated concrete slabs such as balconies [9]. The thermal bridges in buildings cause several negative consequences: high energy consumption for heating and cooling process, non-compliance with energy codes requirements, and uncomfortable spaces due to cold interior surfaces. Furthermore, they cause condensation on cold surfaces that may lead to dampness and mold growth, associated with health concerns caused by poor indoor air quality. Thermal bridging through walls and ceiling studs causes low temperature areas along these assemblies that leads to wall staining, which is also called “ghosting” [10]. Adding more insulation layers to the building envelope while disregarding the impact of thermal bridges may not lead to a significant reduction in the

heat losses, however it may increase the thermal bridging impact beside the augmentation in cost of construction [11],[12].

Disregarding impacts of thermal bridges but adopting highly efficient windows and well insulated walls will not produce an optimum reduction in the building energy usage. The building thermal bridges cause an increase of about 30% in the space heating load [1],[9],[7]. Neglecting the major building thermal bridges, such as balconies, can result in an underestimation of 20% to 70% of the total heat flow through the building envelope [11]. Unaccounted effects of thermal bridges in some buildings can cause an increase in thermal loads by up to 35% than preliminary calculations [6]. Thermal bridge can cause a reduction in the total thermal resistance of the clear wall field by about 40% [14]. Solid metal profiles, that used to fix the building envelopes' insulation layers, diminish the thermal resistance of the assembly to half value, so they are a major cause of thermal bridging [7].

1.4 Types of Building Thermal Bridges

Thermal bridge exists in areas where the heat transfers across the building envelope components, because of the discontinuity in thermal insulation layers [9]. There are different areas of the building envelope with high thermal transmittance (low thermal resistance), through which heat can pass more easily, such as balcony connections, windows frame, exterior wall corners, floor supports, and anchors [15]. The thermal resistance of some of these areas can be increased by adding more insulation materials; on the other hand, some of thermal bridges cannot be solved by increasing the thickness of the insulation layer, for example, wall penetrated by balconies. The amount of heat transferred through the common thermal bridges may exceed the amount of heat transferred through the insulated assemblies [15]. Following is a brief description of the common types of building envelope thermal bridges [16]:

1.4.1 Constructional/Structural thermal bridges

As presented in Figure 1.1, structural thermal bridges exist where a penetration occurs in the insulation layer of the exterior building envelopes. They are very common and easy to identify in building envelope because of their significant negative impact. These types of thermal bridges cause a discontinuity in the insulation layers, for example, projection of balconies, slab edges of buildings, and floor supports.

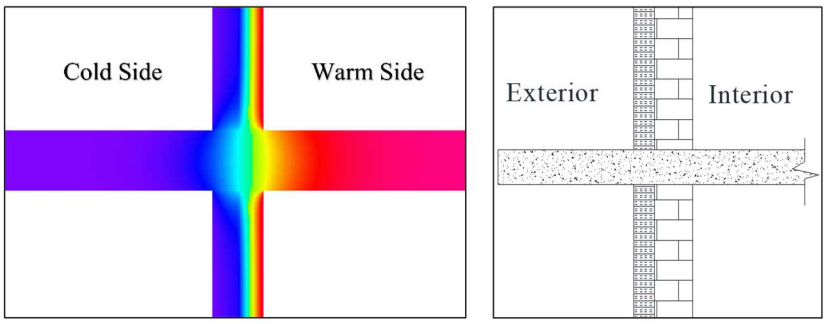

Figure 1.1. Schematic constructional/structural thermal bridges.

1.4.2 Geometrical thermal bridges

As shown in Figure 1.2, these types of thermal bridges exist in the envelopes of building where a difference occurs between the internal thermal absorbing area and external thermal dissipating area. For example, edges, corners of buildings, and window perimeters. The corner thermal bridge occurs at the junction between wall to wall, wall to roof, and wall to floor. These types do not form a discontinuity in the insulation layers.

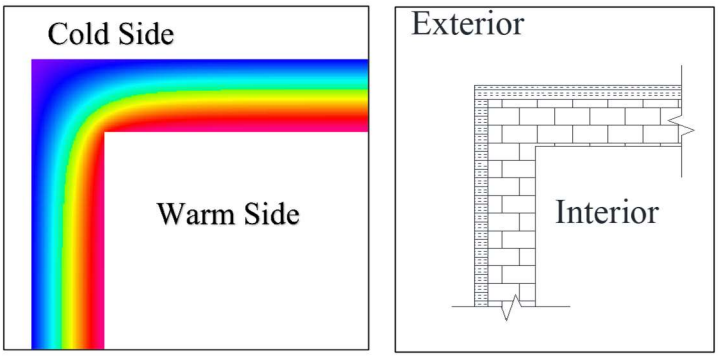

Figure 1.2. Schematic of a geometrical thermal bridge.

1.4.3 Systematic thermal bridges

As shown in Figure 1.3, these types usually appear in a certain series in the building assembly, such as wall's wood or metal studs, and concrete block webs. The joints in walls play a major role of heat loss and gain between indoor and outdoor environments, which is the major cause of the "ghosting" phenomenon.

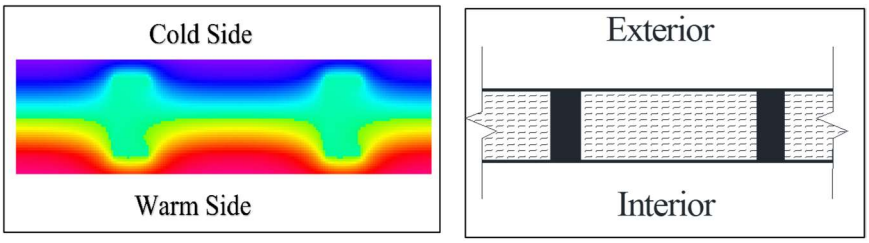

Figure 1.3. Schematic of a systematic thermal bridges

1.5 Linear and Point Thermal Transmittance

The linear thermal transmittance is defined as the difference between the heat flow through a building assembly with thermal bridges, such as balconies, and the amount of heat transferred through a clear wall divided by the effective length of the thermal bridges Figure 1.4. The point thermal transmittance differs from the linear thermal transmittance. The effective length of thermal bridges is not required to calculate the point thermal transmittance. For instance, anchors, and floor supports considered as point thermal bridges and their thermal effect considered as the point thermal transmittance.

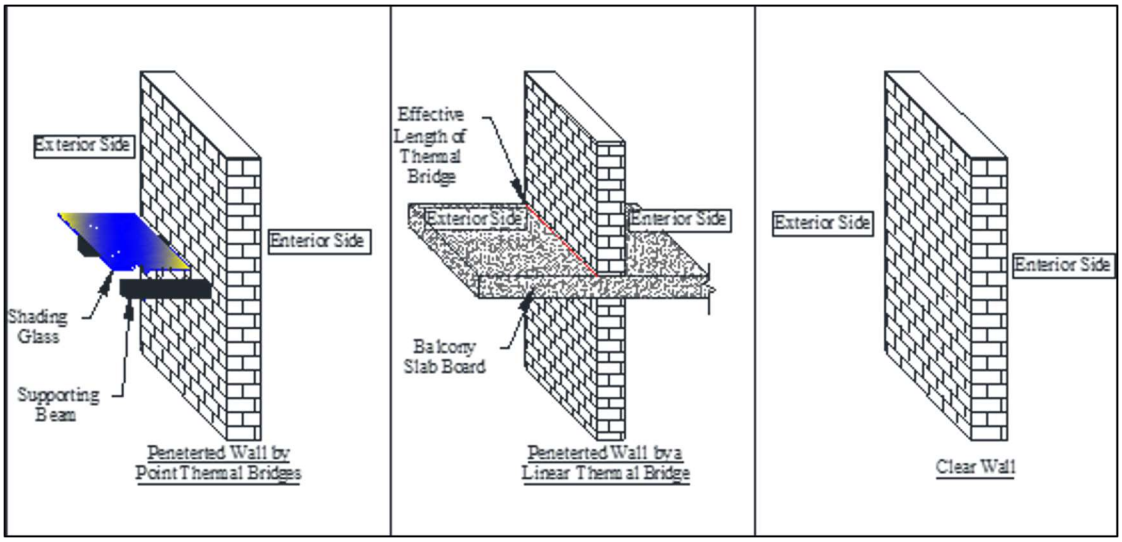

Figure 1.4. Sketches of different wall configurations

The heat transfer across the thermal bridges can be calculated by knowing the linear and/or point thermal transmittance of the thermal bridge as described in following equations:

$$Q_o = U_o * A_o * [T_{in} - T_{out}] \quad (1.1)$$

$$U_o = \frac{1}{R_o} \quad (1.2)$$

$$R_o = \frac{1}{h_{in}} + \frac{x_n}{k_n} + \frac{1}{h_{out}} \quad (1.3)$$

$$L_{3D} = \frac{Q_t}{\Delta T} \quad (1.4)$$

$$\Psi = \frac{L_{3D} - (U_o * A_o)}{l} \quad (1.5)$$

$$\chi = L_{3D} - [U_o * A_o] \quad (1.6)$$

$$Q_t = Q_o + Q_{tb} \quad (1.7)$$

$$Q_{tb} = \left[\left(\sum_{i=1}^{I} \Psi_i * l_i\right) + \left(\sum_{j=1}^{J} n_j * \chi_j\right)\right] * [T_{in} - T_{out}] \quad (1.8)$$

$$Q_t = \left[(U_o * A_o) + \left(\sum_{i=1}^{I} \Psi_i * l_i\right) + \left(\sum_{j=1}^{J} n_j * \chi_j\right)\right] * [T_{in} - T_{out}] \quad (1.9)$$

Where:

Q_o is the rate of heat transfers across the clear wall [W]

U_o is the thermal transmission coefficient of the clear wall [W/ (m^2 K)]

A_o is the surface area of the clear wall [m^2]

T_{in}, T_{out} are indoor and outdoor temperatures [K]

R_o is the thermal resistance of the clear wall [(m^2 K)/W]

h_{in} , h_{out} is the indoor /outdoor convection heat transfer coefficient [(m^2 K)/W]

k_n is the conduction heat transfer coefficient for (n) assembly materials [W/(m K)]

x_n is the thickness for n clear wall layers [m]

Ψ is the linear thermal transmission coefficient [W/(m K)]

χ is the point thermal transmission coefficient [W/K]

L_{3D} is the thermal coupling coefficient from 3-D calculation [W/K]

Q_{tb} is the rate of heat transfers across the assembly via the thermal bridge [W]

Q_t is the total rate of heat transfers across the assembly [W]

l is the effective length of thermal bridge [m]

n is the number of point thermal bridges in the assembly.

Regression models have been developed to estimate the linear thermal transmittance of three common thermal bridges in the building envelope: slab on grade floor to wall intersection, floor to wall intersection, and roof to wall intersection [12]. These models can predict the value of linear thermal transmittance of the three aforementioned thermal bridges with a relative error of less than 5% compared to the results that were calculated using computer software. In Europe, there are three different techniques used to estimate the thermal transmittance coefficient [17]. Selecting the thermal transmittance default values from the European Standard EN ISO 14683 [18] is the most common practice. However, using the default values from the standard may not give a precise estimation of the thermal bridge effects because of the complexity in constructions of some envelope

elements. In addition, applying the thermal transmittance default values may not give an accurate estimation of thermal calculations for North American buildings. This inaccuracy occurs because of the variances in the design and the construction materials used in European buildings. The common construction materials in Europe is concrete or masonry that ensures no interference between more than one type of thermal bridges; however, this is not the case in the North American buildings construction [14].

1.6 Approaches to Reduce the Impact of Thermal Bridges

As mentioned earlier, building envelopes have different types of thermal bridges that cause a rise in the energy consumption, because of the increase in heat loss or gain across the exterior building envelopes. As well, they may result in a problem of moisture condensation and mold growth on interior surfaces. Meeting the requirements of energy code regulations, ensuring suitable mechanical and thermal design, and reducing the proportion of energy loss and gain through thermal bridges have become a priority for many energy and building researchers. Therefore, number of numerical and experimental studies have been published on different types of thermal bridges with the aim to reduce their negative thermal impacts. Some thermal bridging problems can be solved by adding additional insulating barrier layers to ensure the insulation continuity in order to disrupt the heat transfer, while others require specific approaches to reduce their impacts.

1.6.1 Wall-to-roof interface

To solve the issues associated with geometrical thermal bridges, the solution depends on the design of building assemblies and how they interface with each other. In the case of wall to roof interface Figure 1.5 where the wall rises above the roof level, an insulation layer on the wall to roof interior corner is needed to prevent the thermal bridging [15].

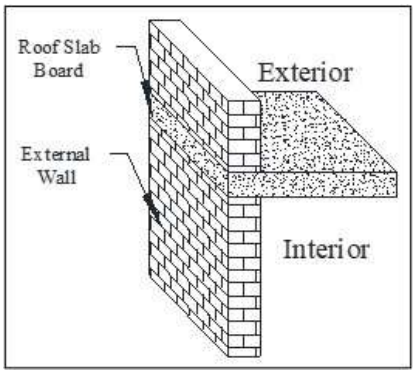

Figure 1.5. Sketch of wall to roof interface

1.6.2 Window perimeters

A window offset (Figure 1.6)can be considered as an essential thermal bridge. In some architectural design, the frames of windows are shifted outside to add some flush to the buildings. This shift causes a discontinuity in the building envelope insulation layer where the heat can transfer around the window frame especially in metal constructions. To eliminate heat from escaping through the window perimeter, an insulated panel is needed. Adding an insulation coat made of silica aerogels (k = 0.03–0.04 W/(m K)) to the window perimeter causes up to a 50% reduction in the energy loss caused by windows' offset thermal bridges [19].

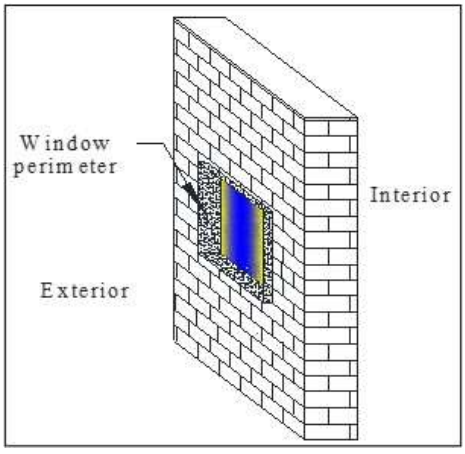

Figure 1.6. Sketch of window perimeter

1.6.3 Interface between building assemblies

Wall-to-wall thermal bridges (Figure 1.2) commonly exist between any two perpendicular walls because of the difference in interface region area from inside to outside. The adequate solution to this type of thermal bridge is adding additional insulation to the interface region. Furthermore, overlying exterior and interior insulation or insulating different planes of the wall is needed to ensure continuous thermal barrier [15].

1.6.4 Sun-shade structures

The sun-shade elements (Figure 1.7) are used in building constructions to reduce the radiation heat gain during the summer. Sometimes, these elements have a negative impact on thermal loads during the winter. Isolating these elements from the building envelope is required to diminish heat bridging from warm indoor to cold outdoor environments. Using lapped insulation at anchors of the sun-shades is a good way to eliminate these type of thermal bridges [15].

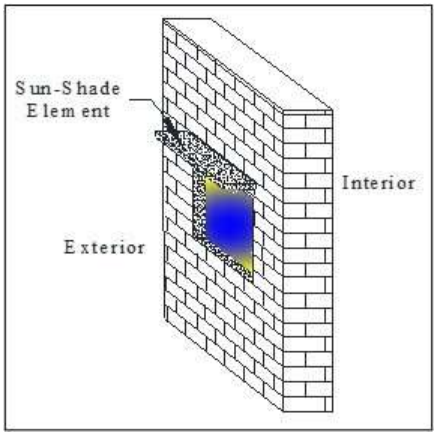

Figure 1.7. Sketch of sunshade element

1.6.5 Exterior wall studs.

The thermal bridge caused by studs (Figure 1.3) exists when the insulation is applied only for the area between studs. In the case of metal construction, using wood studs instead

of steel will reduce heat loss; otherwise, an exterior insulation layer is needed [20]. Increasing the space between the studs by 20 cm, in case of not adding an external insulation layer, will cause an increase in the overall thermal resistance of the wall by 25% [21].

1.6.6 Balconies extended slab.

In general, the thermal bridging through the balcony slab (Figure 1.1) is considered as the most challenging problem [22]. Among all thermal bridge types, the balcony thermal bridge causes the highest percentage of energy loss. The balcony slab board penetrates the barrier layers of the building envelope and creates a direct connection (i.e., heat flow path) between spaces with different thermal conditions. The balcony slabs work as "heat transfer fins" in buildings [20]. Compared with all other types of thermal bridges, balcony thermal bridges have a significant negative impact on energy performance because they present a large cross-sectional area ratio of exterior building envelopes [9]. Because of its greater impact on energy performance of buildings, the next section will concentrate on solutions of this type of thermal bridges.

1.7 Minimizing Impacts of Balcony Thermal Bridges

Researchers working on thermal bridging mostly focused on addressing the importance and the calculation methods to determine the amount of heat transferred through building thermal bridges. After demonstrating the negative impacts of thermal bridges on buildings energy performance and occupants' comfort, researchers started focusing on finding solutions for the issue. So far, a number of numerical and experimental research studies were published on finding solutions to diminish the heat loss across the balcony slabs.

Wakili et al. [22] developed a balcony board sample with a thermal break made of glass fiber reinforced polymer (GFRP) as compression elements. The thermal performance of the new balcony board was analyzed numerically by using the TRISCO 3D computer program [23]. A specimen of the new balcony board and a wall made of exterior insulated brick (U-value = 0.2 W/(m^2 K)) were built and tested in a hot-box (ΔT= 30 ^oC). Both numerically and experimentally, the linear thermal transmittance and the temperature of the inner corner between the lower surface of the balcony and the wall surface were measured. Then the results were compared with conventional balcony board (balcony slab without thermal break). Both the experimental and the numerical analysis gave almost same results for temperature profile along the specimen surface. Comparing the inside corner temperature in case of the new balcony board and the conventional balcony showed that using the thermal break caused a rise in the inside corner temperature by up to 4 ^oC depending on the structural and the strength of the innovative thermal break. The study demonstrated the positive influence of thermal break on the linear thermal transmittance. The innovative thermal break caused a decrease of about 60% in the linear thermal transmittance compared to the linear thermal transmittance of the conventional balcony board.

Karabulut et al. [24] studied the effects of insulating the surfaces of two different thermal bridge types (intermediate floor beam wall, and extended balcony board). This study focused on the impact of external and internal insulation layers and the effect of the insulation layer thickness on the thermal bridging. Thermal analyses in this study were done by using ANSYS FLUENT simulation tool [25]. The specimen wall was built of brick that is penetrated by the concrete slab with a 35 ^oC temperature difference across the wall. The impact of insulating the building envelope was presented by measuring the temperature variation along the penetrated wall. The internal insulation scenario produced a 65% to 80% reduction in the heat flux through the wall depending on the

thickness of the insulation material. However, the case of internal insulation did not cause any reduction in the heat flux through the concrete slab. Therefore, the interior insulation was not a good solution to eliminate the thermal bridging. The researchers studied the effect of exterior insulation on the heat flux through the penetrated wall. In this scenario, the inner surface temperature did not drop as it did in the case of internal insulation. The heat flux through the wall was very low compared to the interior insulation scenario, which means the external insulation layer has a good effect in reducing the heat transfer. Changing the thickness of the insulation layer had a significant influence on the inner temperature variation and the heat flux through the assembly. The influence of covering the balcony slab with insulation material with various thicknesses was also investigated. In comparison with the uninsulated balcony board, this approach caused an important change in temperature variation and heat flux through the inner surface of the assembly. The lowest surface temperatures were recorded at the interior corner where the reinforced concrete component joined the wall assembly.

In 2016, the same research group published another research study [26]. The objectives of this research were the same as the previous one, but the study was extended to different building and insulation materials. The new study emphasized the effects of different configurations of insulation layers applied on the same building geometry. The conclusion of this study supported the results from the previous research, i.e., the importance of adding insulation layers to the building envelope and the effectiveness of external insulation.

In recent years, a number of studies were carried out to investigate the significance of using a commercially available thermal break products (Figure 1.8) [27] to reduce the heat loss through the balcony thermal bridge. A typical commercially available thermal break product is built by using different insulation materials such as extruded/expanded polystyrene or mineral wool and contains reinforcing bars to deal with shear, tensile, and

compression forces [27]. A Canadian study [9] investigated the importance of installing the commercially thermal break in the construction of the balcony slab. The numerical analysis was carried out using HEAT 3 software [28]. The study predicted that using the thermal break would produce an increase in the internal slab-wall corner temperature up to 4.5 ^{o}C higher than the non-thermally broken balcony. The study concluded that using the thermal break would cause a 7% to 8% reduction in space heating energy demand.

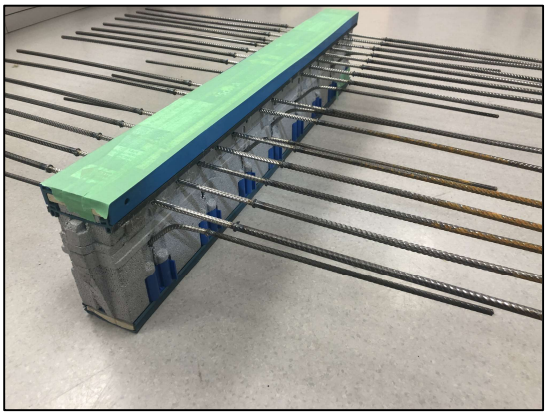

Figure 1.8.Commercially available thermal break product

A study by Ge et al. [29] on a twenty-six-story building, located in Toronto, Canada, investigated the impact of the commercial balcony thermal break on the internal slab surface temperature of seven different wall configurations, using simulation tool THREM [30]. Furthermore, the researchers presented the effects of the thermal break on the building heating and cooling loads by using *e*Quest energy simulation tool [31]. The study concluded that installing the traditional balcony thermal break caused a 4.1 to 6.4^{o}C increase in the internal slab temperature, depending on the wall assembly configuration. The thermal break caused a 5 to 13% reduction in the annual heating energy consumption, and less than 1% reduction in annual cooling energy consumption. The performance of thermal break is higher when window to wall area ratio is reduced, walls are well-insulated, and other types of wall thermal bridges are eliminated.

A field study [32] evaluated the influence of thermal break in the balcony construction on the thermal performance and energy saving of high-rise multi-unit residential buildings located in Chicago, IL, USA. The study was done by installing thermocouples on both the slab board of a thermally broken balcony and the conventional balcony slab (non-thermally broken balcony) to measure the temperature gradient. During the cold season, the temperature readings indicated that temperature gradient through the thermally broken balconies was 2.5 to 4.5 ^{o}C lower than those of the conventional balconies, which means lower heat losses through the building envelope. Implementation of the thermal break caused a reduction in the building energy consumption by up to 3%. In a 20-storey building with continuous balconies geometry around the building perimeter on each storey, the annual energy saving cost can be up to $6000 US based on utilities rate of Illinois, USA.

Goulouti et al. [33], [34] studied the impact of replacing the stainless-steel bars in the conventional thermal break with fiber-reinforced polymer materials that have low thermal conductivity, about 170 times less than stainless-steel thermal conductivity. The innovative thermal break was built in a PVC box filled with aerogel materials (k = 0.013 W/(m K)) to ensure high thermal resistivity. The tension stainless-steel bars in the conventional thermal break were replaced by the aramid fiber-reinforced polymer bars. The compression bars were replaced by glass fiber-reinforced polymer bars attached to a hexagonal foam sandwich to transmit the shear force. Generally, this study focused intensively on the structural performance of the innovative thermal break. ANSYS FLUENT software was used to investigate the thermal performance of the new thermal break. The study concluded that thermal losses diminished by 41%, in the case of ideal building envelope that has the lowest energy consumption. In addition, the study showed that very low values of linear thermal transmittance could be achieved (Ψ < 0.15 W/(m K)).

Murad et al. [35] studied the impacts of including insulated concrete curb, which is made of 25.4mm Extruded and Expanded Polystyrene (XPS and EPS), underneath the sliding door of the balcony. Eight different scenarios were thermally investigated by using THERM simulation tool. The commercial balcony thermal break was one of the scenarios that was used for comparison. The objectives of this study were to measure the interior wall-balcony corner temperature and the distance from the sliding door to the point where the slab surface temperature reaches the space temperature. The study concluded that the installation of the insulated concrete curb under the sliding balcony door increased the interior temperature and reduced the distance from the sliding door to the point of the same indoor temperature. These results improved when the insulated curb was combined with using the commercial balcony thermal break.

Another comprehensive research study [9], evaluated the influence of different building design parameters, such as balcony slab thickness, projection span of the balcony, effects of floor finishing, and impact of radiant heating system, on the equivalent thermal resistance value of the wall assembly (Eq. R-value). The study indicated that an increase of 2 inches to the thickness of the balcony slab would cause about 12% reduction in the wall Eq. R-value. The change in the balcony projection depth had insignificant impact on wall Eq. R-value. The indoor floor finishing and radiant in-floor heating system had almost no effects on the wall Eq. R-value. This study also presented various solutions to reduce the balcony thermal bridging, such as balcony structure cut-outs with and without insulation, concentrated reinforced steel bars with and without insulation, insulated outer balcony surfaces, and installed conventional thermal break. HEAT3 software was used to analyze the performance of the above solutions. The research concluded, in the case of well-insulated walls, the first two scenarios made no positive impact on the wall assembly Eq. R-value except when the insulation was added to the section area that is free of steel bars. In these cases, compared to the traditional balcony slab case, the wall

Eq. R-value would increase by around 50%. Insulating the outer surface of the balcony made a significant increase in the wall Eq. R-value by around 60%. Using the commercial thermal break caused an increase in the wall Eq. R-value to double value.

A case study by Ge and Baba [36] presented the effect of the building thermal bridges on the energy consumption of a two-story residential building. Two different climates were chosen, Quebec City, QC, Canada as a cold climate location, and Phoenix, AZ, USA as a hot climate location. A whole building energy analysis was performed using WUFI Plus program [37]. The thermal bridge impact was modeled using three different methods, direct 3D simulation method, equivalent U-value method, and equivalent wall method. These three methods were used to calculate the difference in annual heating and cooling loads. In comparison to using the 3D simulation method in calculating the annual heating and cooling loads, the study indicated the followings: in cold climate, use of equivalent U-value method caused an underestimation of 8 to13%, and use of equivalent wall method caused an underestimation of 4% to 9%; while in hot climate, use of equivalent U-value method and equivalent wall method caused an underestimation of 17%, and 14% respectively.

Another study reported by Baba and Ge [38] investigated the effect of the balcony thermal bridge on the energy performance of a high-rise building in different locations in Canada. The researchers studied the impact of the balcony thermal bridge on the building thermal loads by using the equivalent U-value method and a simulation tool, WUFI Plus program. The effect of implementing the commercial balcony thermal break on the building thermal loads was investigated. The study presented effects of the balcony thermal bridge on three different configurations of balcony slabs. The researchers discovered that the divergence in calculated annual thermal loads between the two used methods was higher in the milder climate. The thermal break reduced the energy consumption in the heating process by 7.1% to 8.8%, and its effectiveness improved in

well-insulated building envelopes. The thermal break reduced the difference between the results of the methods. This study demonstrated the importance of the balcony thermal bridge and the effect of increasing the balcony slab ratio on the building thermal loads, particularly the heating load.

A numerical and experimental analysis study conducted by Dikarev et al. [39] investigated the thermal effect of the balcony thermal bridge on the temperature gradient in the interior floor and roof slab surfaces. The researchers studied the impact of implementing the commercial balcony thermal breaks on energy loss through slab boards that penetrate the building envelopes. Two samples were tested; one was a wall penetrated by slab board (conventional case), while the other sample was a wall penetrated by a thermally-broken slab board (thermal break case). Both samples were placed in a guarded hot box to measure the temperature gradient along the slab board using a number of thermocouples. Furthermore, a three-dimensional steady-state numerical approach was performed using ANSYS FLUENT. The numerical analysis was applied to validate and compare the experimental analysis. The conclusion of this study was that the balcony commercial thermal break has a significant influence in reducing the energy loss through the balcony slab board. This thermal break produced an increase in temperature of 8 ^{o}C higher than the conventional case at a particular point on the slab.

A research study by Real et al. [40] investigated the use of structural lightweight aggregate (SLWA) in concrete instead of the normal weight aggregate (NWA) to diminish the negative impact of thermal bridges in the building envelopes. Because of the porosity in the composition of SLWA, this aggregate has a low thermal conductivity compared to NWA. It was observed that an increment of 1.0% in aggregate porosity caused a reduction in its thermal conductivity by 0.6%. This advantage of SLWA had been tested numerically by THERM software on four different types of structural lightweight aggregate concrete (SLWAC) with different properties. The study confirmed that the thermal conductivity

of 1850 kg/m^3 density of SLWAC ranges from 0.58 to 0.86 W/(m K), which is lower than the thermal conductivity of NWC by about 50% to 70%. The study concluded that the SLWAC has a significant effect on the steady state condition because of its lower thermal conductivity, and on the unsteady state conditions because of its higher specific heat capacity. In this research, the whole building energy performance was analyzed using EnergyPlus software program [41]. The total energy usage of the sample in the case study indicated that using SLWAC in construction reduced the annual energy consumption by 0.9 to 1.3 kWh/m^2 (6 to 11% saving in energy) compared to usage of NWC. The SLWAC has a significant effect in reduction of heating loads rather than cooling loads because, in the hot climate, the solar gain has more crucial effect on cooling loads than thermal bridges.

Larbi et al. [42] evaluated the performance of an innovative thermal break that can be used in steel balconies attached to a concrete slab. The new thermal break is built of a 10mm rigid PVC plate and 10mm of acoustic insulation layer. This thermal break is installed between the end-plate of the steel beams and the concrete wall or floor to minimize the impact of the point thermal bridges created by steel beams. A 3-D steady state simulation analysis using TRISCO was implemented to calculate the point thermal transmittance values by applying different configurations: the thickness of the PVC plate and the insulation layer of the building envelope, the material of fastening parts (stainless steel or carbon steel), and installation of an additional insulation layer around the beams at the connection areas. The numerical analysis showed that the innovative thermal break caused a reduction in the impact of the thermal bridge 20% to 65% compared to a similar structure built without installing the innovative thermal break. The range of reduction depends on the combination of the construction configurations mentioned above. Moreover, in comparison with carbon steel as a fastening system, stainless steel caused a 17% to 37% reduction in the impact of the thermal bridge.

Zhang et al. [43] have assessed how balcony thermal bridges affect heating energy demand in apartment buildings. They found that using thermal breaks like thermal break and thermal break with GFRP rebars reduced heat loss by approximately 60.9-66.5% and 70.1-75.0%, respectively, with TB-GFRP being more effective by 8.0-9.2%. These measures can help reduce heating energy demand by about 5.6-8.0% for TB and 6.6-9.3% for TB-GFRP, with TB-GFRP saving an additional 0.9-1.5% compared to TB, especially in buildings with radiant floor heating systems. These percentages highlight the significant energy-saving potential of these thermal breaks.

Borelli et al. [44] have utilized a two-dimensional steady-state finite element model (FEM) to replicate the thermal bridge between the wall and the floor. They employed a regression algorithm to determine the linear transmittance ψ for numerous node configurations.

Aghasizadeh et al. [45] conducted a study on thermal bridges at the connection points between balconies and walls. They explored three types of connections: concrete-to-concrete, concrete-to-steel, and steel-to-steel. Their findings showed that the most effective solution in each case involved adding an EPS insulating layer between the exterior and interior structures to interrupt heat transfer. The 3D simulations revealed that the concrete-to-concrete connection had the highest linear transmittance, while the concrete-to-steel connection had the lowest. Overall, implementing EPS thermal bridge insulation resulted in a 12.2% reduction in heat losses.

In a related study by Romero et al., [46] thermal bridges associated with three distinct building envelope improvements were investigated. Their findings indicate that the installation of external façade insulation and insulation at joints required to support insulating panels can reduce thermal bridge transmittances by approximately 20% and up to 63.4%, respectively.

Borelli et al. [47] created a regression-based simulation to assess the thermal transmittance of linear thermal bridges at wall-to-floor nodes, considering different construction scenarios. The accuracy of this method was thoroughly validated against industry standards. The study highlights the significant impact of construction choices on heat loss in these bridges. The resulting correlations provide a practical tool for analyzing ground contact thermal bridges in various scenarios, offering ease of use and accuracy. This methodology can also be extended to other types of thermal bridges, such as roller shutter boxes and window sills.

Saied et al. [48] underscored the importance of thermal bridges in slab-on-grade constructions. Their study highlighted variations in thermal bridge calculation standards across regions, the influence of ground thermal properties, and the significance of insulation solutions. They advocate for exterior insulation, acknowledging that its effectiveness depends on factors such as thickness and depth. They also emphasize the need to consider economic and feasibility factors when implementing retrofitting solutions. Notably, the L-type insulation emerged as a highly effective option, reducing thermal bridge effects by 54% without requiring soil drilling.

1.8 Conclusions

It is obvious from the published literatures and technical reports that further research and development initiatives are needed to reduce the impact of the balcony thermal bridge on building energy efficiency. Development of innovative thermal breaks, using advanced thermal insulation and structural materials, is a top priority. Moreover, most of the published literatures on thermal bridge and breaks were based on numerical simulation. The lack of experimental benchmarking of simulation results may lead to an under or overestimation of the actual results and the future performance of the buildings.

Chapter 2: Construction and Calibration of a Unique Hot Box Apparatus

The content of this chapter was published in the following journal:

> *A. Alhawari and P. Mukhopadhyaya, "Construction and Calibration of a Unique Hot Box Apparatus," Energies, vol. 15, no. 13, Art. no. 13, Jan. 2022, doi: 10.3390/en15134677.*

2.1 Abstract

A variety of mathematical models are available to estimate the thermal performance of buildings. Nevertheless, mathematical models predict the thermal performance of buildings that might differ from the actual performance. The hot box is a widely-used test apparatus to assess the actual thermal performance of various building envelope components (walls, roofs, windows) in the laboratory. This paper presents the process of designing, constructing, and calibrating a unique small-scale hot box apparatus. Despite its smaller metering area (1.0 m × 1.0 m), this apparatus met the key requirements (below ±0.25 °C fluctuations in chambers' air temperature, and below 2.0% variation from the point-to-point temperature in reference to the temperature difference across the specimen) as prescribed in the ASTM C1363 and ISO 8990 standards. The walls of this apparatus are uniquely constructed using vacuum insulation panels or VIPs. The efficient and novel use of VIPs and workmanship during the construction of the apparatus are demonstrated through the temperature stability within the chambers. The achieved range of temperature steadiness below ±0.05 °C and point-to-point temperature variation below 1.0% of the temperature difference across the specimen allow for this apparatus to be considered unique among the calibrated hot box categories reported in the literature. In addition, having an affordable, simple-to-operate, and high-accuracy facility offers a great opportunity for researchers and practitioners to investigate new ideas and solutions. The apparatus was calibrated using two extruded polystyrene foam (XPS) specimens with thicknesses of 2″ and 4″. The calibration exercise indicates small

differences between results obtained numerically, theoretically, and experimentally (below 3.0%).

2.2 Introduction and Background

Energy consumption in the building sector has increased significantly over time to meet the expected living standards of the occupants. In developed countries, 20% to 40% of the total energy consumption is consumed by the building sector [49], [50]. Therefore, reducing building energy consumption will help meet the requirements of energy codes. Consequently, it will diminish the negative impacts associated with the energy production process, such as air pollution and global warming. For example, using high thermal resistive insulation materials in building envelopes and making buildings more airtight are the key steps to reducing the amount of energy consumed for heating and cooling processes. The appropriate selection of insulation materials/components and the determination of their representative thermal properties are critical steps toward high energy-efficient buildings.

Different approaches are employed to measure the thermal properties of the building envelope materials in the laboratory. The most common devices used to measure the thermal properties, in the case of one-dimensional heat flow, are the guarded hot plate (see ASTM C177 standard [51]) and the heat flow meter (see ASTM C518 standard [52]). However, there are some limitations to using these devices because they can be used only to test homogeneous building materials that can be represented by a small-size specimen. In the case of large-scale and nonhomogeneous building assemblies, hot box test apparatuses are employed to determine the thermal properties of such components. The hot boxes are used to measure the thermal performance of nonhomogeneous building components with multi-dimensional heat flows. More details and history of hot boxes are presented in the next paragraphs.

The concept of a hot box test apparatus was first introduced about a century ago in the USA [53]. The hot box was initially introduced as an analogous testing method to the guarded hot plate (Figure 2.1a), which is used to evaluate the thermal properties of homogeneous building materials [54]. Unlike the guarded hot plate, the hot box is used to test large-scale, homogeneous/non-homogeneous specimens, which represent building envelope assemblies. The hot box consists of two chambers, i.e., a metering chamber and a climate chamber, which, respectively, serve as indoor and outdoor environments. During hot box testing, the specimen is placed between the chambers, and heating and cooling systems are incorporated to create a steady temperature difference across the specimen. The hot box setups are typically classified under two categories: (1) calibrated hot box (Figure 2.1b), and (2) guarded hot box (Figure 2.1c). The major distinction between the two systems is the existence of a guarded chamber that surrounds the metering chamber in the case of the guarded hot box. The guarded chamber helps to maintain the difference in temperature between the metering and guarded chambers, keeping it very small so as to minimize the heat loss via the metering walls. In the case of the calibrated hot box, the surrounding environment is treated as a guarded chamber, and heat transfer through the metering walls needs to be measured. According to the ASTM C1363 standard, the calibrated hot box must be used when the area of specimens is smaller than the opening of the metering chamber, where a surrounding panel is needed. However, the guarded hot box is a suitable choice when the building element to be tested has an area larger than the opening of the metering chamber and is free of high-conductive elements that continue outside the opening of the metering chamber. It is to be noted that there are more studies with calibrated hot boxes reported in the literature than studies with guarded hot boxes [55].

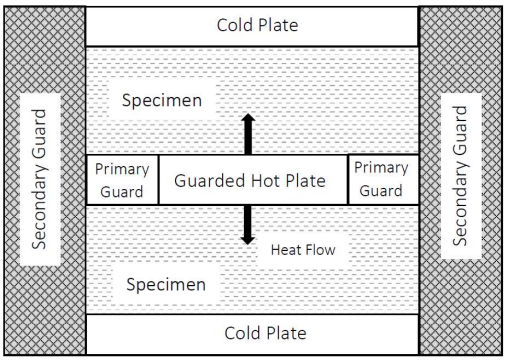

(a)

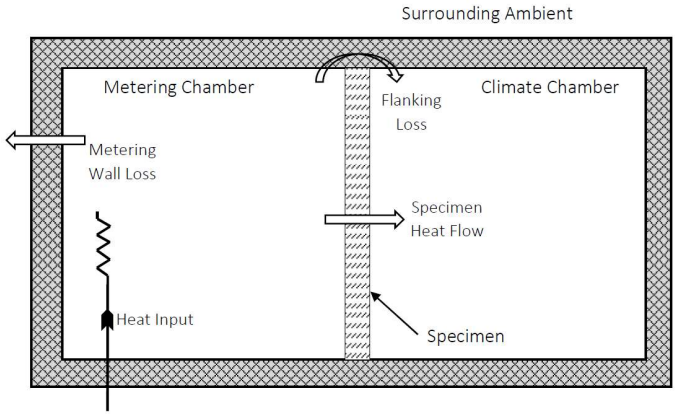

(b)

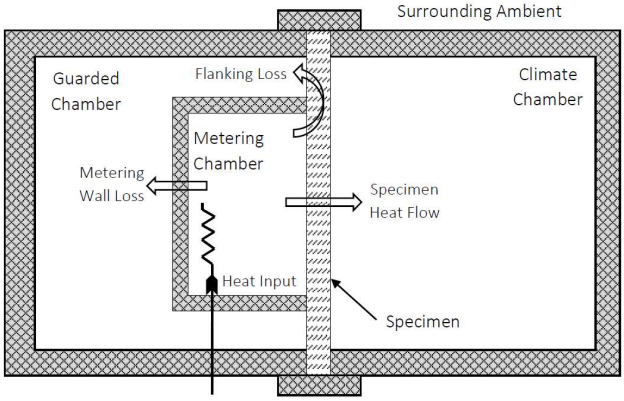

(c)

Figure 2.1. Schematics of: (a) guarded hot plate; (b) calibrated hot box; (c) guarded hot box.

The utility of laboratory tests with hot boxes was recognized by the building envelope designers/engineers/researchers, and several hot boxes were built to evaluate the thermal

performance of different building components, including fenestration systems [56], [57], [58]. In the early 1970s, Mumaw [59] developed a large-size calibrated hot box facility to measure the properties of large-scale wall sections of areas up to 2.7 m by 4.2 m. Soon after, from the 1970s to the 1990s, numerous studies were published on the construction and calibration of hot box test apparatuses [60]–[70]. All of these publications were used as the basis for the ASTM C 1363 standard [71], which was first published in 1997 and was recently updated in 2019. In Europe, an identical standard, ISO 8990, was released in 1996 [72]. Both standards illustrate specific requirements that should be followed during the stages of construction and operation to obtain repeatable and representable results.

2.3 Literature Review

Due to our recent concern about the issues related to global warming [73], more regulations and policies have been introduced in building codes to boost the energy performance of building envelopes, which consequently helps to reduce the carbon footprints of buildings. One important criterion to ensure the requirements of building codes are met is accurately specifying and determining the thermal characteristics of building envelope materials/systems, and the guarded hot box test apparatus is routinely used for this purpose. Though hot box test apparatuses are usually available in commercial research laboratories [74]–[77], several thermal investigations have been performed using test facilities that are available in academic/university laboratories. In academic laboratories, hot boxes are usually distinct in size and structure, and are usually inexpensive and relatively simple and easy to operate. The following paragraphs present studies using hot box facilities in academic institutions, which are comparable to the hot box presented in this paper.

Asdrubali and Baldinelli [78] studied the accuracy of three different hot box standards (ISO 8990; ASTM C1363-05; and GOST 26602.1-99) using a calibrated hot box. The

chamber walls of the hot box were constructed with an EPS (240 mm thick) inserted between two panels of wood (19 mm, each) with an overall thermal resistance of 7.5 m2·K/W (R-42.3). The opening area of the apparatus was 2.7 m × 2.0 m and temperature fluctuation inside the chambers was lower than ±0.20 °C. A few years later, Ricciardi et al. [79] employed the same apparatus to investigate the thermal properties of two panels with an area of 1.23 m × 1.48 m that were made of waste paper (12 mm thick) and textile fibers (20 mm thick). The authors did not provide any information regarding temperature stability inside the chambers.

Seitz and MacDougall [80], at Queen's University, Canada, designed and constructed a small-scale calibrated hot box. The size of the metering area was 1.18 m × 1.37 m, and the apparatus was built to evaluate the thermal characteristics of non-conventional building materials such as a straw bale of a maximum thickness of 41 cm. The hot chamber was constructed using layers of expanded polystyrene coated by two layers of plywood of a total thickness of 130 mm. The total thermal resistance of the chamber wall was 2.91 m^2·K/W (R-16.5). To provide a cold environment on the side of the specimen, an environmental chamber was employed. Air temperature variation from point to point was below 3.0 °C, and the air temperatures inside the chambers at steady state fluctuated within ±2.0 °C.

Buratti et al. [81], [82] developed a small-scale calibrated hot box to evaluate the thermal conductivity of different coating materials. The testing facility consisted of a hot chamber and a test specimen frame with opening area of 0.46 m × 0.46 m. The hot chamber and the specimen frame were made of expanded polyurethane (200 mm thick) and two panels of wood (each of 20 mm thick). So, the total thermal resistance of the walls was 8.78(m^2 K)/W (R-50). The laboratory room was considered a cold chamber. During the test, the hot chamber air temperature fluctuated by about ±0.10 °C, and the specimen surface temperature varied within a range of 0.60 °C on the hot face and 0.40 °C on the cold face.

Alongi et al. [83] developed an apparatus at Politecnico of Milano, Italy to experimentally investigate the thermal behavior of air-permeable concrete specimens at different pressure differentials. The apparatus envelope/wall consisted of polystyrene panels protected by laminated panels on both sides (140 mm total thickness). The total thermal resistance of the apparatus wall was 4.35 (m^2 K)/W (R-25). The maximum specimen area that could be tested in this apparatus was 1.0 m × 1.0 m and had a thickness of 33 cm. The design of this apparatus was different because authors were not only looking to investigate the thermal performance of tested samples under steady-state conditions, but also to study the impact of airflow through air-breathing wall samples. Thus, the apparatus was fitted with an air circulation system that controlled the velocity and direction of the airflow. The authors indicated that temperature fluctuation inside chambers was always within the range of ±0.30 °C.

Chowdhury and Neogi [84] investigated the thermal performance of common wall and roof constructions used in residential buildings in India using a guarded hot box facility. The facility was constructed according to the ISO 8990 standard. Extruded polystyrene insulation panels (250 mm thick) were used for chamber's walls, which lead to a total thermal resistance of 8.80 m^2·K/W (R-50). The dimensions of the apparatus' metering chamber and metering area were 1.75 m × 1.50 m and 0.50 m × 0.50 m, respectively. The authors presented a detailed description of the apparatus calibration process and testing methodology. At steady state, temperature fluctuation within the chambers was about ±0.06 °C.

Barbaresi et al. [85] developed a prototype hot box for the preliminary assessment of thermal properties of wall elements and insulation panels at the University of Bologna, Italy. The apparatus was used to test a small specimen of a maximum area of 1.0 m × 1.0 m and consisted only of a hot chamber made of 100 mm of expanded polystyrene panels and a layer of wood with a total thermal resistance of 2.0 m^2·K/W (R-11.5). The laboratory

space was treated as a cold chamber. The temperature inside the hot chamber fluctuation was high, as presented in the graphs; however, the authors stated that the apparatus provided results with low error compared to the value measured by a guarded hot plate. Additionally, they mentioned that this apparatus can only be used for preliminary evaluations, not for certification purposes.

Shen et al. [86] constructed a small-scale hot box with a 355 mm × 355 mm metering area to establish a relationship of thermal properties between full-scale and scaled-down concrete sandwich wall panels. Whereas the full-scaled specimens were tested using the finite element method, the scaled-down specimens were tested in the hot box. The walls of the hot chamber were built of a layer of extruded polystyrene panel (25.4 mm thick) that was finished with a layer of plywood (19.1 mm thick). An insulation blanket layer was added to the outer surfaces to reduce the impact of temperature fluctuations in the laboratory. The apparatus was calibrated using an extruded polystyrene sample before testing the concrete sandwich wall panel; however, the degree of stability of the chamber's temperature was not specified. The authors concluded that using a small-scale hot box is practicable and inexpensive, but it cannot replace full-scale hot box measurements.

Most recently, Tejeda et al. [87] and Boukhelf et al. [88] studied the hygrothermal behavior of different concrete wall systems. In both studies, small-scale hot boxes of the metering area of around 1.0 m × 1.0 m were incorporated to perform the experimental analysis. The chamber walls of both hot boxes were made of extruded polystyrene (50 mm thickness) that was coated by protection layers from both inside and outside. The first group reported that the temperature of the air inside the chambers fluctuated by below 1.0 °C, though the second group reported less temperature variation below 0.30°C.

The present study introduces the construction and calibration processes of a unique small-scale calibrated hot box apparatus for academic research. A description of the apparatus and its components including the novel use of insulation materials in wall structures, and the calibration procedure of the apparatus using two extruded polystyrene foam panels of different thicknesses are presented. This apparatus is intended to be used for testing and validating various research questions. As a case study, a test specimen representing a lightweight steel frame (LSF) wall system (clear wall, i.e., wall area containing only insulation and necessary framing materials) was tested using this apparatus. Table 2.1 lists and compares the studies available in the published literature on hot boxes fabricated in academic research laboratories across the world, and also includes the recommendations provided by the relevant ASTM and ISO standards.

Table 2.1. Detailed description of selected studies utilizing comparable test apparatus.

Publication Authors/Year	Size of Metering Area	Size of Metering Chamber	Apparatus Typology	Thickness of Chamber Walls (Core Materials)	Thermal Resistance of Chambers Walls	Point-to-Point Air Temp. Variation	Max. Temp. Fluctuations at Steady State
ASTM C1363 (2019) [71]	> 1.50 m²	>1.50 m²	GHB/CHB	-	> 0.83 (m² K)/W (R-4.7)	< 2.0% of ΔT and <2 K	< ±0.25 °C
ISO 8990 (1996) [72]	> 1.50 m × 1.50 m	>1.50 m × 1.50 m	GHB/CHB	-	-	< 2.0% of ΔT and < 2 K/m	< 1.0% of ΔT
Asdrubali, Baldinelli (2011) [78]	2.70 m × 2.0 m	2.70 m × 2.0 m	CHB	240 mm (EPS)	7.46 (m² K)/W (R-42)	-	±0.2 °C
Seitz et al. (2015) [80]	1.18 m × 1.37 m	1.18 m × 1.37 m	CHB	130 mm (EPS)	2.91 (m² K)/W (R-16.5)	< 3.0 °C	±2.0 °C
Buratti et al. (2016) [81], [82]	0.46 m × 0.46 m	0.50 m × 0.50 m	CHB	220 mm (Polyurethan)	8.78 (m² K)/W (R-50)	0.4 °C	±0.1 °C
Alongi et al. (2017) [83]	1.00 m × 1.00 m	1.22 m × 1.22 m	CHB	140 mm (Polystyrene)	4.35 (m² K)/W (R-25)	-	±0.3 °C
Chowdhury et al. (2019) [84]	0.50 m × 0.50 m	1.75 m × 1.50 m	GHB	250 mm (XPS)	8.80 (m² K)/W (R-50)	-	±0.06 °C
Barbaresi et al. (2020) [85]	1.00 m × 1.00 m	1.00 m × 1.00 m	CHB	100 mm (EPS)	2.0 (m² K)/W (R–11.5)	-	±4.0 °C
Shen et al. (2021) [86]	0.35 m × 0.35 m	0.44 m × 0.44 m	CHB	25.4 mm (XPS)	0.88 (m² K)/W (R-5)	-	-
Tejeda et al. (2021) [87]	1.00 m × 1.00 m	Not available	CHB	50 mm (XPS)	1.76 (m² K)/W (R-10)	-	±1.0 °C
Boukhelf et al. (2022) [88]	1.30 m × 1.35 m	Not available	CHB	50 mm (XPS)	1.76 (m² K)/W (R-10)	-	±0.3 °C
Current study	**1.00 m × 1.00 m**	**1.00 m × 1.00 m**	**CHB**	**185 mm (XPS + VIP)**	**9.15 (m² K)/W (R-52)**	**0.2 °C**	**±0.05 °C**

The table above (Table 2.1) presents a comparison between the hot box introduced in this study and the ones described in the relevant literature. The comparison was made considering five major characteristics: (1) the type of the apparatus, (2) the size of the apparatus and its metering area, (3) the type and thickness of the core insulation material used in the chamber walls, (4) the total thermal resistance of the chamber walls, and (5) the temperature stability inside the chambers. It is clear from Table 2.1 that the developed apparatus has thinner walls. It has also the highest thermal resistance due to the novel use of VIPs. Furthermore, the significant achievement of the apparatus is the high level of temperature stability within the chambers. The point-to-point air temperature variations and the maximum temperature fluctuations at steady state condition reported from this study were the lowest compared with the hot box constructions reported in the literature.

2.4 Description of the Apparatus

The apparatus was designed to test a variety of wall configurations, including the ones associated with balcony penetration. The apparatus consists of eight major components: (i) environment chambers, (ii) specimen frame, (iii) heating system, (iv) cooling system, (v) radiation baffles, (vi) air circulation systems, (vii) temperature sensors, and (viii) heat flux sensors. Further details about these major components are depicted below.

2.4.1 Environment Chambers

The hot (metering) and the cold (climate) chambers are identical in dimension at 1.0 m × 1.0 m wide and 1.0 m deep (Figure 2.2a,b). Despite what is stipulated in ASTM C1363, the minimum size of the metering area is 1.5 m^2 and the metering area of this apparatus is 1.0 m^2 because of several restrictions, such as the laboratory height and door size. The walls of the chambers are assembled using very high thermal resistive materials. The walls are constructed of one layer of 25 mm (1.0 in) vacuum insulation panels (VIP) attached to

four 25 mm (1.0 in) layers of extruded polystyrene (XPS), with two layers on each side. As a protection to the apparatus, a 16 mm (5/8 in) plywood layer is used on the outer surface. As interior skin, a 16 mm (5/8 in) fiberglass-mat-faced gypsum (DENSGLASS®) sheathing is used to prevent any moisture management issues. As specified by the ASTM 1363 standard, the surface's emittance needs to be greater than 0.80 to avoid any radiative heat transfer with the specimen. Hence, all interior surfaces have been colored black. The total thermal resistance of the chamber walls is about 9.15 (m^2 K)/W (R-52) according to the manufacturer's specifications for the used materials. At the back of each chamber, there is a small aperture for wiring access and coolant pipe connections.

(a) (b) (c)

Figure 2.2. (a) Environment chamber; (b) interior view of the chamber; (c) specimen frame

2.4.2 Specimen Frame

The specimen frame (shown in Figure 2.2c above) consists of two pieces to facilitate the installation of specimens: the base and the U-shape. In addition to a 25 mm (1.0 in) VIP layer, the base is constructed of three layers of high-density extruded polystyrene foam (XPS-100) 76 mm (3.0 in) thick. This type of XPS was chosen to guarantee handling heavy specimens. The U-shape component is assembled from layers identical to those used in chamber walls described in the previous section. The frame is stationary while the chambers are transportable, with four wheels attached to the bottom of each one. To

minimize heat loss via interfaces between chambers and the specimen frame, layers of neoprene rubber are glued to the interfaces, which work as a gasket. Table 2.2, below, presents the properties of the materials used in constructing the apparatus.

Table 2.2. Materials' properties [89]–[93].

Material	Properties			
	Density (Kg/m^3)	Thermal Conductivity (W/(m K))	Specific Heat Capacity (J/kg·K)	Compressive Strength (kPa)
Extruded polystyrene: XPS-20/XPS-100	25/48	0.028	1470	173/690
Vacuum insulation panel (VIP)	220	0.0051	850	100
Plywood	550	0.125	1880	~35 × 10^3
Fiberglass-mat-faced gypsum (DENSGLASS®)	700	0.128	880	3445
Neoprene foam	160	0.0384	2500	25

2.4.3 Heating System

The ASTM C1363 standard illustrates that the thermal stability of the metering chamber can be obtained through two different methods [94]. The first is supplying constant power to the chamber, and the second is controlling the temperature within the chamber. The first method is adopted in this study. The disadvantage of this approach is the long operation time to reach thermal stability, because of the thermal mass of materials constructing the metering chamber. A ceramic heat bulb is used as a heat source in the metering chamber (Figure 2.3a). The heat supply by the bulb is adjusted by a regulated DC power supply (Figure 2.3b).

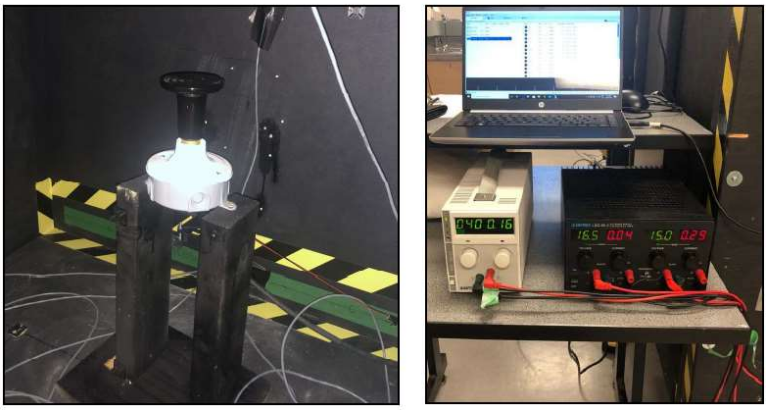

(a) (b)

Figure 2.3. (a) Ceramic heat bulb; (b) DC power supply regulator.

2.4.4 Cooling System

The air to water cooling system has been adopted as a cooling system. The system is required to remove the heat transferred from the metering chamber or surrounding space to reach stable conditions. A refrigerating circulation bath (chiller) attached with a precise temperature controller was used as a main cooling system component (Model: AP7L-20R). Inside the climate chamber, two small evaporators connected in series are mounted at the back of the chamber. For efficient heat exchange between the air in the climate chamber and the coolant inside the evaporators, four small fans are attached to the evaporators; two pairs are attached to each evaporator.

2.4.5 Radiation Baffles

There are multiple reasons for having baffles parallel to the surfaces of the sample. Baffles prevent any radiative heat exchange from any heat source device such as fans and heaters inside the chambers. Thus, all heat-generating devices need to be installed behind the baffle. Baffles also help to obtain a uniform airflow of a constant velocity by adjusting the distance between the specimen and the baffle. The space between the specimen side and the baffle is recommended by the ASTM C1363 standard to be between 140 and 200 mm. The surface of the baffles facing the specimen should have an emittance greater than 0.80

to prevent any radiative heat exchange with the specimen. Moreover, materials that are used to construct the baffles should have a high thermal resistance (1.0 $m^2 \cdot K/W$ is recommended by standards). Because of all the aforementioned reasons and recommendations, the baffles of this apparatus are made of 50 mm (2 in) of extruded polystyrene insulation panels. The distance between the specimen and the baffles is adjustable depending on the specimen geometry and air velocity requirement. Figure 2.4a, below, shows the baffle element.

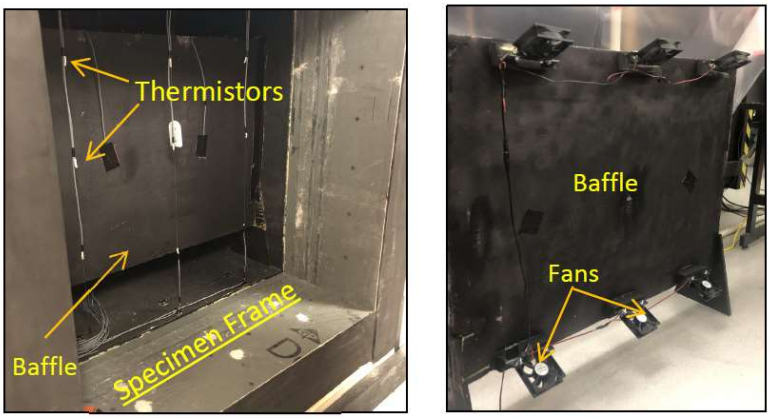

(a) (b)

Figure 2.4. (a) Radiation baffle element; (b) fans attached to the baffle.

2.4.6 Air Circulation Systems

Attaining uniform temperatures and velocities in the air curtains is required in regard to obtaining accurate results. The uniform temperature in both chambers can be acquired by circulating the air in the curtains at constant velocities. To maintain temperature uniformity in the air curtains, twelve small fans are used, six in each chamber. To achieve natural air movement, fans are mounted to circulate the air downwards in the hot chamber and upwards in the cold chamber at constant velocities. According to the ASTM C1363 standard, the maximum air velocity of 0.50 m/s is allowed to ensure the natural convection air condition in the metering chamber. Figure 2.4b shows the fans' positions for the hot and cold chambers. The fans are attached to the back of the baffles to avoid

any heat radiation between them and the specimen. The speed of the fans is adjusted by controlling the power supply through a DC power-regulated device. The air velocity inside the air curtains is measured using a hot wire anemometer. During all measurements, the air velocity is below the limit mentioned above.

2.4.7 Temperature Sensors

To measure the temperatures of the air inside the chambers, a number of thermistors are installed. According to the product datasheet, the operating temperature limits of the thermistor are from −55 °C to 125 °C with a tolerance of 1.0%, and are readable to ±1.0 K. There are two data acquisition boards, one for each chamber. Each board has 48 channels, so a total of 48 thermistors can be installed inside each chamber and on each surface of the specimen. In each chamber, nine thermistors were installed in the air curtain between the baffle and specimen about 100 mm away from specimen surfaces. An adequate number of temperature sensors for the specimen can be installed based on the area and the geometry. Figure 2.5, below, shows the location of the thermistors in the space between the faces of the specimen and the baffle. Four sensors (two in each chamber) are placed on the surfaces of baffles that are facing the specimen. Measurements of the baffles surface temperatures are required to determine if there is any contribution of radiative heat transfer between the baffle and the specimen, which can occur if there is a difference in temperature.

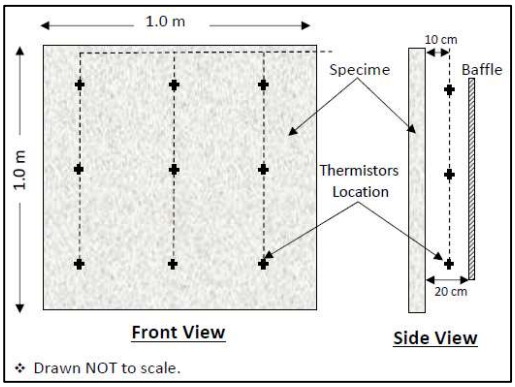

Figure 2.5. Scheme of temperature sensors' layout.

2.4.8 Heat Flux Sensors

Two heat flux transducers have been installed, one for each chamber. According to the specification datasheet, these sensors can be used within a temperature range of −50 °C to 120 °C, and a heat flux range of ±150 kW/m^2. The transducer has a sensing area of 84 cm^2. The heat flux sensors are connected to precision instrumentation amplifiers. The amplifiers' job is to convert the differential voltage output readings from micro and mille ranges to higher ranges. The output data from the amplifier are then transferred to the data acquisition system. The heat flux transducers can be used to measure the thermal heat flux transferred through the test specimen or via the walls of the chamber in the process of calibration. Before use, the heat flux sensors have been calibrated according to the procedure indicated in the product datasheet.

2.5 Calibration Procedure

The calibration process is essential for the hot box to determine its performance and the accuracy of its measurements. Calibration procedures can be accomplished numerically, theoretically, or experimentally. According to the literature, the experimental approach is usually implemented to perform the calibration procedure, where materials with uniform thermal properties are used. For example, boards of extruded (XPS) and expanded (EPS) polystyrene rigid foam insulation are recommended. In the current study, two samples of XPS of different thicknesses (2.0 and 4.0 in) with areas equal to the aperture of the apparatus (1.0 m^2) were selected for calibration. The calibration process was completed in two steps under three temperature gradients. The first step was completed by comparing the amount of heat flow via the specimens obtained experimentally with the amount calculated both theoretically, assuming a one-dimensional heat transfer, and numerically, using a three-dimensional finite element

program (HEAT3) [95]. The second step of calibration is to experimentally estimate the amount of associated metering and flanking losses.

2.5.1 Temperature Stability

Maintaining stable temperatures in air curtains, which refers to the air space between the surfaces of the baffles and the specimen's surfaces, is a key point for obtaining accurate results when investigating the material properties using the hot box apparatus. Incorporating low thermal conductivity materials in the walls of the hot box is helpful for reducing temperature fluctuations as well as the impact of instability of the ambient temperature of the laboratory space. The two selected samples were used to perform the initial experiments. Despite challenges in ensuring that the surrounding environmental temperature remained within a stable range, very small fluctuations in the air curtains' temperatures of metering and climate chambers were noticed. As mentioned earlier, nine thermistors in each chamber were used to measure the temperature of the air adjacent to the surfaces of the specimen (as shown in Figure 2.5). In order to show the stability of the temperature inside the chambers, the air curtains' temperature profiles of the test conducted on the 2″ XPS specimen are presented in Figure 2.6. These figures illustrate the degree of air temperature stability inside the chambers while the ambient air temperature swings by about 3 °C (as shown in Figure 2.7). The ambient air temperature was measured by placing five thermistors around the hot chamber. Several reasons for the fluctuation in the laboratory temperature are related to the age of the building, such as the building's poor thermal insulation and airtightness. Moreover, other devices running in the same space were accounted for as heat sources.

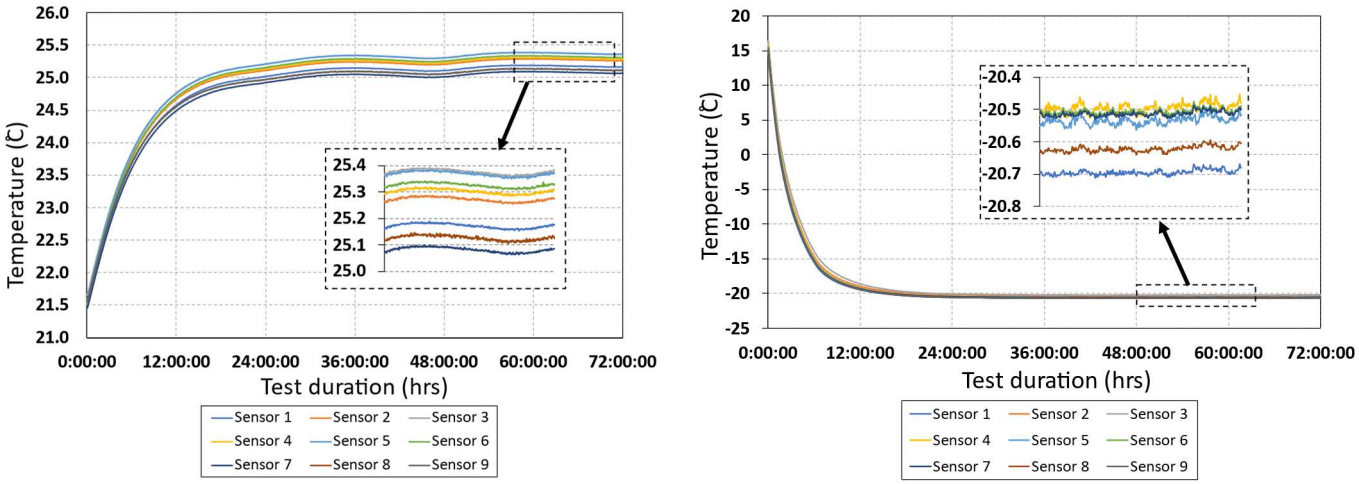

(a) (b)

Figure 2.6. Air curtain temperature profile of: (a) metering chamber; (b) climate chamber.

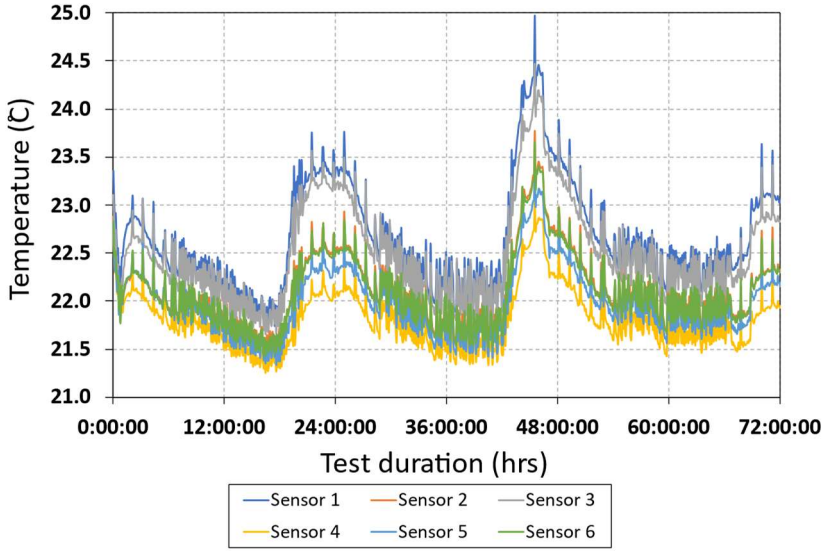

Figure 2.7. Laboratory temperature profile.

2.5.2 Experimental, Numerical, and Theoretical Thermal Analyses

The performance of the apparatus was assessed by measuring the heat flux through known thermal properties specimens, which are two XPS boards in this study. The boards had thicknesses of 2.0 in and 4.0 in. These specimens were tested under three different temperature gradients, as listed in Table 3. The size of each specimen was equal to the box aperture area (1.0 m^2). As mentioned above, the heating control system of the

apparatus was a constant power supply into the metering chamber; thus, the temperature readings are not presented as the same fixed values in all cases. The average temperature of the air in the curtains was measured using nine thermistors located about 100 mm away from the surfaces of the specimens. The precision of the measurements using this apparatus was evaluated by estimating the rate of heat flow through the designated specimens via three different methods:

Theoretical calculation: the heat flux was estimated according to Equations (2.1) and (2.2), where the average values of the measured temperatures of the specimen surfaces $T_{h,s}$ and $T_{c,s}$ were employed:

$$q_S = \frac{\left(T_{h,s} - T_{c,s}\right)}{R} \quad (2.1)$$

$$R = \frac{x_S}{\lambda_S} \quad (2.2)$$

Numerical analysis: the HEAT3 program was incorporated to estimate the heat flux, where the average values of the measured air temperatures are assumed. In both the theoretical and numerical analysis, the thermal conductivity of the tested samples was assumed to be a constant value equal to 0.028 W/(m K). According to the ASHREA handbook and the ISO 12567-1 standard, the cold (exterior) and hot (interior) sides' surface film coefficients (h_e and h_i) were assumed to be 25 W/m^2·K and 7.7 W/(m^2 K).

Experimental measurements: the average heat flux value collected using the heat flux sensor was considered. The heat flux sensor is located at the center of the specimen panel. The average value was collected over a period of more than 6 h after reaching the steady-state conditions, as indicated in [94]. In general, the steady state was considered to have been achieved when the temperature measurements in the air curtains started to vary arbitrarily by less than 1.0% over a period of time [72].

Ultimately, the theoretical and numerical computed heat flux values were then compared to the average value of data measured experimentally. The differences are also presented as percentages in Table 2.3 and Figure 2.8.

Table 2.3. Comparison between theoretical, numerical, and experimental heat flowrates.

Parameters	Units	2″ XPS Specimen			4″ XPS Specimen		
		Test 1	Test 2	Test 3	Test 1	Test 2	Test 3
Metering Chamber Air Temperature	°C	21.13	21.75	21.65	20.88	21.1	21.65
Climate Chamber Air Temperature	°C	−7.91	−12.51	−16.96	−8.18	−12.76	−15.96
Specimen Hot Surface Temperature	°C	19.97	20.39	20.13	20.25	20.38	20.86
Specimen Cold Surface Temperature	°C	−6.46	−10.78	−15.01	−7.43	−11.90	−14.97
Calculated Heat Flow Rate	W/m²	14.57	17.18	19.37	7.64	8.91	9.81
Simulated Heat Flow Rate	W/m²	14.6	17.22	19.4	7.62	8.88	9.87
Measured Heat Flow Rate	W/m²	14.82	17.44	19.63	7.55	8.67	9.61
Difference Between Measured and Calculated	W/m² (%)	−0.25 (−1.72)	−0.26 (−1.51)	−0.26 (−1.34)	0.09 (1.18)	0.24 (2.69)	0.28 (2.83)
Difference Between Measured and Simulated	W/m² (%)	−0.22 (−1.51)	−0.22 (−1.28)	−0.23 (−1.19)	0.07 (0.92)	0.21 (2.36)	0.26 (2.63)

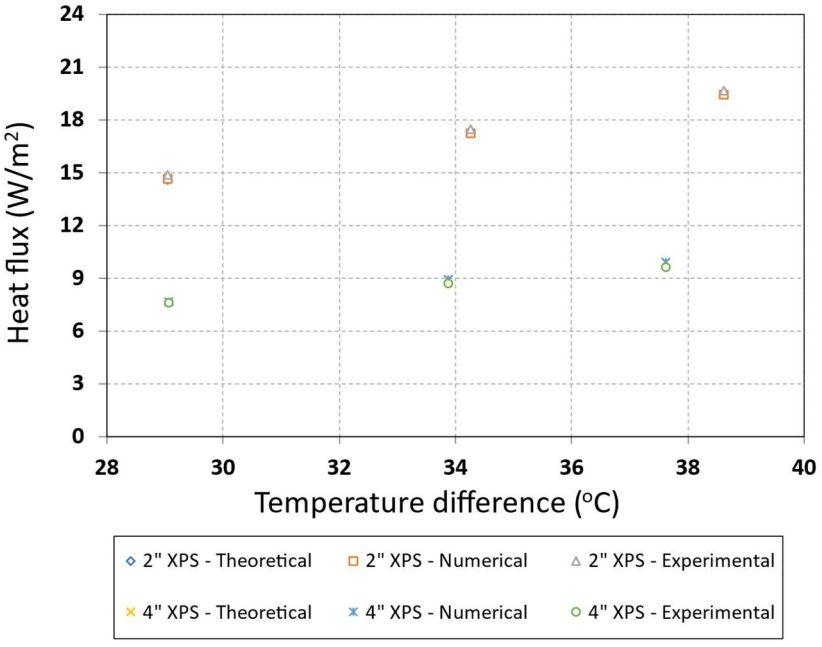

Figure 2.8. Comparison between theoretical, numerical, and experimental heat flow rates.

2.5.3 Energy Balance

The main objective of the hot boxes is to measure the amount of heat that flows through the tested specimen when the air conditions of both sides reach steady-state conditions. During the test, stability in both temperature and air velocity are required within the air curtains in both chambers for a period of time. When the steady-state conditions are established, the amount of heat flowing through the specimen is then calculated. The standards stipulate that the heat loss through the walls of the metering chamber must be less than 10% of the amount of heat transferred through the specimen. This apparatus has been constructed to be well insulated; nevertheless, a small percentage of the supplied heat into the metering chamber will transfer through its walls. Moreover, some heat will be lost through the interface areas of the apparatus components. It is impractical to fabricate a completely insulated apparatus; therefore, the heat transfer across the walls of the metering chamber (metering loss), and the heat flow at the edges of the specimen and frame (flanking loss), needs to be characterized to obtain precise results. Moreover, the apparatus contains different parts, such as wires and access openings, which might cause thermal loss to the surrounding space. Due to the complexities of estimating metering and flanking loss separately, all forms of heat losses are combined in a single quantity known as an extraneous loss. Flanking loss was first accounted for as a part of the extraneous loss by Lavine at el. [96]. They defined flanking loss as the heat flow increment between the chambers in reference to specimen heat flow in absence of any edge effect. Figure 2.9 shows a scheme of various types of heat flow paths.

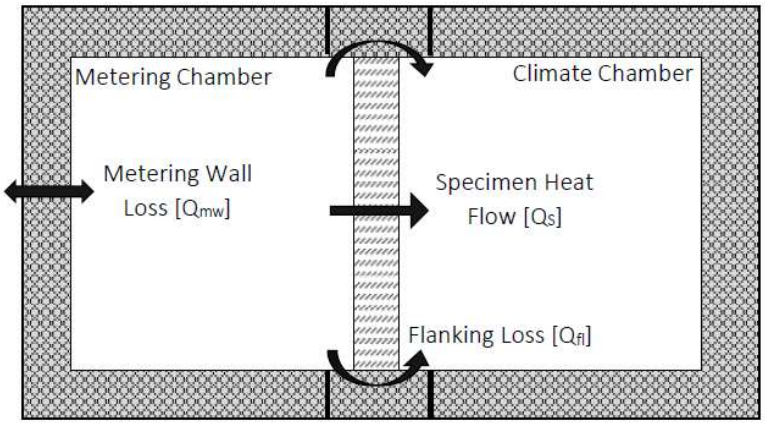

Figure 2.9. Scheme of heat flow paths.

The net amount of heat transferred through the specimen (Q_s) is calculated by subtracting total heat loss from the net amount of energy input into the metering chamber. The net amount of supplied energy is presented through the total heat dissipated by the heater (Q_{in}) and air circulation system (Q_f). The electric power consumed by the heater and fans is metered and considered to be totally converted into heat. As mentioned above, the heat loss includes the metering wall loss (Q_{mw}) and flanking loss (Q_{fl}). Equations (2.3)–(2.6) represent the calculation procedure using the data obtained experimentally.

$$Q_{in} + Q_f = Q_S + Q_{mw} + Q_{fl} \quad (2.3)$$

$$Q_S = [Q_{in} + Q_f] - [Q_{mw} + Q_{fl}] \quad (2.4)$$

$$Q_{extr} = Q_{mw} + Q_{fl} \quad (2.5)$$

$$Q_{extr} = [Q_{in} + Q_f] - Q_S \quad (2.6)$$

The total amount of extraneous loss (Q_{extr}) can be estimated either theoretically by applying the regression Equations (2.7)–(2.9) below [94], or experimentally by testing known thermal characteristic materials, such as polystyrene foam panels (presented next). Finite element methodologies can be also used to estimate the thermal balance of the hot box.

$$A_{eff} = A_i + 0.54 \cdot L \cdot \Sigma e_i + 0.60 \cdot L^2 \quad (2.7)$$

$$Q_{mw} = \frac{\lambda_{eff} \cdot A_{eff} \cdot (T_{mw,i} - T_{mw,e})}{L} \quad (2.8)$$

$$Q_{fl} = \lambda_{eff} \cdot (A/L)_{eff} \cdot \left(T_{env,h} - T_{env,c}\right) \quad (2.9)$$

where A_{eff} is the metering chamber's effective area normal to the heat flow, A_{in} is the interior area of the metering chamber in m^2, and L is the wall thickness of the metering chamber in m; e_i is the sum of metering chamber's interior edges lengths in m; λ_{eff} is the effective thermal conductivity; $T_{mw,i}$ and $T_{mw,e}$ are the temperatures of the interior and exterior surfaces of metering chamber; $(A/L)_{eff}$ is the effective area/path length of the entire specimen frame; and $T_{h,env}$ and $T_{c,env}$ are the air temperatures inside the metering and climate chambers.

According to the ASTM C1363 standard, reasonable results are obtained when the metering box walls, and flanking losses are at a minimum. The first type of losses can be minimized by using high thermal resistance materials in the construction of the box walls. Flanking loss can be reduced by designing an apparatus with a large metering area, which is not the case here because of the restrictions described earlier. Another strategy to diminish the flanking loss is to incorporate low thermal conductivity materials at the interface between the specimen edges and its frame. Calculating the metering walls and flanking losses accurately is very challenging due to the non-uniformity of the wall layers of the chambers and the specimen frame based on the design requirements. Thus, losses are estimated experimentally using insulation panels of known thermal properties. From the perspective of a thermal bridging analysis, specimens containing any types of thermal bridges can be tested to address the impact of the thermal bridge. This apparatus is beneficial to evaluations of the performance of some novel solutions for thermal bridging problem. The relation between the measured heat flow through the calibration panels of

1.0 m^2 area and the associated extraneous losses are presented in Table 2.4 and Figure 2.10.

Table 2.4. Extraneous loss associated with hot box measurements.

Parameters	Units	2″ XPS Specimen			4″ XPS Specimen		
		Test 1	Test 2	Test 3	Test 1	Test 2	Test 3
Temperature Difference	°C	29.25	34.26	38.61	29.06	33.86	37.61
Mean Temperature	°C	6.62	4.62	2.35	6.35	4.17	2.85
Measured Heat Flow via the Specimen	W	14.82	17.44	19.63	7.55	8.67	9.61
Total Supplied Energy into Metering Chamber	W	20	24.05	27.51	11.41	13.75	15.72
Amount of Extraneous Heat Loss	W	5.18	6.61	7.88	3.86	5.08	6.11
Percentage of Extraneous Heat Loss *	%	25.90	27.48	28.64	33.83	36.95	38.87

* Percentages are calculated in respect to total amount of energy supplied into the metering chamber.

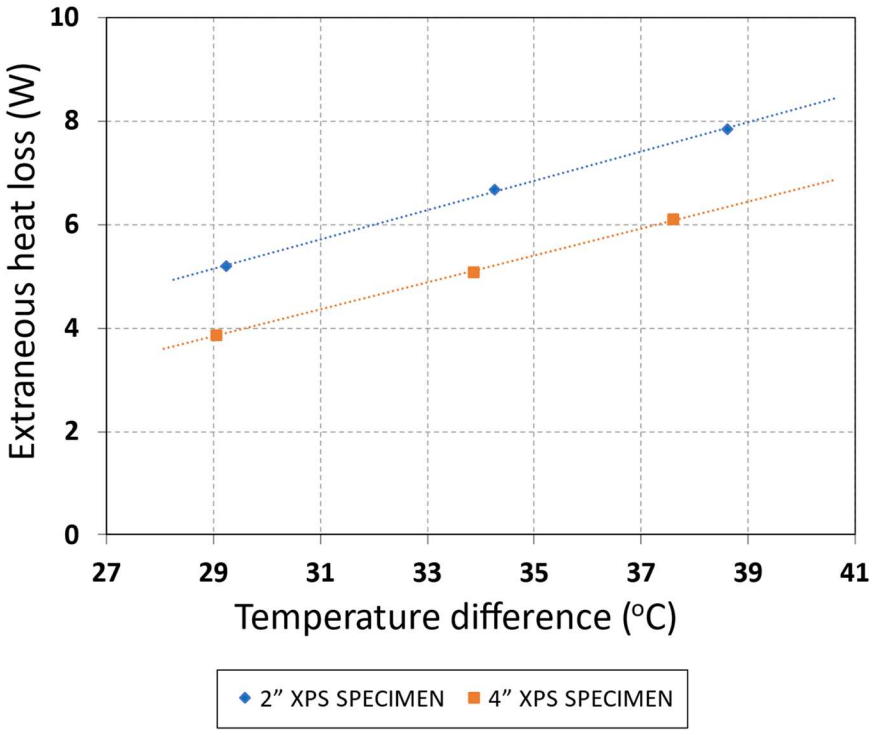

(a)

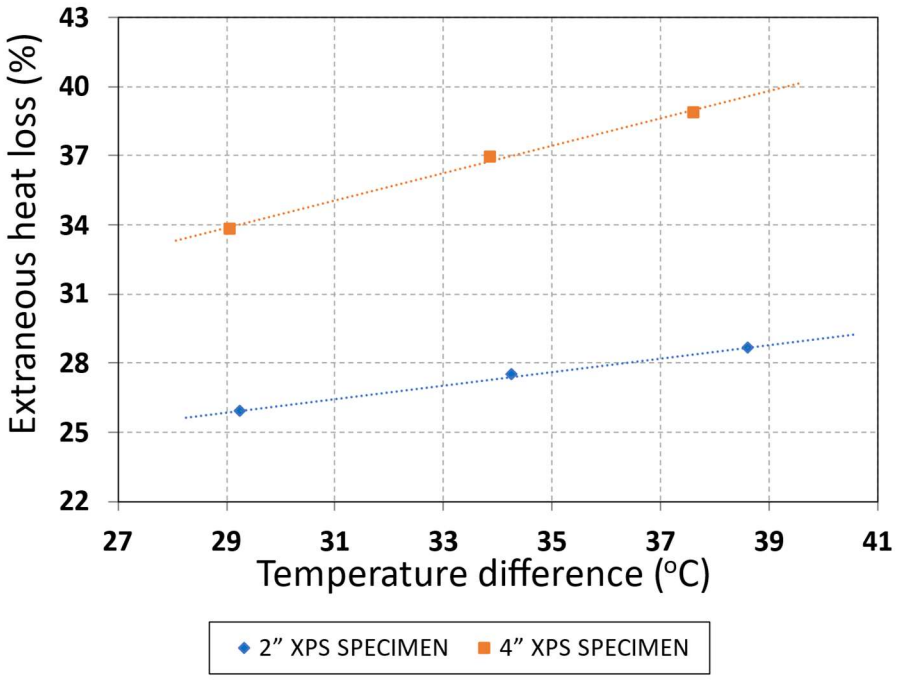

(b)

Figure 2.10. Relation between temperature gradients and extraneous heat loss as: (a) an amount; (b) a percentage.

2.6 Summary of Observations and Conclusions

This paper presents the process of the construction and calibration of a unique small-scale calibrated hot box apparatus that has unprecedented temperature stability. The walls of this hot box have been constructed with vacuum insulation panels (VIPs) sandwiched between layers of extruded polystyrene (XPS) boards. The walls have high thermal resistance (R-52); thus, specimens with high thermal resistance can be tested using this apparatus. The apparatus can be used to evaluate the thermal characteristics of traditional and novel building envelope components of sizes up to 1.0 m (height) × 1.0 m (width) × 0.4 m (thickness). The major findings from this study are outlined below:

Although the temperature of the surrounding space fluctuates by ±1.50 °C, at the steady state, the temperature fluctuation inside the chambers and the temperature variation from point to point across the specimen's surface remain below ±0.05 °C and 0.20 °C,

respectively. These values are the lowest among all studies reported in the literature using a calibrated hot box apparatus.

During the calibration procedure, the differences between the results obtained experimentally and the ones computed both numerically and theoretically were always below 3.0%. These observations clearly demonstrate the uniqueness of this calibrated hot box apparatus with the unprecedented temperature stability and reliability of the test results.

Chapter 3: Mitigating Balcony Thermal Bridging: Experimental and Numerical Investigation of Innovative Solutions for Energy-Efficient Building Envelopes

The content of this chapter has been prepared for review and subsequent publication:
A. Alhawari and P. Mukhopadhyaya."Mitigating Balcony Thermal Bridging: Experimental and Numerical Investigation of Innovative Solutions for Energy-Efficient Building Envelopes"

3.1 Abstract

Heat transmission through building envelopes is heavily influenced by various thermal bridges, with balcony thermal bridges being a common type that significantly affects the energy performance, durability, and indoor air quality of buildings. Numerous studies highlight the importance of addressing balcony thermal bridges. To tackle this issue, researchers have explored various solutions, one notable approach being the introduction of thermal break elements within balcony structures.

The effectiveness of thermal breaks has been usually quantified through numerical simulations. However, the practical/real effectiveness of thermal break remains unsupported, primarily due to a lack of experimental investigations. This study aims to evaluate, experimentally and numerically, a conventional balcony slab (i.e. without thermal break), a balcony slab with a commercially available thermal break, and also three novel approaches such as using glass fiber-reinforced polymer (GFRP) rebars and partially replacing conventional concrete with an aerogel-concrete mixture to minimize the impacts of balcony thermal bridges. Thus, five balcony slabs (750 mm x 350 mm x 20 mm) were constructed and tested in the laboratory using a hot box apparatus and they were also numerically modelled using a 3-D simulation tool (HEAT3).

The results from the experimental and numerical investigations show similar trend. The experimental observations show the commercial thermal break can reduce the thermal transmittance values by 61.5% whereas the novel approaches can improve it further up to 67.65 % compared to the conventional balcony. Similarly, the numerical observations show corresponding thermal transmittance reductions are 62.36 % and 70.27 %.

3.2 Introduction

Reducing energy consumption in buildings has been a key concern for building researchers and property owners, driven by the need to mitigate the negative environmental impacts of greenhouse gas/carbon emissions, and higher energy bills. According to the Global Alliance for Buildings and Construction (GlobalABC) [97], buildings are responsible for consuming 35% of total energy, with residential buildings sector alone accounting for 22%. Moreover, buildings and construction industry are responsible for emitting 38% of the global CO2 emissions. In Canada and the United States, the buildings sector consumes 33% and 40% of total energy, respectively [2], [3]. In fact, the total energy consumption of the buildings and construction sector has increased by 7% from 2010 to 2019 [98]. Therefore, constructing highly efficient buildings has become essential step toward sustainable future.

Naturally, heat flows from hot to cold spaces and the rate of heat transfer increases as the temperature difference between the spaces increases. In cold climates, the demand for energy during the heating season is high due to the significant temperature difference between indoor and outdoor environments. In fact, 63% of the energy consumed in Canadian homes is used for space heating [5]. Therefore, well-insulated building envelopes are required to reduce heat loss. Various insulation materials act as thermal barriers and are commonly used in building construction. Thermal barrier continuity is crucial for achieving high thermal performance. However, discontinuity of thermal

barriers is unavoidable in some parts of buildings due to penetrations of structural elements with higher thermal conductivity relative to insulation materials. When those highly conductive elements pierce through the thermal insulation layer, they create direct thermal pathways between the interior and exterior environments, referred to as thermal bridges or thermal bridging.

Thermal bridges negatively impact building thermal efficiency by increasing thermal loss and creating cold regions along interior surfaces of building envelopes, which may lead to condensation and mold growth. Neglecting thermal bridging can reduce the thermal efficiency of well-insulated building assemblies. Thermal bridging consequences worsen as other building envelope components become more insulated [99], [100]. Building envelopes commonly suffer from thermal bridging due to changes in building geometry, such as extended balcony boards, slab edges, and interfaces between building assemblies. The balcony thermal bridge is accounted as the most challenging type due to the large cross-sectional area of the building envelope and high-conductive components of the balcony slab. Addressing thermal bridging is crucial for energy code compliance and achieving high thermal performance while maintaining comfortable indoor spaces. Balconies are desirable features in multistory residential buildings, so it is essential to mitigate the impact of balcony thermal bridges. In the last decades, thermal bridging issue have become a global concern where numerous research studies have been conducted to characterize their impact on buildings.

3.2.1 Literature review

As discussed above, the thermal bridging is a critical consideration in thermal analysis. The importance of considering thermal bridging problem in thermal investigation were emphasized in different studies. Theodosiou and Papadopoulo [101] utilized computational methods to highlight the significant impact of thermal bridging exclusion

on thermal loss and heating requirements. They concluded that disregarding thermal bridges could result an underestimation of up to 35% in thermal loss and 30% in heating requirements. Kosny et al. [102] conducted a numerical investigation on the impact of thermal bridges on building thermal performance, and their findings showed that thermal bridges within the building envelope could reduce the total thermal resistance of the envelope by up to 40%. The significance and consequences of thermal bridging by balconies have also been highlighted. Finch et al. [103] conducted numerical simulations and concluded that extended concrete boards, such as balconies and slab edges, are the second source of thermal loss in high-rise buildings after windows and external doors. Additionally, it has been numerically reported by Theodosiou et al. [104] that extended balcony concrete boards could have a substantial effect of more than 30% on the total heat transfer through the building envelope. Ge et al. [105] also conducted numerical investigations and found that balconies with cross-sectional areas equal to 4% of the total exterior wall could increase heating loads by up to 11%, depending on the thermal efficiency of the other envelope components.

After examining the adverse effects of thermal bridging, particularly the balcony thermal bridge, researchers have turned the attention to assessing the efficacy of existing solutions. The primary approach of these solutions centers on minimizing the discontinuity of the insulation layers in the building envelope. To date, the most successful solution for thermal bridging involves creating a gap between the ceiling and balcony slabs and filling it with materials that have low thermal conductivity. An innovative solution called thermal break was developed. The novel product is consisting of low thermal insulation materials to mitigate heat loss, and steel rebars with low thermal conductivity to deal with tensile, shear, and compressive forces. Researchers have investigated the commercially available thermal break product [106], which consists of a rigid insulation material and stainless steel rebars. In comparison to the traditional

balcony slab (non-thermally broken), the thermal break causes a rise of up to 4.5 °C in the interior wall-ceiling corner temperature. Furthermore, according to a numerical study [107], the thermal break results in a reduction of 7% to 8% in space heating energy demand.

The numerical study by Ge et al. [105] found that the implementation of the commercially available thermal break can cause a temperature rise of up to 6.4 °C in the interior wall-ceiling corner and a 13% decrease in annual heating energy consumption, depending on the wall-assembly configuration. An experimental and numerical investigation of partially replacing the stainless-steel rebars in a fabricated thermal break with glass fiber-reinforced polymer (GFRP) elements was also conducted by Ghazi Wakili et al. [108]. The reinforcement section of the fabricated thermal break was made from GFRP to address compression forces and stainless-steel bars to address tensile and shear forces. The results of the study showed that the fabricated thermal break caused a temperature rise of up to 4 °C in the interior wall-ceiling corner and a decrease of around 60% in the linear thermal transmittance compared to the conventional balcony.

The full use of fiber-reinforced polymer elements of unique shapes to build a special thermal break product was investigated numerically by Goulouti et al. [109], [110]. The innovative thermal break was built inside a PVC box filled with aerogel materials. Glass fiber-reinforced polymer bars attached to a hexagonal foam sandwich were installed to address both compressive and shear stresses. In addition, loops made of aramid fiber-reinforced polymer were designed to address tensile forces. The study concluded that thermal losses could be reduced by 41%, in the case of an ideal building envelope with the lowest energy consumption, and extremely low values of linear thermal transmittance could be achieved.

Most of the previous studies on the thermal impacts of balcony thermal bridges and their practical solutions have primarily been conducted using mathematical models with various finite element software. Additionally, simplified methodologies such as ISO 10211 [111] have been used to estimate the impact of linear thermal bridges, which is acceptable for standard design processes but it has been suggested for further improvement [13], [112], [113]. However, the lack of experimental analyses may result in an unrealistic estimation of the actual performance. Despite numerous research efforts to evaluate the effectiveness of commercially available thermal breaks using simulation-based approaches, no experimental study has been reported in the literature that clearly investigate the performance of this product. Therefore, the actual performance of the product remains to be investigated experimentally.

3.3 Aim of the work

This study aims to address the lack of experimental work and establish correlations between numerical and experimental analyses. It focuses on two main objectives: (1) investigating the impact of implementing a commercially available thermal break, and (2) evaluating the effectiveness of new approaches to further reduce the heat loss through thermal bridges in balcony structures. By combining numerical simulations and experimental testing, the study aims to provide critical insights for improving energy efficiency and sustainability in building design, particularly concerning balcony thermal bridging.

3.4 Materials and Methodologies

In this research, various concrete board specimens, which representing balcony boards, were analyzed through experimental and numerical methods. Also, a uniform panel made of extruded polystyrene and plywood boards was tested. Table 3.1 summarized the cases analyzed in this research. Firstly, the thermal characteristics of an extended

conventional balcony were evaluated as a worst-case scenario in respect to thermal performance. Secondly, the effectiveness of the commercially available thermal break product was evaluated as a benchmark solution for the balcony thermal bridge issue. Finally, novel concepts were explored for further energy enhancements. Throughout the research, five different balcony boards were built and investigated experimentally under different conditions. Additionally, detailed modules representing the balcony boards were replicated and simulated using HEAT3 software. The dimensions and components of all evaluated specimens are presented in the following subsection.

Table 3.1. Summary of the analyzed cases.

Case	Schematic	Description and purpose
1. Uniform panel.	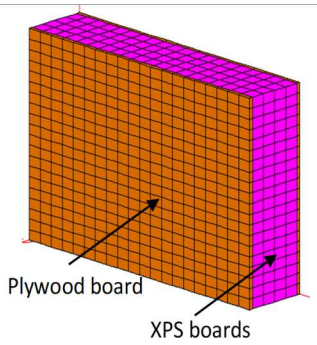	An assembly consisting of two XPS boards sandwiched between two plywood boards. This specimen was employed to estimate the heat losses associated with hot box testing, such as flanking loss and metering wall loss.
2. Conventional slab.	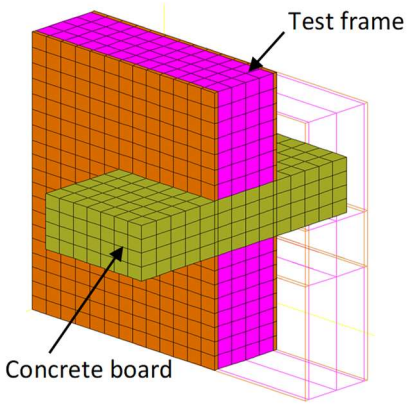	The investigation into the impact of balcony thermal bridging began with the analysis of a concrete board, which serves as a representation of a typical balcony construction. This board was placed within a test frame panel, identical to the uniform panel configuration described above. This arrangement exemplifies the most challenging scenario in terms of the significant impact of balcony thermal bridging.

3. Thermally interrupted slab by commercially available thermal break.	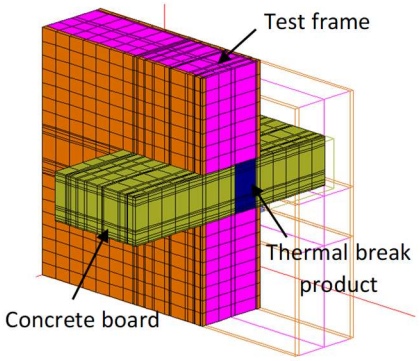	The study incorporated the utilization of a commercially available thermal break product, acknowledged as one of the most effective solutions to date for addressing the balcony thermal bridges. This specific case served as a benchmark to measure the efficacy of the innovative techniques introduced in this study.
4. Thermally interrupted slab with enhanced thermal break of GFRP rebars.	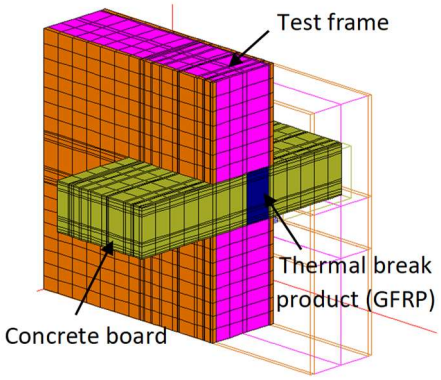	The reinforcement section of the commercially available thermal break consists of stainless steel rebars, which exhibit high thermal conductivity. We studied the potential enhancements in thermal efficiency attainable through the substitution of these rebars with Glass Fiber Reinforced Polymer (GFRP) rebars, known for their comparably diminished thermal conductivity properties.
5. Partial replacement of standard concrete with aerogel-concrete on one side of the slab (warm side).	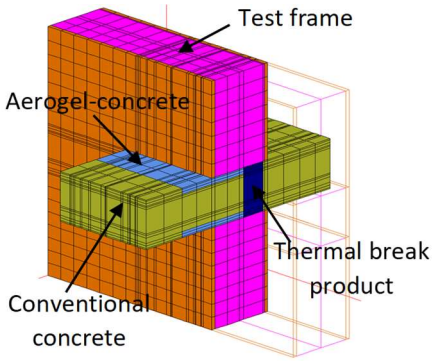	The exploration of potential enhancements in the thermal performance of the building envelope entailed a proposal to partially substitute the traditional concrete with an innovative composite known as "aerogel-concrete." This unique mixture has reduced thermal conductivity compared to conventional concrete. To initiate this approach, we initially applied the technique to the warmer side of the concrete board.

6. Partial replacement of standard concrete with aerogel-concrete on both sides of the slab.	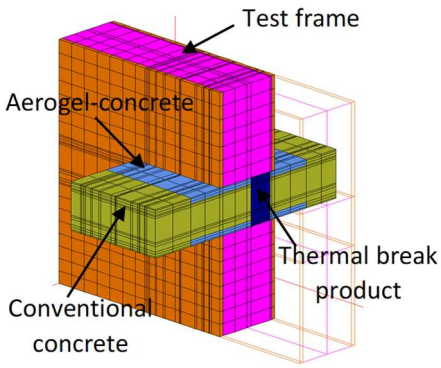	The same composite blend utilized in the previous scenario was employed to assess the further enhancements in thermal performance achievable through the partial replacement of conventional concrete on both faces of the concrete board.

3.4.1 Description of the tested specimens

I. Uniform panel: A 100 cm x 100 cm assembly consisting of two 101.6 mm extruded polystyrene insulation (XPS) boards bonded together. Two 12.7 mm plywood sheets were added to the outer surfaces of the XPS panels to provide support for the heavy specimens since panel with an aperture was used for concrete boards testing (see Figure 3.1). Initially, the uniform panel was utilized to estimate the extraneous heat loss associated with hot box examinations, which will be addressed later.

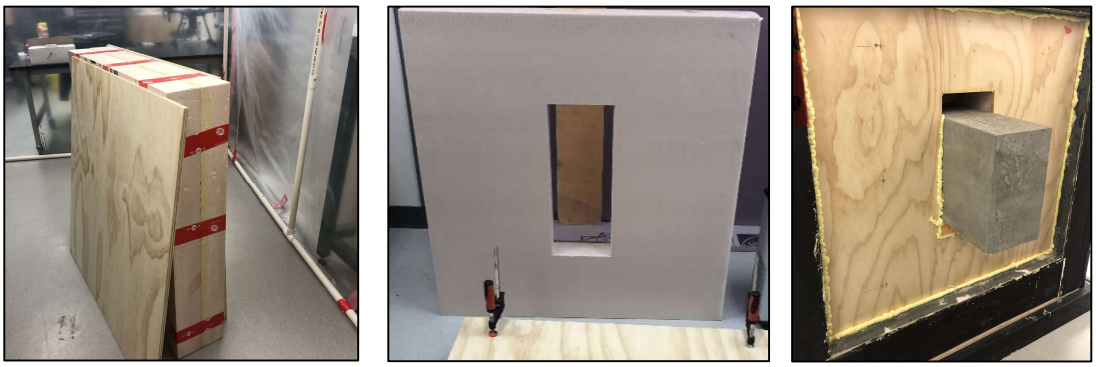

(a) (b) (c)

Figure 3.1. (a) Uniform panel; (b) Uniform panel with an aperture; (c) Uniform panel in use to support the concrete board prior testing.

II. Conventional slab: A concrete board, measuring 75 cm x 35 cm x 20 cm high, was poured in the laboratory to mimic a standard residential balcony slab as shown in Figure 3.2. The dimensions of the board were selected based on two key factors:

Promoting optimal air circulation within the hot box and facilitating easy handling by two people for installation/removal for testing. All concrete boards utilized in the study were made from C35/M35 concrete grade.

Figure 3.2. Conventional slab.

III. Thermally interrupted slab: A concrete slab was cast with dimensions, components, and steel bar sizes identical to subsection II. An 80 mm thick thermal break product was integrated into the slab, placed around 40 cm and 27 cm away from the end, extending into the hot and cold chambers as shown in Figure 3.3. This interruption prevents the concrete and main steel bars from continuing from the hot side to the cold side. The thermal break consists of polystyrene rigid foam, stainless steel rebars, steel fiber reinforced ultra-high performance concrete elements to deal with compression forces, and fire resistance plates. The commercially available thermal break products are varying in thickness, stainless-steel bar specifications, and are used for various applications.

(a) (b)

Figure 3.3. Thermally interrupted slab: (a) Prior to the pouring of concrete; (b) Tested specimen.

IV. Thermally interrupted slab with glass fiber reinforcement: In contrast to subsection III, in this scenario, the stainless-steel rebars of the commercially available thermal break was replaced with glass fiber reinforced polymer (GFRP) rebars as presented in Figure 3.4. The GFRPs offer advantages such as low thermal conductivity, high tensile strength, lightweight, and corrosion resistance. However, they have a lower modulus of elasticity compared to steel [114]. Studies by Ghazi et al. [108] and Goulouti et al. [109], [110] has explored the thermal effects of incorporating lower thermal conductivity elements and replacing stainless steel rebars, respectively. In this study, the hypothetical scenario involves replacing all tensile and shear stainless steel rebars of the commercially available thermal break with sand-coated GFRP rebars was proposed. This scenario allows evaluating the impact of complete replacement of stainless steel by GFRP on heat flow through the balcony slabs.

(a) (b)

Figure 3.4. Thermally interrupted slab with glass fiber reinforcement: (a) Upgraded thermal break; (b) The setup prior to the pouring of concrete.

V. Thermally interrupted slab with aerogel-concrete at warm surfaces: The proposed modification involves replacing a portion of concrete at the surface near the thermal break with low thermal conductivity concrete mixture (aerogel-concrete) [115]–[120]. We use a novel mixture called "high-performance aerogel concrete (HPAC)" with 47 vol.% aerogel granules that introduced in 2015 by Fickler et al. [117] and later in 2018 by Welsch and Schnellenbach-Held [120]. This mixture has low thermal conductivity and relatively high compressive strength in comparison with the aerogel concrete mixtures presented in other studies (see Table 3.2). Two layers of this concrete blend, each 2.5 cm thick and 25 cm long, replace the conventional concrete at the top and bottom surfaces near the thermal break from the hot side (interior), as shown in Figure 3.5. The optimal dimensions of these layers are determined through a parametric study that is discussed later.

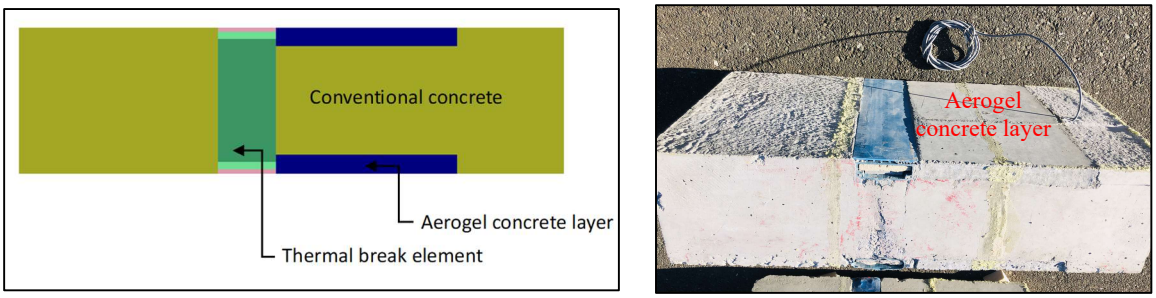

(a) (b)

Figure 3.5. Thermally interrupted slab with aerogel-concrete layers at warm surfaces: (a) Schematic; (b) Casted specimen.

Table 3.2. Properties of conventional concrete and aerogel-concrete.

Property	**Normal-weight concrete [40]**	**Aerogel-concrete with various aerogel volumetric percentage [120]**	
		47 vol.%	70 vol.%
Dry bulk density (kg/m3)	2000 - 2600	1340	690.4
Compression strength (MPa)	57.7	25	4.79
Thermal conductivity (W/(m K))	1.65 – 2.0	0.26	0.137

VI. Thermally interrupted slab with aerogel-concrete at both surfaces (warm and cold):

In addition to the setup described in V, this configuration includes 25 cm thick and 15 cm long aerogel-concrete layers on the cold surfaces of the concrete slab, as represented in Figure 3.6. The length of these layers is determined by the size of the tested concrete board in the cold chamber, ensuring partial replacement of conventional concrete rather than the entire replacement.

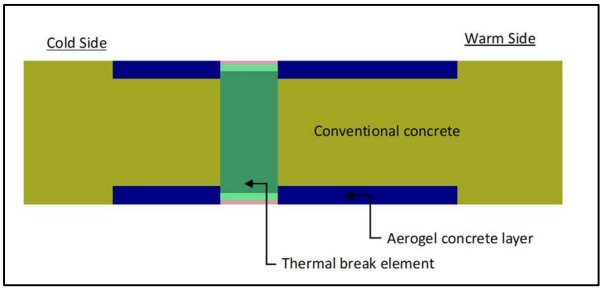

Figure 3.6. Thermally interrupted slab with aerogel-concrete at both surfaces

3.4.2 Numerical simulation

The numerical analysis was performed using a three-dimensional heat transfer simulation program based on a finite element method, HEAT3, developed by BLOCON and the Department of Building Physics, Lund University. The software was validated per EN ISO 10211:2007 standard [121]. The computation in HEAT3 is built based on the multi-dimensional partial differential heat conduction equation or Laplace Equation ((3.1). In the case of steady-state calculation, the left-hand side of equation (3.1) is equal to zero. Also, the internal heat generation is often zero. Thus, the change in the temperature is approximated by values at distinct points depending on the computational mesh.

$$\rho\, C_p\, \frac{\partial T}{\partial t} = k\left(\frac{\partial^2 T}{\partial x^2} + \frac{\partial^2 T}{\partial y^2} + \frac{\partial^2 T}{\partial z^2}\right) + I \qquad (3.1)$$

In the current research, detailed models identical to specimens investigated experimentally were simulated under steady-state conditions. The purpose of the numerical analysis was to examine the consistency in results obtained experimentally and numerically and to calculate the percentages of difference between the two methodologies. Table 3.3 presents the thermal properties of materials incorporated in the structure of the metered samples that are assumed for numerical calculations.

Table 3.3. Properties of incorporated materials

Material	**Thermal conductivity (W/(m K))**
Reinforced concrete	2.20
Extruded polystyrene insulation	0.028
Plywood	0.125
Polystyrene hard foam (Neopor®) [122]	0.031
Stainless steel rebars	25

High strength, fiber-reinforced concrete [122]	0.83
High-density polyethylene	0.52
High temperature insulation board [123]	0.20
GFRP [108]	0.40
Aerogel concrete [117]	0.26

For numerical analysis, following assumptions were adopted:

- The interior (hot) and exterior (cold) surface film resistance values are equal to 0.13 (m^2 K)/W and 0.04 (m^2 K)/W, respectively, which comply with the ranges presented in both ASHRAE Handbook and ISO 6946 standards.
- The thermal properties of the incorporated material are assumed constant regardless of temperature changes.
- All layers are assumed tight to adjacent interfaces, so contact resistances between the layers are negligible.
- The impacts of air leakage within the assembly and solar heating are neglected.
- The reinforced concrete slab is assumed to be homogeneous with a uniform thermal conductivity, whereas the reinforcement rebars are considered implicitly in the slab.
- The commercially available thermal break structural components are represented and modeled explicitly. Moreover, the structural details with circular shapes are denoted by elements with square/rectangular shapes while maintaining the same cross-sectional area due to the software limitations.
- The edges of the concrete slab inside the hot chamber were treated as adiabatic surfaces due to the continuous span of the interior floor slab. In the experiments, these surfaces were covered with thick pieces of extruded polystyrene insulation as shown in Figure 3.7.

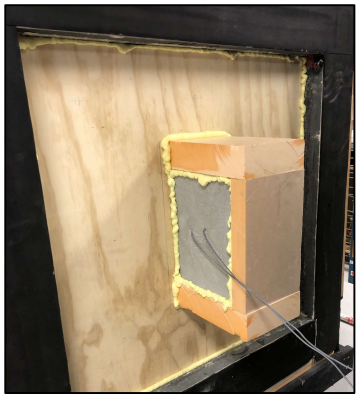

Figure 3.7. The warm side of the tested concrete board

3.4.3 Parametric study

A parametric study was completed to investigate the impact the aerogel-concrete layers' dimensions on the heat flow through the extended concrete slab. The aerogel-concrete layers partially replaced the conventional concrete on the top and bottom surfaces of the interior slab as shown above (Figure 3.5). In the study, the layers' thickness varies between 7 mm to 25 mm, and length varies between 50 mm to 500 mm with 50 mm increments. The study was accomplished by simulating forty combinations (Table 3.4) using HEAT3 software and adopting the same assumptions listed above. The interior and exterior ambiance temperatures are +22 ^{o}C and -10 ^{o}C, respectively. The percentages of improvement are computed relative to the case of implementation of the commercially available thermal break only without any replacement of conventional concrete with aerogel concrete. Overall, the study aimed to analyze how varying the dimensions of the aerogel-concrete layers affects the heat flow through the extended concrete slab, providing insights into the thermal performance of different layer configurations.

Table 3.4. Percentages of reduction in heat flow rate via concrete slab in respect to warm side.

Layer length	Aerogel-concrete layer thickness			
	7 mm (1/4″)	13 mm (1/2″)	19 mm (3/4″)	25 mm (1″)
50 mm	3.82 %	5.07 %	6.38 %	7.30 %
100 mm	4.23 %	5.80 %	7.52 %	8.89 %
150 mm	4.81 %	6.79 %	8.84 %	10.54 %
200 mm	5.24 %	7.50 %	9.80 %	11.70 %
250 mm	5.47 %	7.93 %	10.39 %	12.44 %
300 mm	5.62 %	8.18 %	10.74 %	12.92 %
350 mm	5.70 %	8.33 %	10.97 %	13.20 %
400 mm	5.75 %	8.41 %	11.10 %	13.35 %
450 mm	5.77 %	8.49 %	11.17 %	13.45 %
500 mm	5.80 %	8.51 %	11.22 %	13.53 %

From the data presented in the table above, increasing the thickness and length of the aerogel-concrete layers reduces heat flow through the slab. However, it comes to a point where further changes have minimal impact. For example, when the layers' length increases from 400 mm to 500 mm, the heat flow is only reduced by 0.18 % with layer thickness equal to 25 mm. Moreover, the heat flow diminished as the layers' thicknesses increased, though this study is limited to 25 mm since replacement of more concrete may lead to construction failure.

The study also examined the scenario where aerogel-concrete layers replaced part of the conventional concrete on the top and bottom surfaces of both the warm and cold sides (Figure 3.6). Two specific layer thicknesses (19 mm and 25 mm) mentioned in Table 3.4 were considered for installation on both sides, with varying lengths ranging from 50 mm to 500 mm.

The analysis revealed that implementing aerogel concrete on both sides resulted in a reduction in heat flow through the concrete slab. With a layer thickness of 25 mm, the

heat flow was reduced by approximately 3.6%, while a layer thickness of 19 mm achieved a reduction of around 3.0%. This suggests that using aerogel-concrete layers on both the warm and cold sides can provide effective insulation and contribute to decreasing heat transfer through the slab. The specific thickness of the layers influenced the degree of heat flow reduction, with the thicker 25 mm layer exhibiting slightly better performance compared to the 19 mm layer.

3.4.4 Laboratory work

The experimental analysis was carried out employing a calibrated hot box apparatus designed and calibrated in the Building Science Laboratory at The University of Victoria, BC, Canada [124].

3.4.5 Brief description of the test facility

The test setup used in the study consists of three main components: the metering/hot chamber, climate/cold chamber, and specimen frame. The walls of the apparatus are primarily made of vacuum insulation panels (VIPs) covered by extruded polystyrene boards. The utilization of VIPs provides excellent thermal resistance and ensures temperature stability within a narrow range of ±0.05 °C [124].

Several other components are incorporated in the apparatus. A ceramic heat bulb is employed to maintain the temperature inside the hot chamber, while a refrigerated circulation bath/chiller, connected to two heat exchangers mounted inside the room, provides lower temperatures in the cold chamber. Small fans are attached to the back surface of radiation baffles placed in each chamber to circulate the air and maintain uniform temperatures during measurements.

The power consumption of the heat bulb and fans in the hot chamber is monitored by a DC power supply regulator and assumed to be completely converted into heat. To

measure temperatures accurately, thermistors with a high accuracy of 1.0% tolerance are used to measure the temperatures of air curtains near the specimen surfaces, the laboratory space surrounding the apparatus, the surfaces of both the specimen panel and concrete slab, and the inside of the concrete boards.

Heat flux sensors are utilized to measure the heat flow when testing the uniform panel. The air velocities in the curtains are controlled within the ranges specified by the ASTM C1363-19 standard. This is achieved by measuring the air velocities with a hot wire anemometer and adjusting the fan speed in both chambers accordingly. To ensure proper air circulation around the concrete boards during testing, they are installed vertically inside the specimen board, as shown in Figure 3.8.

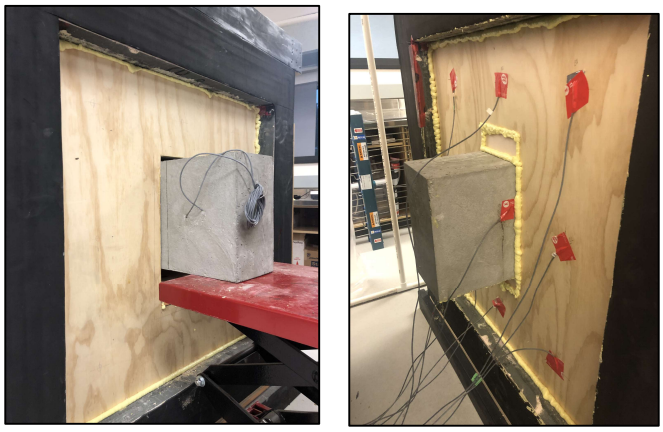

(a) (b)

Figure 3.8. (a) Placing the specimen into the chamber; (b) Specimen ready for testing.

3.4.5.1 Construction of samples

The concrete specimens were cast in the laboratory, starting with the conventional slab of 75 cm in length, 35 cm in width, and 20 cm in thickness. The materials used to construct the samples were Portland cement, sand, aggregate (20 mm size), and water. The ratio of cement: sand: aggregate: water was 1.0 : 1.5 : 2.6 : 0.43, following the IS 10262-2009 standard. The steel rebars were designed as per the CSA A23.3-04 standard. As main bars,

six (10M) steel rebars of 70 cm in length were distributed at a 150 mm distance and divided into two rows. As distribution bars, ten (10M) steel rebars of 30 cm in length were utilized.

Moving to the case of the thermally interrupted slab, the commercially available thermal break product was installed (Figure 3.9), which caused a discontinuity in the main steel bars throughout the concrete board. The utilized thermal break element has a thickness of 80 mm and stainless-steel rebars with a diameter of 8 mm and 6 mm for tensile and shear rebars, respectively.

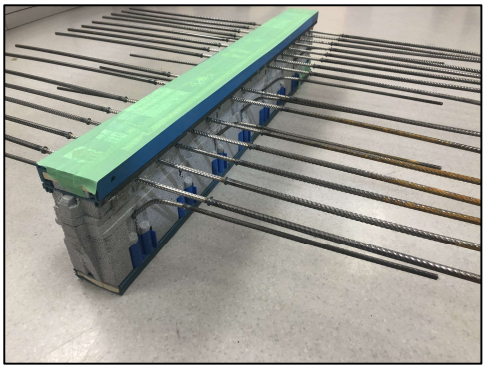

Figure 3.9. Thermal break product

In the case of GFRP reinforcement thermal break, the tensile and shear rebars of the incorporated thermal break are replaced with sand coated GFRP rebars instead. Six sand-coated GFRP rebars of 12 mm diameter were implemented (Figure 3.10), maintaining the same number and diameter of steel rebars used in the case of the conventional slab. The rest of the components of the thermal break remained the same.

Figure 3.10. GFRP rebars

Finally, for the aerogel-concrete approaches, the HAPC mixture was made based on the literature [120] by mixing the specified quantities of the following materials and chemical additives: Portland cement, silica aerogel granule, silica suspension, superplasticizer, organic stabilizer, and water (Figure 3.11).

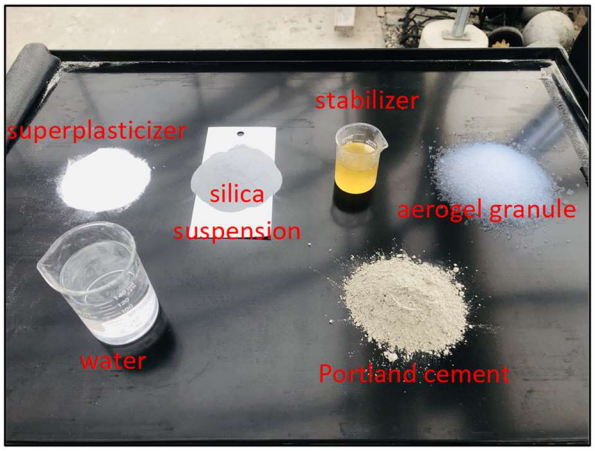

Figure 3.11. Aerogel-concrete ingredients

3.4.6 Estimation of extraordinary losses

3.4.6.1 Metering box wall loss (Q_{mw})

The amount of heat transferred between the metering (hot) chamber and the laboratory space (surrounding) is referred to as a metering wall box loss. This heat amount needs to be estimated and subtracted from the total heat supplied into the metering chamber. Four

experiments were performed in this regard by adjusting and maintaining same temperature in both hot and cold chambers, as presented in Table 3.5 and Figure 3.12. That means the heat flow through the specimen and around the specimen's edges are neglected, so any heat amount that is supplied into the metering chamber will go to the surrounding space. Throughout all experiments of this study, the temperature of the metering chamber was always higher than the surrounding temperature to ensure all heat transfers outwards of the chamber. A correlation between the metering box wall loss (Q_{mw}) and the difference in temperature between the metering chamber (T_h) and the surrounding (T_{surr}) was established (3.2).

$$Q_{mw} = 1.0872\ (T_h - T_{surr}) \tag{3.2}$$

Table 3.5. Measurements of estimation of metering box wall loss.

Supplied heat into metering chamber* $\boldsymbol{Q_{in}}$ (W)	**Chambers temp.** $\boldsymbol{T_h}$ (°C)	**Surrounding temp.** $\boldsymbol{T_{surr}}$ (°C)	**Temp. difference** $\boldsymbol{T_h - T_{surr}}$ (°C)
2.53	24.94	22.80	2.14
3.13	24.56	21.76	2.80
4.35	25.81	21.81	4.00
5.40	27.45	22.36	5.09

* The supplied heat amounts are equal to metering box wall loss since metering and climate chambers are maintained at the same temperature.

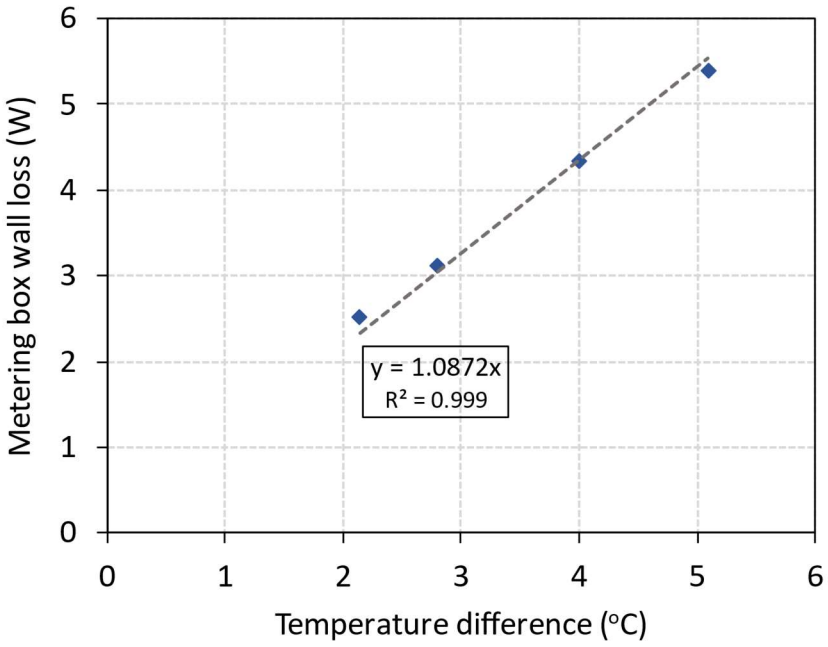

Figure 3.12. Correlation between metering box wall loss and temperature difference.

3.4.6.2 Flanking loss (Q_{fl})

Flanking loss is defined as the heat amount that transfers from the metering chamber to the climate chamber at the interaction of the metered specimen and the interior specimen frame wall. As demonstrated in the ASTM C1363 standard, this type of loss needs to be characterized by testing a homogeneous panel of uniform and predictable thermal properties. In this study, the uniform panel (described in I) was incorporated to predict the amount of flanking loss. A series of tests were performed under different temperature gradients to estimate the flanking loss. Since the metered specimen was constructed of uniform layers, two heat flux sensors positioned at the center of the specimen (one on each side) were used to measure the heat flux via the uniform panel (Q_{sp}). Then, the flanking loss (Q_{fl}) was determined by subtracting the heat flows through the uniform panel and metering box wall loss (Q_{mw}) from the total heat input to the metering chamber, including heat supplied by the heater (Q_h) and fans (Q_f), as in equation (3.3).

$$Q_{fl} = Q_h + Q_f - Q_{sp} - Q_{mw} \quad (3.3)$$

Table 3.6. Measurement data collected/calculated to estimate the flanking loss.

Test #	Energy Supplied Q_{in} (W)	Metering chamber temp. T_h (°C)	Climate chamber temp. T_c (°C)	Temp. of surrounding T_{surr} (°C)	Measured heat flux via sample* q_{sp} (W/m²)		Metering box heat loss Q_{mw} (W)	Flanking loss Q_{fl} (W)
					Exp.	Num.		
1	12.26	25.78	-20.46	23.42	5.78	6.09	2.57	3.91
2	10.50	24.40	-14.95	22.38	5.04	5.18	2.20	3.26
3	9.71	24.85	-9.95	22.98	4.54	4.58	2.03	3.14
4	9.11	24.88	-5.00	22.53	4.03	3.94	2.55	3.53
5	8.55	25.12	-0.06	22.35	3.47	3.32	3.01	2.07
6	7.25	25.32	4.59	22.95	2.77	2.73	2.58	1.90

* The amounts of heat flow via the uniform panel (Q_{sp}) are equal to the heat flux amounts since the panel has an area of 1.0 m².

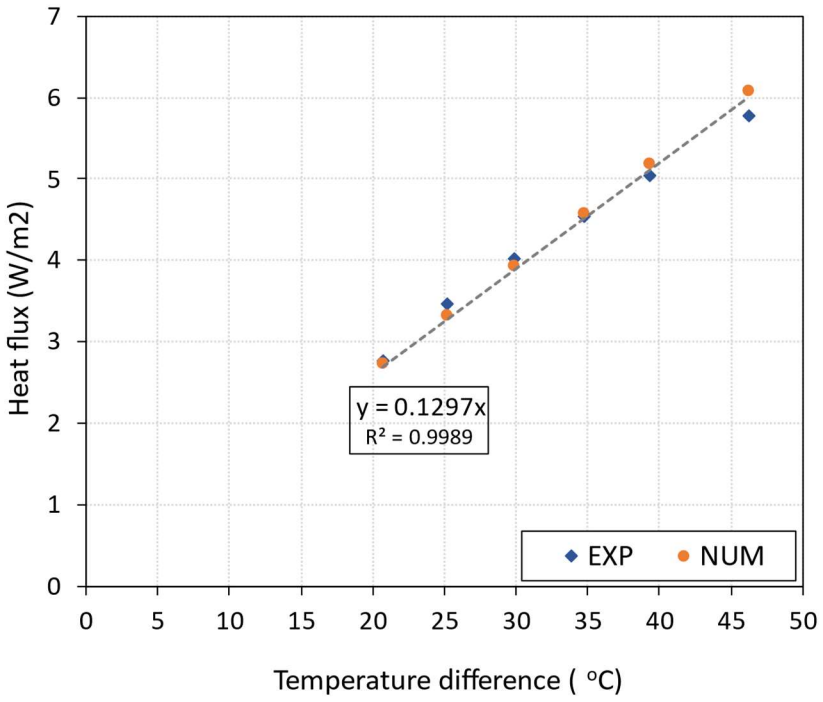

Figure 3.13. Relation between heat flux via uniform panel and temperature difference

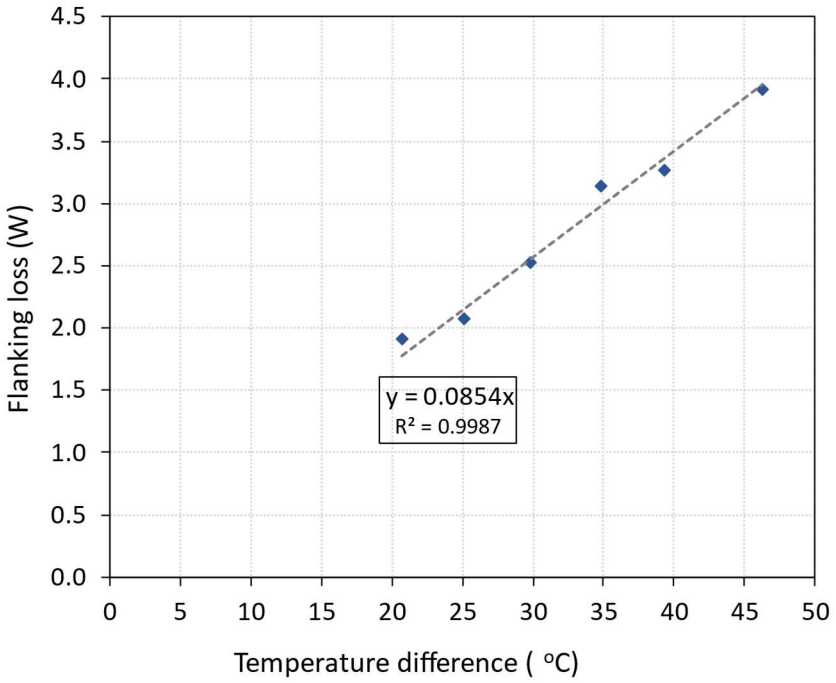

Figure 3.14. Relation between flanking loss and temperature difference

Based on these characterization measurements and data presented in Table 3.6, a correlation (equation (3.4) was established between flanking loss and temperature difference between the metering chamber (T_h) and the climate chamber (T_c). Additionally, the heat flux (q_{sp}) in (W/m^2) via the uniform panel was presented as a function of temperature difference based on the measured data (equation (3.5), as shown in Figure 3.14. These correlations will be employed to determine the flanking loss and the heat transfers via the specimen panel while testing the concrete board specimens. It can be noticed that intercept set to zero since the temperature difference is equal to zero, there will be no heat exchange between the chambers.

$$Q_{fl} = 0.0854 * (T_h - T_c) \quad (3.4)$$

$$q_{sp} = 0.1297 * (T_h - T_c) \quad (3.5)$$

3.4.7 Measured data.

The laboratory work to test all specimens continued for approximately ten months. Six test rounds were conducted under different temperatures for each previously defined case. The average temperature of the air spaces adjacent to both sides of the metered specimen (T_h, T_c) was measured using eight thermistors. Additionally, the average temperature of the surrounding ambient (T_{surr}) was monitored using six thermistors placed in the airspace adjacent to the apparatus. Thermistors were also employed to measure the temperature at various locations on the metered slab ($T_{hs1}, T_{hs2}, T_{in1}, T_{in2}, T_{cs}$), as shown in Figure 3.15. The collected data are presented in Table 3.7, Table 3.8, Table 3.9, Table 3.10, and Table 3.11.

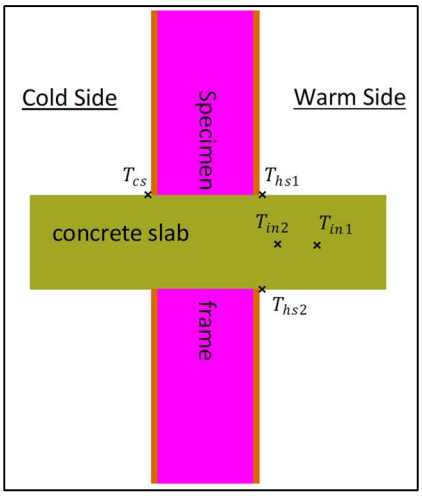

Figure 3.15. Locations of temperature sensors

Table 3.7. Collected measurements of conventional slab.

#	Q_{in} (W)	T_h (°C)	T_c (°C)	T_{diff} (°C)	T_{surr} (°C)	T_{hs1} (°C)	T_{hs2} (°C)	T_{in1} (°C)	T_{in2} (°C)	T_{cs} (°C)
1	25.98	24.38	-19.90	44.28	22.16	17.01	15.30	17.85	12.03	-15.07
2	21.93	23.31	-15.81	39.12	22.13	16.72	15.21	17.56	12.32	-11.53
3	18.78	22.63	-11.56	34.18	21.59	16.68	15.51	17.46	12.72	-7.87
4	18.78	24.20	-6.69	30.89	22.00	19.00	17.76	19.40	14.97	-3.59
5	16.26	24.47	-2.40	26.87	22.17	20.01	18.92	20.04	16.28	0.50

6	14.38	24.13	2.10	22.03	21.23	20.48	19.56	20.22	17.17	4.47

Table 3.8. Collected measurements of thermally interrupted slab.

#	Q_{in} (W)	T_h (°C)	T_c (°C)	T_{diff} (°C)	T_{surr} (°C)	T_{hs1} (°C)	T_{hs2} (°C)	T_{in1} (°C)	T_{in2} (°C)	T_{cs} (°C)
1	17.49	24.73	-20.45	45.18	22.13	21.68	21.78	20.26	16.70	-17.75
2	15.30	23.57	-16.16	39.72	21.23	20.87	20.96	20.53	16.74	-13.86
3	14.38	24.28	-11.75	36.03	21.87	21.79	21.88	21.36	17.85	-9.69
4	13.31	24.37	-7.23	31.60	21.54	22.14	22.21	21.62	18.50	-5.42
5	12.12	24.80	-2.66	27.46	22.18	22.92	22.99	21.74	19.51	-1.00
6	10.46	24.88	1.97	22.91	22.24	23.32	23.37	22.26	20.28	3.42

Table 3.9. Collected measurements of thermally interrupted slab with GFRP reinforcement.

#	Q_{in} (W)	T_h (°C)	T_c (°C)	T_{diff} (°C)	T_{surr} (°C)	T_{hs1} (°C)	T_{hs2} (°C)	T_{in1} (°C)	T_{in2} (°C)	T_{cs} (°C)
1	18.3	24.90	-19.82	44.72	20.91	22.99	22.26	20.20	17.92	-17.51
2	17.26	24.90	-16.74	41.64	20.97	22.16	22.40	20.31	18.24	-14.65
3	15.09	24.84	-11.38	36.22	21.17	22.45	22.66	20.64	18.87	-9.48
4	12.9	24.85	-7.24	32.09	22.05	23.00	22.9	20.01	21.57	-5.68
5	13.31	24.67	-5.25	29.92	20.73	22.67	22.84	20.88	19.48	-3.72
6	12.12	25.04	-0.70	25.75	21.18	23.45	23.31	21.51	20.41	0.59

Table 3.10. Collected measurements of thermally interrupted slab with aerogel-concrete at interior surfaces.

#	Q_{in} (W)	T_h (°C)	T_c (°C)	T_{diff} (°C)	T_{surr} (°C)	T_{hs1} (°C)	T_{hs2} (°C)	T_{in1} (°C)	T_{in2}* (°C)	T_{cs} (°C)
1	17.49	25.42	-18.43	43.85	21.93	22.96	22.96	20.50	-	-15.59
2	15.09	24.22	-15.08	39.30	21.77	22.03	22.03	19.60	-	-12.70
3	14.38	24.22	-11.24	35.46	21.15	22.21	22.20	19.78	-	-9.09
4	13.31	24.37	-7.08	31.45	21.22	22.57	22.56	20.17	-	-5.19
5	12.12	24.59	-2.59	27.18	21.40	23.03	23.02	20.68	-	-0.99
6	10.46	24.81	1.99	22.82	21.69	23.51	23.50	21.22	-	3.33

*Damages thermistor

Table 3.11. Collected measurements of thermally interrupted slab with aerogel-concrete at the interior and exterior surfaces.

#	Q_{in} (W)	T_h (°C)	T_c (°C)	T_{diff} (°C)	T_{surr} (°C)	T_{hs1} (°C)	T_{hs2} (°C)	T_{in1} (°C)	T_{in2} (°C)	T_{cs} (°C)
1	18.06	24.60	-20.79	45.39	21.20	22.26	21.97	19.87	15.52	-18.75
2	17.49	24.51	-18.83	43.34	20.96	22.27	21.95	18.97	15.10	-16.90
3	14.18	24.35	-11.14	35.49	21.61	22.47	22.19	19.81	16.24	-9.46
4	13.12	24.54	-4.41	28.95	20.97	22.99	22.76	20.55	17.54	-3.11
5	12.30	24.56	-0.81	25.37	20.62	23.20	22.99	20.86	18.21	0.31
6	11.35	24.98	2.88	22.11	20.99	23.80	23.61	21.55	19.23	3.85

3.5 Results and discussion

3.5.1 Heat flow analyses

In this section of the study, we calculated the amount of heat transferred through the slab board (Q_{slab}) for each case. We used equations and measured data from the previous section to estimate the heat amounts. Additionally, we conducted simulations to obtain alternative estimates. To compare the results obtained through measurements and simulations. Then, we calculated the percentage difference between the two approaches. This step provides an assessment of the consistency between simulation results and measured data.

I. Case of conventional slab

Table 3.12. Thermal analysis for conventional slab.

Test #	T_{diff} (°C)	T_{mean} (°C)	**Experimental Analysis**					**Numerical Analysis**		**Diff.***
			Q_{in} (W)	Q_{mw} (W)	Q_{fl} (W)	Q_{sp} (W)	Q_{slab} (W)	Q_{sp} (W)	Q_{slab} (W)	|%|
1	44.28	2.24	25.98	2.42	3.78	5.34	14.44	5.42	14.27	1.23
2	39.12	3.75	21.93	1.27	3.34	4.72	12.60	4.79	12.60	0.06
3	34.18	5.54	18.78	1.13	2.92	4.12	10.61	4.19	11.02	3.74
4	30.89	8.75	18.78	2.39	2.64	3.73	10.03	3.79	9.95	0.73
5	26.87	11.04	16.26	2.50	2.29	3.24	8.22	3.29	8.66	5.18

6	22.03	13.12	14.38	3.16	1.88	2.67	6.67	2.70	7.10	6.24

* Absolute values of difference percentages between experimental and numerical concrete slab heat flow (Q_{slab}).

II. Case of thermally interrupted slab.

Table 3.13. Thermal analysis for thermally interrupted slab.

Test #	T_{diff} (°C)	T_{mean} (°C)	**Experimental Analysis**					**Numerical Analysis**		**Diff.***
			Q_{in} (W)	Q_{mw} (W)	Q_{fl} (W)	Q_{sp} (W)	Q_{slab} (W)	Q_{sp} (W)	Q_{slab} (W)	|%|
1	45.18	2.14	17.49	2.83	3.86	5.45	5.35	5.54	5.48	2.38
2	39.72	3.71	15.30	2.55	3.39	4.79	4.57	4.87	4.82	5.22
3	36.03	6.27	14.38	2.62	3.08	4.35	4.33	4.41	4.37	0.81
4	31.60	8.57	13.31	3.08	2.70	3.81	3.71	3.87	3.83	3.11
5	27.46	11.07	12.12	2.85	2.35	3.31	3.61	3.36	3.33	8.08
6	22.91	13.42	10.46	2.87	1.96	2.76	2.87	2.81	2.78	3.18

* Absolute values of difference percentages between experimental and numerical concrete slab heat flow (Q_{slab}).

III. Case of thermally interrupted slab with GFRP reinforcement.

Glass fiber reinforced polymer (GFRP) products are a type of composite material that combines glass fibers and a polymer matrix. The fibers and matrix are mechanically bonded together to create a product with enhanced properties. One of GFRP advantages is the low isotropic thermal conductivity compared to materials like steel. However, the longitudinal thermal conductivity of GFRP products can be higher. The thermal conductivity of GFRP products can vary depending on several factors, including the type of fiber, fiber orientation, fiber volume fraction, and the polymer used in the composite [125].

In the case of sand coated GFRP rebars, the literature does not provide a specific value for the thermal conductivity. Furthermore, the manufacturer of the products that was

used in this study does not provide this information either. As a result, we had to perform multiple simulations using different values for the thermal conductivity of the sand coated GFRP rebars to reach an acceptable range of difference between results obtained numerically and experimentally, which reached for other cases. Based on that, a value of 6.90 W/(m² K) was chosen to represent the thermal conductivity of the sand coated GFRP rebars, as presented in Table 3.14.

Table 3.14. Thermal analysis for thermally interrupted slab with GFRP.

Test #	T_{diff} (°C)	T_{mean} (°C)	Experimental Analysis					Numerical Analysis		Diff.* |%|
			Q_{in} (W)	Q_{mw} (W)	Q_{fl} (W)	Q_{sp} (W)	Q_{slab} (W)	Q_{sp} (W)	Q_{slab} (W)	
1	44.72	2.54	18.3	4.34	3.82	5.39	4.75	5.48	4.35	8.82
2	41.64	4.08	17.26	4.28	3.56	5.02	4.40	5.10	4.05	8.39
3	36.22	6.73	15.09	4.00	3.09	4.37	3.63	4.44	3.52	3.17
4	32.09	8.81	12.98	3.03	2.77	3.87	3.29	3.93	3.03	8.26
5	29.92	9.71	13.31	4.28	2.55	3.61	2.86	3.67	2.82	1.41
6	25.75	12.17	12.12	4.20	2.20	3.11	2.61	3.15	2.43	7.31

* Absolute values of difference percentages between experimental and numerical concrete slab heat flow (Q_{slab}).

IV. Case of thermally interrupted slab with aerogel-concrete at interior surfaces.

Table 3.15. Thermal analysis for interrupted slab with aerogel-concrete at interior surfaces.

Test #	T_{diff} (°C)	T_{mean} (°C)	Experimental Analysis					Numerical Analysis		Diff.* |%|
			Q_{in} (W)	Q_{mw} (W)	Q_{fl} (W)	Q_{sp} (W)	Q_{slab} (W)	Q_{sp} (W)	Q_{slab} (W)	
1	43.85	3.50	17.49	3.80	3.74	5.29	4.66	5.37	4.77	2.25
2	39.30	4.57	15.09	2.66	3.36	4.74	4.33	4.81	4.27	1.44
3	35.46	6.49	14.38	3.33	3.03	4.28	3.75	4.34	3.86	2.91
4	31.45	8.65	13.31	3.43	2.69	3.79	3.40	3.85	3.42	0.50
5	27.18	11.00	12.12	3.47	2.32	3.28	3.05	3.33	2.96	3.15
6	22.82	13.40	10.46	3.40	1.95	2.75	2.36	2.80	2.48	5.08

* Absolute values of difference percentages between experimental and numerical concrete slab heat flow (Q_{slab}).

V. Case of thermally interrupted slab with aerogel-concrete at the interior and exterior surfaces.

Table 3.16. Thermal analysis for thermally interrupted slab with aerogel-concrete at both surfaces.

Test #	$\boldsymbol{T_{diff}}$ (°C)	$\boldsymbol{T_{mean}}$ (°C)	**Experimental Analysis**					**Numerical Analysis**		**Diff.***
			$\boldsymbol{Q_{in}}$ (W)	$\boldsymbol{Q_{mw}}$ (W)	$\boldsymbol{Q_{fl}}$ (W)	$\boldsymbol{Q_{sp}}$ (W)	$\boldsymbol{Q_{slab}}$ (W)	$\boldsymbol{Q_{sp}}$ (W)	$\boldsymbol{Q_{slab}}$ (W)	|%|
1	45.39	1.91	18.06	3.70	3.88	5.48	5.01	5.56	4.74	5.51
2	43.34	2.84	17.49	3.86	3.70	5.23	4.70	5.32	4.52	3.93
3	35.49	6.61	14.18	2.98	3.03	4.28	3.88	4.35	3.71	4.69
4	28.95	10.07	13.12	3.88	2.47	3.49	3.27	3.55	3.02	7.85
5	25.37	11.87	12.30	4.28	2.17	3.06	2.79	3.11	2.65	5.35
6	22.11	13.93	11.35	4.34	1.89	2.67	2.46	2.71	2.31	6.23

* Absolute values of difference percentages between experimental and numerical concrete slab heat flow (Q_{slab}).

In summary, we have investigated the impact of thermal break product on reducing heat flow through a cantilever concrete slab. The commercially available thermal break effectively minimizes heat transfer and improves the building's thermal performance. When comparing the conventional balcony with the thermally broken one, we found that the heat flow reduction through the slab ranged between 57% to 64%. The percentage of reduction varied depending on the temperature difference between the apparatus' chambers, where higher temperature gradients led to greater reductions in heat flow, as shown in Figure 3.16.

Additionally, we explored other techniques to enhance the thermal performance of building envelope. One approach involved the replacement of the thermal break stainless steel rebars and adding aerogel-concrete layers to the surfaces of the concrete board. As

presented in Figure 3.17, more improvements, range between 9% to 17% were achieved in comparison to the thermally broken board using the commercially available thermal break. In the case of adding aerogel-concrete layers on both surfaces (warm and cold side), no thermal enhancement was observed in reference to the case of applying aerogel concrete on one side through the experimental analysis. The reasons behind that are the short span of the tested concrete boards, which made it challenging to add longer aerogel-concrete layers to the slabs effectively, and exposed edges, from where heat can easily flow.

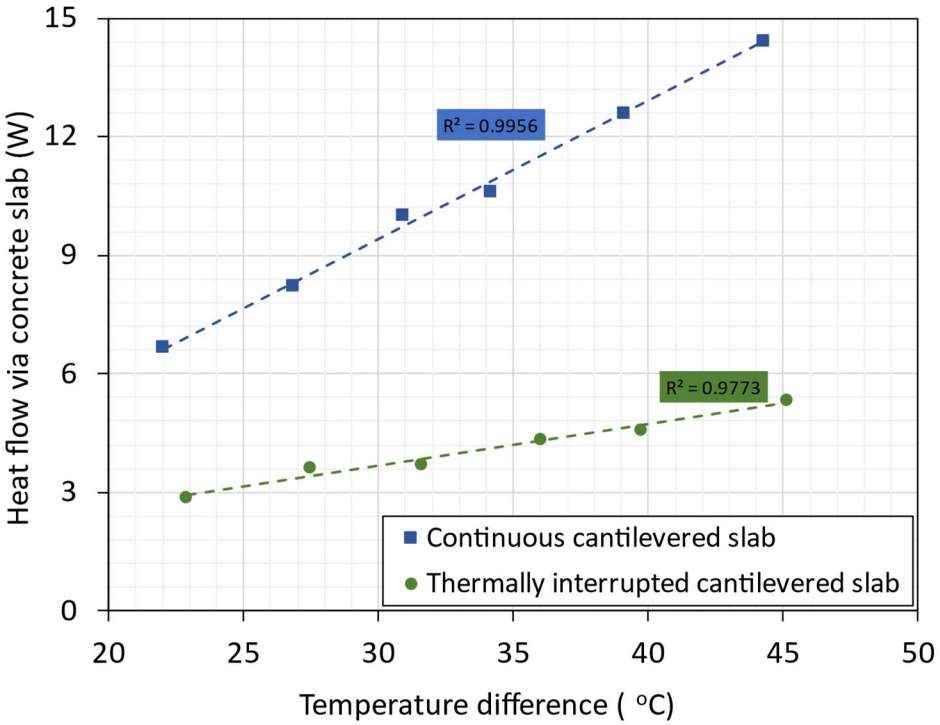

Figure 3.16. Heat flow rate in case benchmark cases

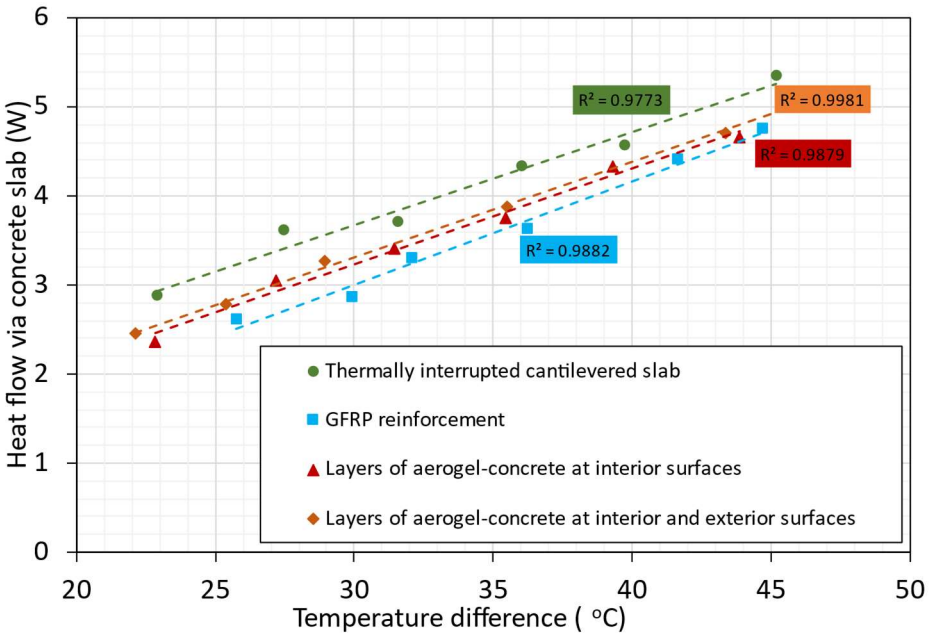

Figure 3.17. Heat flow rate for enhanced cases

The linear thermal transmittance (ψ) values of all studied cases were determined. These values are used as measures of enhanced thermal performance. For conventional slab, ψ is equal to 0.901 W/ (m K) and 0.921 W/(m K) based on experimental measurements and numerical analysis, respectively. For thermally interrupted balcony slab, implementing the commercially available thermal break, ψ is equal to 0.347 W/ m based on both experimental measurements and numerical analysis. For thermal interrupted slab with thermal break of GFRP rebars, ψ is equal to 0.921 W/ (m K) and 0.274 W/(m K) based on experimental measurements and numerical analysis, respectively. Finally, for thermal interrupted slab with aerogel-concrete layers, ψ is equal to 0.308 W/ (m K) and 0.311 W/(m K) based on experimental measurements and numerical analysis, respectively.

3.5.2 Temperature analysis

The experimental measurements also incorporated to examine the improvements in the interior surface temperature. To understand this further, relationships were established between the air temperature in the climate chamber (T_c) and the difference between the

air temperature in the metering chamber and the interior surface temperature of the slab ($T_h - T_{hs}$).

The primary objective of these analyses is to demonstrate how the studied approaches can reduce the potential for condensation on interior surfaces. Condensation becomes more likely when there is a significant difference between the interior temperature and the slab surface temperature, especially with high moisture content in indoor air. Therefore, reducing the temperature gradient between the interior space and the slab surfaces can effectively decrease the risk of condensation.

For instance, considering the scenario where the cold chamber temperature is set to -20°C. In the case of a conventional slab, the temperature difference ($T_h - T_{hs}$) is higher than 8°C (Figure 3.18), which indicates a higher risk of condensation. However, when the improvement approaches are applied, this temperature difference remains consistently below 3°C (Figure 3.19), demonstrating a substantially lower risk of condensation.

These results clearly show that the applied approaches have a positive impact on reducing the potential for condensation on interior surfaces. By minimizing the temperature difference between the interior space and the slab's interior surface, the risk of condensation-related issues, such as moisture buildup and mold growth, can be effectively mitigated. This contributes to a more comfortable and healthier indoor environment.

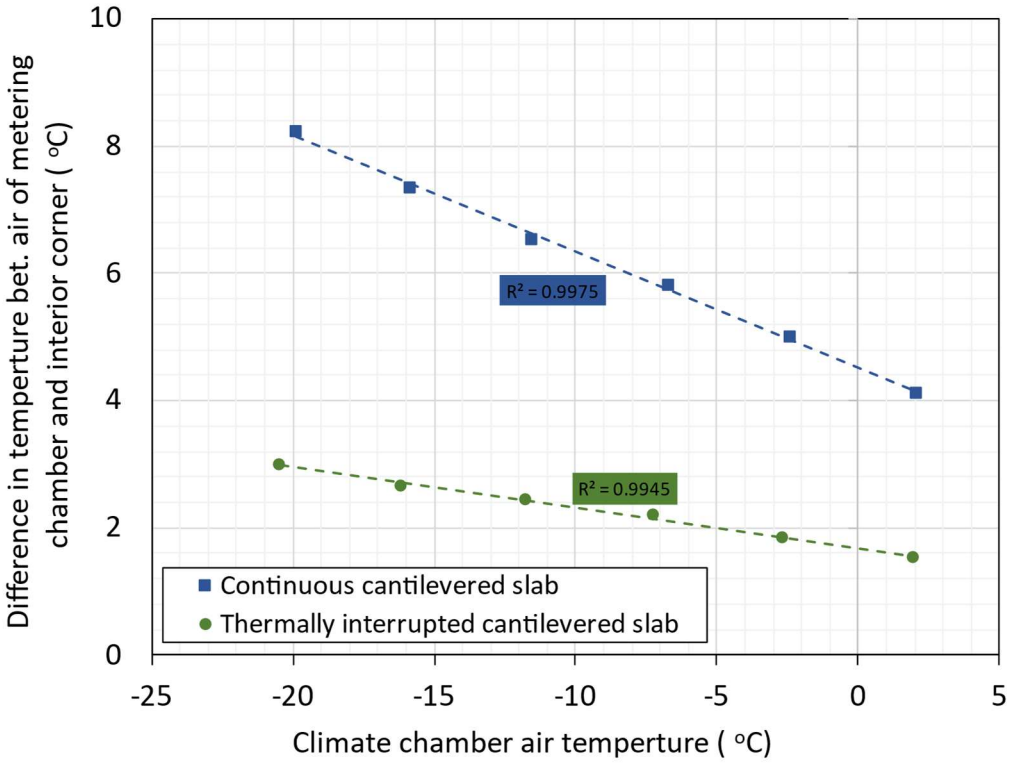

Figure 3.18. Temperature analysis for conventional and thermally interrupted slabs

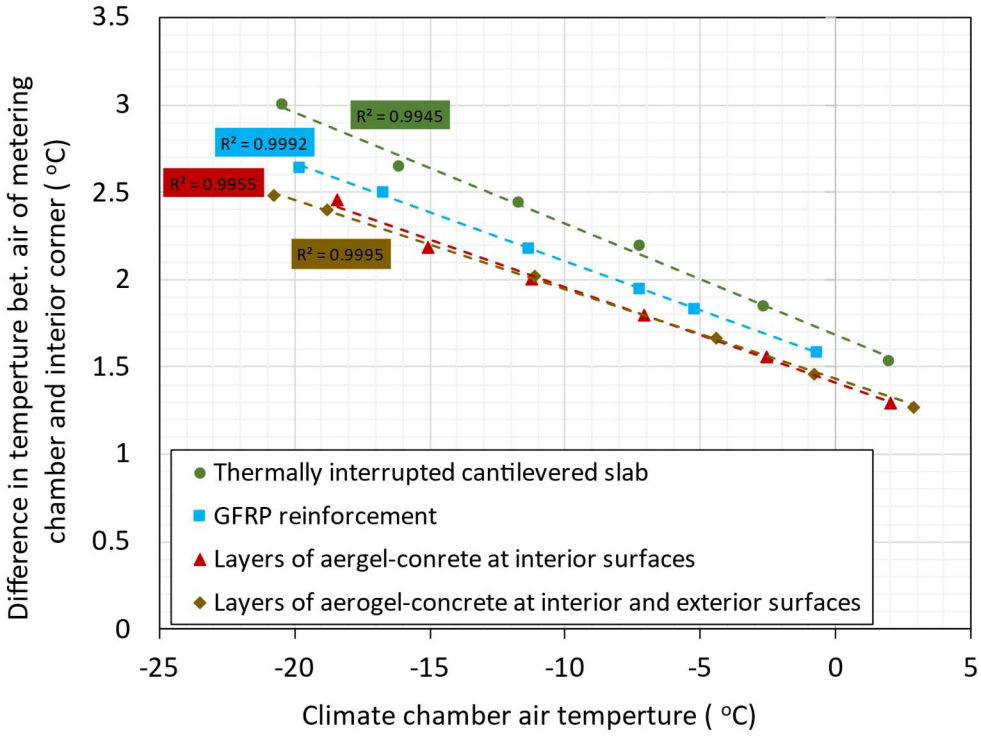

Figure 3.19. Temperature analysis for enhanced slabs

3.6 Conclusions

This study evaluated the thermal characteristics of a conventional balcony and explored various approaches to reduce the heat loss through the balcony slab. The combination of experimental measurements and numerical simulations demonstrated excellent consistency between the results obtained utilizing both methods, which validates the reliability of the simulation approach.

The investigations involved six different specimens, including a uniform panel, conventional slab, and four thermally interrupted slabs with different modifications. These configurations help assessing the effectiveness of a commercially available thermal break and two novel concepts, incorporating glass fiber reinforced polymer (GFRP) rebars and partial replacement of the conventional concrete by the aerogel concrete. The results demonstrated that the thermally interrupted slabs reduce heat loss and risk of condensation, leading to better indoor environment/comfort.

The findings indicated significant improvements toward reducing the heat loss through balcony thermal bridges. The improvements were presented by calculating the average value of linear thermal transmittance (ψ) for the cases presented in this study:

- The ψ value for the conventional balcony slab is 0.901 W/(m K) in experimental measurements and 0.921 W/(m K) in numerical analysis, which shows 2.17% difference between the two approaches.
- The use of commercially available thermal breaks significantly reduces the linear thermal transmittance, with a ψ value of 0.347 W/(m K) observed in both numerical and experimental results. When compared to the conventional balcony slab case, there is a reduction of 61.50% in the experimental analysis and 62.36% in the numerical analysis.

- The replacement of traditional concrete with aerogel concrete results in a decrease in the ψ value, bringing it down to 0.308 W/(m K) in experimental analyses and 0.311 W/(m K) in numerical analysis. In comparison to the conventional balcony slab case, these reductions represent 65.86% and 66.25% decrease in the experimental numerical analysis, respectively.
- The replacement of the stainless steel rebars of the thermal break with GFRP rebars leads to a further reduction in the ψ value, reducing it to 0.291 W/(m K) in experimental analyses and 0.274 W/(m K) in numerical analysis. When compared to the conventional balcony slab case, these reductions amount to 67.65% in the experimental analysis and 70.27% in the numerical analysis.

The study also examined the change in interior slab surface temperatures. With the introduction of thermal breaks in the balcony slab, there was a noticeable reduction in the temperature difference between the air inside the metering chamber and the interior surface of the slab. Initially, the temperature difference was above 8°C, but it decreased to below 3°C. This improvement underscores the effectiveness of thermal breaks in mitigating the risk of condensation on interior surfaces.

Overall, this research provides valuable insights into optimizing balcony board configurations for enhanced energy efficiency in building constructions. The consistency between experimental and numerical results adds confidence to the findings.

Chapter 4: Impact of Cladding Attachment Structural Elements on the Thermal Performance of Exterior Insulated Steel-Framed Walls

The content of this chapter has been submitted for review and subsequent publication:
A. Alhawari, V. Gretka, I. Lee, P. Roppel, P. Mukhopadhyaya."Influence of Cladding Attachment Structural Elements on the Thermal Performance of Lightweight Steel-Framed Walls."Journal of Building Engineering

4.1 Abstract

The thermal transmittance characteristics of the building envelope significantly influences the whole building energy performance. Lightweight steel framed (LSF) systems with cladding attached back to structures using thermal clips or bracket systems are widely used in heating dominated climates. Thermal bridging associated with the cladding structural elements that bypass the exterior insulation to attach the cladding cannot be avoided, but their impact can be significantly mitigated. This study investigates the thermal influence of a generic aluminum cladding attachment system that has varying levels of complexity associated with thermal breaks, and rail penetration into the insulation. A total of five configurations were assessed besides a reference configuration, which was devoid of any cladding attachment structure. Three-dimensional finite element software (HEAT3) and a small-scale calibrated hot box apparatus were employed to perform the analyses. The objectives were to show the influence of the cladding attachment elements and demonstrate the ability of hot-box measurements and numerical simulations to quantify the influence. Results show a small deviation between numerical simulations and experimental measurements, ranged between -0.85% and 3.70%. The variations in thermal transmittances properties of the investigated wall assemblies are presented, which vary from 40% to 57% compared to the reference case. These findings highlight the significant influence of the structural elements that bypass

exterior insulation and how small variations of the same system can impact the whole thermal performance.

4.2 Introduction

The energy demand is rapidly growing annually. Worldwide, about a 21% increase in energy consumption was reported between 2009 and 2019 [126]. Moreover, energy generation and consumption are primary sources of air pollution problems. Energy generation and consumption contribute about 75% of global greenhouse gas emissions [127]. Hence, many nations adopted various regulations and policies to minimize energy usage in every aspect of our economy and daily-life to diminish the associated negative impacts. The following discussion primarily concerns residential high-rises and their energy consumption focusing on the performance of building envelopes. In Europe, the building sector is a massive energy consumer of about 43% of energy demand [128]. Buildings are also responsible for 36% of carbon dioxide emissions [129], [130]. In Canada, about 63% of the energy used in residential buildings is for space heating [5]. Accordingly, it is crucial to have energy-efficient buildings with highly insulated and airtight buildings envelopes.

The building envelope is the separator between the interior space and the outdoor environment, which represents a significant exposed area to the outdoor conditions. Hence, the envelope design and structure play a critical part keeping the indoor spaces within a comfortable range for the occupants. In other words, making the exterior walls of buildings highly insulated will help conserve energy and mitigate the environmental pollution problems. Accordingly, it is crucial to have building envelope assemblies that are thermally efficient, airtight, and minimize material-use to meet the necessary thermal performance. Exterior insulated steel-framed composite wall assemblies with an air and

moisture barrier applied to the exterior sheathing is a proven and effective way to provide high levels of airtightness and thermal performance.

4.2.1 Lightweight Steel Framing (LSF)

In recent years, lightweight steel framing (LSF) structures have been used intensively in cold climates for several reasons. A LSF structure is composed of three main components (as shown in Figure 4.1): (i) steel frame, (ii) sheathing panels, and (iii) insulation layers. Given its mechanical strength and sustainability, a LSF structure offers additional advantages such as cost efficient use of materials, fire resistance, lightweight construction, easy prefabrication, high possibility to reuse, and high recycled content [131],[132]. Yet, LSF structures have some drawbacks. In climates with higher daily temperature fluctuations, LSF structures experience weakness due to the lack of thermal mass (thermal inertia), which leads to uncomfortable indoor environment [133]–[135]. In case of inappropriate thermal design, the LSF structures have a disadvantage because of the high thermal conductivity of its main structural component (i.e., steel frame). The steel studs create thermal bridges that can significantly reduce the thermal performance of the buildings if not adequately mitigated. In general, in addition to increasing the risk of condensation on the cold surfaces, thermal bridges can be responsible for up to a 30% increase in the energy consumption of buildings [136]. Therefore, the influence of thermal bridges on the performance of the LSF structure needs to be addressed accurately during the design stages.

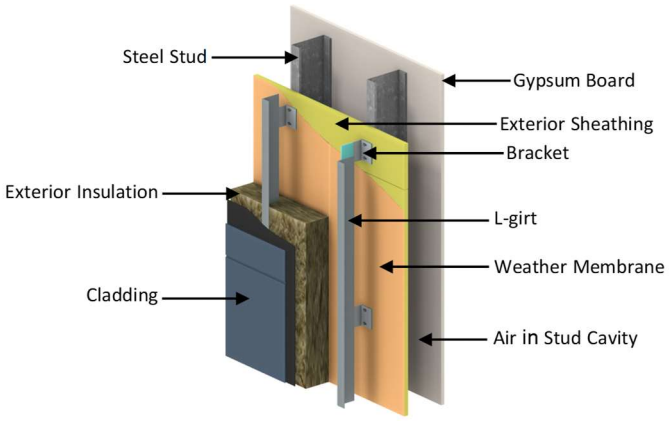

Figure 4.1. Exterior insulated steel-framed composite wall assembly. [137]

4.3 Research Background

Several studies were completed to assess and improve the thermal performance of steel-framed wall assemblies, with particular focus on quantifying the impacts of thermal bridging. A computational study by Kosny and Christian [21] indicated that the continuous layer of exterior thermal insulation reduces the impact of thermal bridging in the wall assembly. In addition, increasing the steel studs spacing was analyzed in the same study, where 15% to 20% improvement in the thermal resistance could be reached, depending on the thickness of the insulation layer. Martins et al. [138] adopted different approaches (i.e. using slotted steel studs, and inserting rubber strips between steel studs and OSB) to mitigate thermal bridging related to steel framing and concluded that the transmittance can be improved by about 8%. Other studies ([139], [140]) were conducted to evaluate the thermal performance of the LSF system when reducing the area of steel components. Nevertheless, the reduction in the steel structure's areas needs to be applied carefully concerning the mechanical strength of the construction.

Besides the steel structure, insulation materials impact the thermal performance of steel-framed walls. Some researchers have investigated insulation materials (aerogel blankets and vacuum insulation panels or VIPs) that have a lower conductivity than conventional

insulation to reduce overall wall thickness. However, these materials have several drawbacks, such as cost, constructability, and embodied carbon [138]. Kontogeorgos et al. [141] numerically investigated the impact of adding a VIP layer at the inner side of the exterior steel-framed walls of a two-story building. They concluded that the overall thermal resistance could be enhanced by about 33% when adding a VIP layer to the wall system. Also, the effect of the location of VIPs within the steel-framed wall was investigated numerically by Rajanayagam et al. [130]. Various wall configurations were modeled where authors claimed that walls containing VIPs of 20 mm thickness reduced the U-value by four times because of the high thermal resistivity of VIPs. A study by Theodosiou et al. [113] explores the impact of point thermal bridges in cladding systems used for energy-efficient building renovations. These bridges, caused by metallic frames and brackets penetrating insulation layers, are often underestimated. Their study uses a detailed numerical analysis and finds that these thermal bridges can constitute a significant portion of a building's heat loss, ranging from 5% to nearly 20% depending on specific factors. Neglecting these bridges can lead to inaccurate energy assessments, highlighting their importance in renovation projects.

Published literatures, reported above, highlight some of the impact of thermal bridging associated with steel-framing. However, this past work overlooked the impact of cladding attachment through exterior insulation that is necessary for attaching cladding back to the structure and is based on numerical analyses. Therefore, thermal performance evaluation of building components can be performed using both laboratory experiments and numerical simulations. The most common devices employed to measure the thermal performance of building envelope materials/systems in the laboratory are the guarded hot plate, the heat flow meter, and the hot box.

Typically, differences exist between experimental and numerical observations due to multiple factors such as assumptions during the modeling process and the geometric

complexity of the investigated component. These deviations between numerical and experimental results may range approximately from 1.0% to 5.0%, as reported for steel-framed wall assemblies by Rose and Svendsen [142]. In another study on steel-framed walls assemblies by Santos et al. [135], differences between the measured and numerically predicted values of thermal transmittances ranged from 1.0% to 14%.

ASHRAE 1365-RP compared numerical and simulated results for 24 steel-framed wall assemblies that was published by several sources [143]. The comparisons were mostly for steady-state conditions but there were also comparisons to transient profiles of heat flux from guarded hot-box measurements. The validation work highlighted the importance of accounting for the impact of the contact resistance between the steel-framing and exterior sheathing to accurately simulate steel-framed wall assemblies when there is insulation in the steel stud cavity. The simulated thermal resistances were on average lower by 1% than the measured thermal resistance for 24 steel framed wall assemblies and ranged between -3.2% and -6.1% when a consistent contact resistance was applied to all the evaluated wall assemblies.

The ASHARE 1365-RP comparisons between simulated and measured results also included some assemblies that had brick veneer and ties, which have some similarities to the cladding attachment system that are evaluated as part of this study. The same methodology and software that was used in ASHRAE 1365-RP was utilized for (BETB) guide [144]. The BETB Guide and Thermal Envelope web application includes results for more than 150 steel-framed wall assemblies with more than 20 proprietary cladding attachment systems that are commonly used in commercial construction in Canada and the USA.

4.4 Objectives and Scope

This paper aims to investigate the influence of thermal bridges created by the cladding attachments for an exterior insulated steel-framed wall assembly using experimental and numerical investigations. Scenarios are evaluated for varying levels of complexity of the structural connections to highlight the impact of each element, such as the impact of thermal breaks and rails that penetrate the exterior insulation.

The paper starts with descriptions of the materials and construction details of wall assemblies, followed by computational assumptions for numerical simulations and depiction of experimental setups. Finally, the results are presented and discussed to conclusions.

4.5 Construction of Test Specimens

An exterior insulated steel-framed wall assembly specimen (900 mm x 900 mm) with 4 inches (101 mm) of mineral wool insulation was constructed in the laboratory without any cladding attachment elements (Figure 1.2). This specimen was subsequently modified to represent different incremental changes to the cladding attachment system to assess the impact of each element that often part of a cladding attachment system. Based on the materials and components used for the wall construction are listed in Table 4.1. The thermal conductivity values for the materials listed in the table were either obtained from the manufacturer's provided data or estimated using default values from the HEAT3 software library.

Table 4.1. Materials and properties.

Material	Thickness [mm]	Thermal conductivity [W/(m K)]
Mineral wool insulation	101	0.036
Aluminum T-Bracket	-	160
Fiberglass mat-faced gypsum	13	0.10

Galvanized steel studs and L-Rails	152	60
Gypsum board	13	0.120
Neoprene	6*	0.193

* Thickness before applying the force.

As a backup wall, the specimen is constructed of two vertical steel studs (152 mm x 42 mm x 18 mm x 1.5 mm) spaced 400 mm apart (16" o.c.). The wall is finished at the interior side with gypsum wallboard (GWB), 13 mm thick, and its exterior side sheathing is a fiberglass mat gypsum board, 13 mm thick. Outward from the sheathing layer: there are two layers of mineral wool thermal insulation (50 mm thickness each). The drywall and sheathing boards are fastened to the steel studs by screws. The insulation layers are affixed to the sheathing board using five insulation fasteners. These fasteners are steel screws inside a high-density polyethylene sleeve. The specimens also contain brackets that penetrate the insulation layers. These brackets are employed to support the cladding by connecting them to the steel studs.

In this study, the cladding attachment bracket is made of aluminum grade 6061-T6 and is T-shaped with dimensions of 76.2 mm deep, 41.27 mm wide, and 6.35 mm thick. Each specimen contains four T-Brackets. Spacers made of neoprene were placed at the interface areas between the T-shaped brackets and sheathing board as thermal breaks. Initial thicknesses of neoprene spacers were 6.0 mm. However, the applied compression force on the T-Brackets causes their thickness to diminish to about a half, which is the thickness adopted in numerical simulations in this study. The cladding always stands outboard of the insulation layer. The cladding and structural elements outboard of the insulation in the rainscreen cavity were excluded from the analysis in this study because of the minimal impact and to focus on the differences between the evaluated scenarios. Figure 4.2 illustrates a schematic diagram of the exterior insulated wall assembly specimen, which was included in the study as a reference case with no cladding attachments.

It is to be noted that the wall systems investigated in this study represent a particular section of the building envelope referred to as a clear wall assembly. The clear wall assembly includes thermal bridging for uniform repeating structural elements such as framing and cladding attachment brackets and does not include thermal bridging at interfaces to other building envelope components, such as the window-to-wall interface, intermediate floor, or roof-to-wall interface. To be consistent with this methodology, the impact of the top and bottom stud tracks was not included because this is included in linear transmittance values.

Membranes and coatings for the moisture and vapor barriers were not included in the tested assemblies because of their negligible impacts on the overall thermal resistance of the wall assembly and desire to focus on the impact of the cladding attachment.

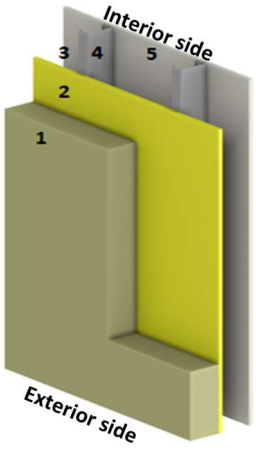

1	Mineral Wool Insulation Layer (101 mm)
2	Fiberglass mat-faced gypsum (13 mm)
3	Steel Studs
4	Air Cavity (152 mm)
5	Gypsum board (13 mm)

Figure 4.2. Schematic diagram of the reference case.

In addition to reference case, five different configurations (see Figure 4.3 and Table 4.2), as depicted below, of the exterior insulated steel framed wall assembly were tested in the laboratory and modeled numerically.

I. Brackets completely penetrate the exterior insulation: Four T-Brackets of 4" (101.6 mm) length were added to the tested wall geometry. The insulation layer and the

brackets are both 4" (101.6); hence, the T-Brackets completely penetrated the insulation and extent to the exterior environment.

II. Brackets partially penetrate the exterior insulation: For this scenario the brackets were reduced to 3" (76.2 mm), which is one inch less than the thickness of the insulation layer and the bracket do not extend to the exterior environment. This is not a realistic cladding attachment scenario but is done to show the incremental change between configuration I and III.

III. Brackets partially penetrate the exterior insulation with exterior rails: In addition to the T-Brackets that do not completely penetrate the insulation, two continuous L-Rails (50.8 mm x 50.8 mm x 1.2 mm) made of galvanized steel were added to the exterior of the wall assembly and screwed into the brackets.

IV. Material isolator at bracket to rail connection: Spacers made of neoprene were added at interface areas of T-Brackets and L-Rails. The initial thickness of the spacers was 6 mm. Thickness was approximately diminished to half thickness because of the compression force produced by the screws. The spacers provide an isolating metal between rail and bracket for dissimilar metals and also as a thermal insulation.

V. Cladding attachment system without thermal insulation or spacer: Configuration IV was evaluated without neoprene at interface areas of both the connection between the bracket and rail and the bracket at the sheathing to assess the impact.

Table 4.2. Summary of materials/components incorporated in the studied configurations.

Materials	**Reference case**	**a**	**b**	**c**	**d**	**e**
Gypsum board	✓	✓	✓	✓	✓	✓
Steel studs	✓	✓	✓	✓	✓	✓
Fiberglass mat-faced gypsum	✓	✓	✓	✓	✓	✓

Mineral wool insulation	✓	✓	✓	✓	✓	✓
Aluminum Brackets	×	✓	✓	✓	✓	✓
Neoprene at brackets and exterior sheathing interface	×	✓	✓	✓	✓	×
L-Rails	×	×	×	✓	✓	✓
Neoprene at bracket and L-Rail interface	×	×	×	×	✓	×

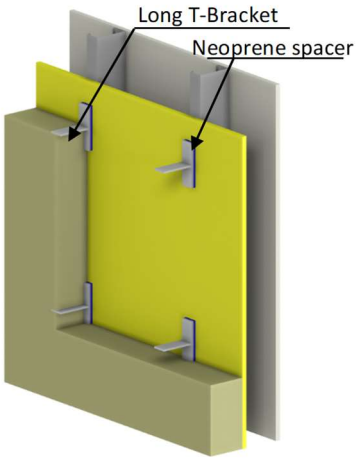

(a) Configuration I

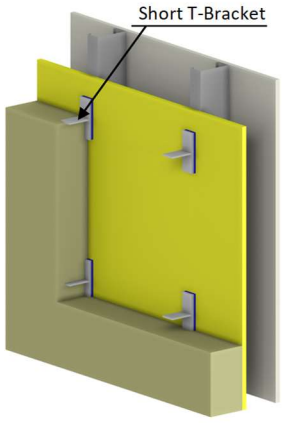

(b) Configuration II

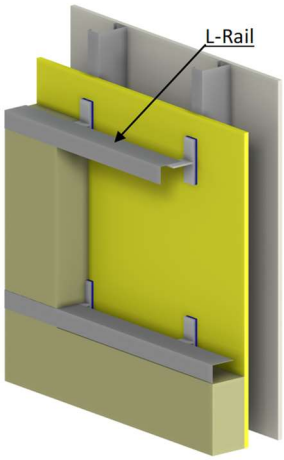

(c) Configuration III

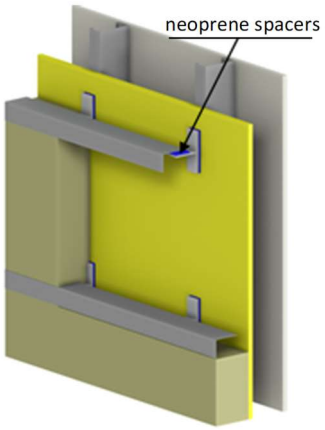

(d) Configuration IV

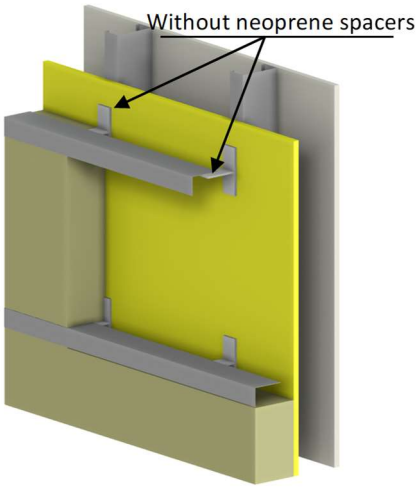

(e) Configuration V

Figure 4.3. Sketches of investigated configurations.

4.6 Methodology

4.6.1 Numerical simulations

The finite element methods (FEMs) are widely used to numerically solve differential equations in different fields such as structural analysis, heat transfer and fluid flow. In the buildings sector, the FEMs are employed to predict the thermal performance of building components such as walls, roofs, windows, etc. In this study, three-dimensional finite element methods software was employed to perform numerical simulations (HEAT3 [95]). Initially, detailed modules representing the tested wall geometries were reproduced in HEAT3 to predict their thermal behavior under different temperatures. Typically, the precision of results obtained by the simulation models depends on the inputs and assumptions of the user. The following parameters were utilized to perform the analyses:

- The thermal conductivity of air within the stud's cavities was assumed to have a solid-equivalent value. From the 2013 ASHRAE Handbook – Fundamental, an equivalent thermal resistance of 0.16 (m^2 K)/W was selected.

- The thermal properties of incorporated materials were considered to be constant regardless of temperature and selected according to International Energy Agency (IEA) report [145] (as represented in Table 1).
- All layers were considered tight to adjacent interfaces and the contact resistances between the layers were excluded from the analysis as their effect is too small as stated in the 2013 ASHRAE Handbook – Fundamentals. Also, ASHRAE RP-1365 [143] concluded that the impact of contact resistance is small for assemblies of lot of thermal resistance outboard of the steel studs, which is this case in this study.
- The impact of both air leakage within the assembly and solar heating were neglected.

4.6.1.1 Boundary conditions

The ambient temperatures of the hot and cold environments adjacent to the walls were set to the same temperature as the experiment. The perimeter surfaces of the modeled wall configurations were considered adiabatic (Figure 4.4). The surface conductance values of building envelope components depend on several factors, such as surface emittance, temperature difference, and surface view to the surrounding objects. According to the ISO 6946 standard [146], the interior (hot) and exterior (cold) surface film resistance values were considered equal to 0.13 (m^2 K)/W and 0.04 m^2 K/W, respectively, which comply with the ranges presented in ASHRAE Handbook [147]. The impact of the interior and exterior surface film resistances on the simulation results has been investigated by changing those values within the range presented in the ASHRAE Handbook of Fundamentals. The handbook illustrates range from 0.12 to 0.2 (m^2 K)/W for interior surfaces and from 0.03 to 0.06 (m^2 K)/W for exterior surfaces. Various combinations of the limits of these two ranges were simulated and compared to the values selected in this study. The impact of changing the interior and exterior surface film resistances was always below 2.5%, which is the case when selecting the high limits of

the ranges (0.2 (m^2 K)/W instead of 0.12 (m^2 K)/W for interior and 0.06 (m^2 K)/W instead of 0.03 (m^2 K)/W for exterior).

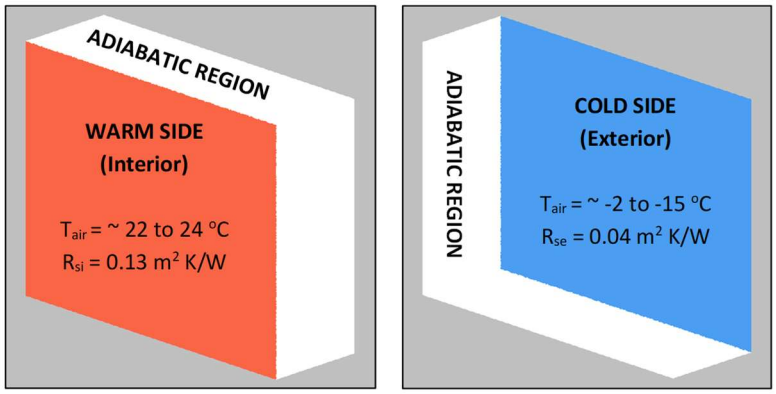

(a) (b)

Figure 4.4. Boundary conditions: (a) Interior side; (b) Exterior side.

4.6.2 Laboratory work

The experimental measurements were performed using a hot box apparatus that was designed and constructed following ASTM C1363 [148]. The apparatus was calibrated experimentally using two extruded polystyrene (XPS) insulation boards. For those boards, the differences between (i) experimental and numerical (3-D), and (ii) experimental and theoretical observations (i.e. heat flow) were below 3.0% [124]. The wall configurations were tested under a wide range of temperatures. Four tests were performed for every specimen under different temperature conditions. The temperature gradients across the test specimens were changed from ~ 24 °C to ~ 40 °C with an increase of ~ 4 °C.

4.6.2.1 Experimental setup

Hot boxes (i.e., calibrated, and guarded) are used to evaluate the thermal performance of large-scale homogeneous and non-homogeneous specimens. The hot boxes investigate representative samples of building components such as walls, roofs, and windows. Furthermore, assemblies that contain thermal bridges within their structure can be

evaluated in the hot box. The hot box apparatus is built based on the principle of controlling the temperature on the sides of the tested specimen until reaching steady-state conditions. According to the ASTM C1363 Standard, a steady state is achieved once the temperatures of air nearby to specimen's surfaces fluctuate randomly. Temperature fluctuations must stay at a minimum or 1.0% of the temperature difference across the test specimen. It is essential to maintain steady-state conditions in air spaces adjacent to the tested sample for a couple of hours to obtain valid results. The ISO 8990-1996 standard [72] illustrates that at least two successive measuring periods of a minimum of three hours each are required to reach a steady-state. Additionally, the ASTM C1363-2019 standard demonstrates that once steady-state conditions are achieved, measurements should be continuous for a period equivalent to five times the time constant.

The calibrated hot box facility consists of three main components. (1) a hot chamber, which represents the indoor environment. (2) a cold chamber, which represents the outdoor environment. (3) a specimen frame, which holds the tested sample. Figure 4.5 shows a schematic of calibrated hot box components. In compliance with above mentioned standards, a small-scale calibrated hot box apparatus was designed, constructed, and calibrated prior to this study, which is employed to perform the experimental measurements of the current study. The test setup can accommodate a wide range of building components with maximum dimensions of 1.0 m wide, 1.0 m high, and 0.4 m thick. More details regarding this test facility can be found in our previous publication [124].

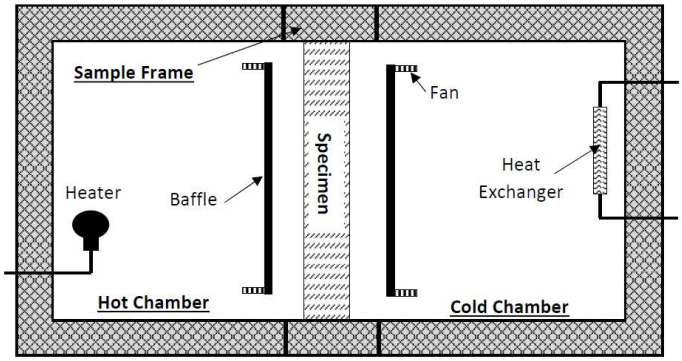

Figure 4.5. Scheme of hot box apparatus

4.6.2.2 Testing procedure

Firstly, the specimen of an area of 90 cm x 90 cm was installed inside the specimen frame. The aperture area of the specimen frame is 1.0 m x 1.0 m. Consequently, a residual gap existed around the specimen's perimeter. Layers of extruded polystyrene insulation (XPS) with a thickness of 50.8 mm were attached to the specimen sides to fill the residual gaps. Simultaneously, the XPS layers around the perimeter of the tested wall assembly helped reduce the extra heat loss at the interface (flanking loss). Similarly, spray foam insulation was used to fill up any small gaps that existed between at interfaces.

Subsequently, the chambers of the apparatus were smoothly shifted towards the specimen frame and interlocked securely. This initiated the operations and data logging processes by cooling the environment chamber and heating the metering chamber. A refrigerating circulation bath (chiller) connected by pipes with two small heat exchangers positioned inside the environment chamber was used as a cooling system. The heat was supplied to the metering chamber by a ceramic heat bulb. A DC power regulator was employed to control the amount of heat supply.

The air temperature inside the chambers ($T_{h,air}$, $T_{c,air}$) were measured using eighteen high accuracy thermistors (nine in each chamber). According to the supplier [149], the tolerance of the thermistors is 1.0% and can operate in temperature ranges from -55 °C to

125 °C. The air temperature inside the metering chamber ranges from 21 °C to 24 °C. The cold side air temperature ($T_{c,air}$) was adjusted to represent different climate zones, approximately from -2 °C to -15 °C. Small fans were employed to circulate the air inside the chambers to avoid air stratification. Each chamber contains six small fans, which are positioned in two rows and attached to the back of the radiation baffle. The air velocities inside the chambers are monitored by adjusting the speed of the circulation fans. The air velocities were measured using a hot wire anemometer. Compliance with the stipulated standards for natural convection conditions was maintained, ensuring an average air velocity around 0.3 m/s in the metering chamber and around 4.5 m/s in the climate chamber.

In our data collection setup, we used two separate data loggers, with one assigned to each chamber. These data loggers were set to record data at five-minute intervals. We waited until the conditions in the chambers stabilized, which met the specific standards mentioned in the previous section. Once we achieved these steady-state conditions, we continued monitoring the data for a minimum duration of six hours. To ensure the reliability of our results across various temperature gradients, we conducted four rounds of testing for each wall configuration. This multiple-round approach was implemented to account for potential variations and ensure the consistency of our findings under different conditions.

In the thermal investigations accomplished using hot boxes, various heat losses are associated with the testing procedure. The amounts of these losses need to be approximate to obtain representative results. Figure 4.6 shows a scheme of heat flow paths associated with the hot box analyses. Descriptions of the heat losses and approximation procedures are presented below.

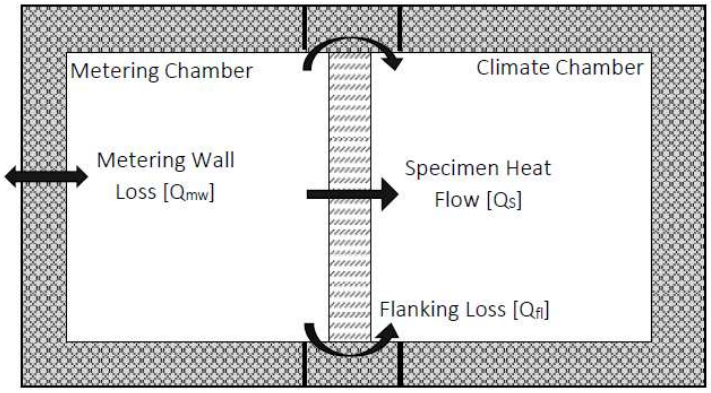

Figure 4.6. Scheme of heat flow paths.

Estimation of metering wall loss: In the hot box measurements, the heat amount crosses the metering chamber walls to the laboratory (surrounding space) is defined as a metering wall loss (Q_{mw}). The metering wall loss occurs due to the differences in air temperature of the metering chamber ($T_{h,air}$) and surrounding space ($T_{surr.}$). In the current study, the temperature of the metering chamber was controlled to be higher than the temperature of the surrounding space. Thus, heat will always transfer outward the metering chamber, which will help prevent any unmetered heat from entering the metering chamber. The temperature of the surrounding space was observed using six temperature sensors distributed around the apparatus. Also, small fans were mounted around the hot box to ensure temperature uniformity and avoid air stratification. The metering wall loss was estimated experimentally by conducting specific experiments. First, both chambers (hot and cold) were maintained at the same temperature while adjusting the temperature of the surrounding space. Then, the amount of energy supplied into the metering chamber was metered. This amount was equal to the amount of heat transferred to the surrounding space. After several measurements, the metering wall loss was approximated and expressed in a correlation as a function of the temperature difference between the hot chamber and the surrounding space (see equation (4.1)).

$$Q_{mw} = 1.0875\left(T_{h,air} - T_{surr}\right) \qquad (4.1)$$

Estimation of flanking loss: Flanking loss is defined as an increase in the heat flow between the hot box's chambers in reference to the amount of heat transfers via the tested specimen in case of the absence of the edge effect [96]. In this study, the flanking heat loss was estimated using FEMs software as per ASTM C1363-19. The boundary conditions and assumptions were utilized as listed above (section 4.6.1). Then, the flanking heat losses were presented as percentages of the total heat. In experimental measurements, the amount of flanking loss was calculated based on the percentages obtained numerically. In other words, the flanking heat loss is the product of the multiplication of the obtained percentages by the total amount of heat supplied into the metering chamber after subtracting the amount of metering wall loss.

4.6.3 Measured data

Table 4.3 illustrates the collected average measurements of the surrounding space temperature and air curtains temperature of metering and climate chambers. The air curtains represent the air space between specimen surfaces and the baffle elements placed in hot and cold chambers. The table also presents the amount of supplied heat into the metering chamber. The heat was dissipated by the heater ceramic bulb and air circulation fans and measured by DC voltage regulators. The data were recorded when reaching the steady state, which usually happened several hours after operating the system.

The hot box apparatus used in this study provides high-temperature stability and slight variations between temperature readings recorded by the sensors, which were placed at different levels. Furthermore, significant temperature gradients between both specimens' adjacent environments were reached, which helps obtain better accuracy in measured thermal transmittance values. Figure 4.7 shows a sample of measured temperatures collected in this study, where temperature uniformity can be observed.

Table 4.3. Measured data.

Specimen	Round of testing	Supplied power	Average temp. of surrounding space	Average temp. of hot chamber	Average temp. of cold chamber
	#	(W)	(°C)	(°C)	(°C)
Reference case	1st	8.55	21.92	22.31	-1.63
	2nd	10.65	21.52	22.73	-4.76
	3rd	12.09	21.55	22.68	-9.30
	4th	14.55	21.10	23.12	-13.85
Configuration I	1st	11.35	21.40	23.31	-1.79
	2nd	11.38	21.31	22.11	-6.36
	3rd	14.55	21.84	23.55	-10.72
	4th	17.05	21.00	23.62	-14.80
Configuration II	1st	9.85	21.00	22.21	-1.81
	2nd	11.35	21.50	22.60	-6.06
	3rd	14.55	21.30	23.59	-10.35
	4th	17.05	21.70	24.56	-14.74
Configuration III	1st	11.35	21.46	21.88	-1.74
	2nd	13.05	21.66	21.75	-6.28
	3rd	15.10	21.91	21.96	-10.71
	4th	17.05	21.80	21.87	-14.96
Configuration IV	1st	11.35	21.65	22.49	-1.76
	2nd	13.05	22.70	22.39	-6.09
	3rd	14.95	21.25	22.08	-10.50
	4th	17.05	21.25	22.25	-14.81
Configuration V	1st	12.26	21.90	22.61	-1.70
	2nd	14.07	21.80	22.34	-6.29
	3rd	16.61	21.10	22.08	-10.79
	4th	17.90	21.30	22.20	-13.49

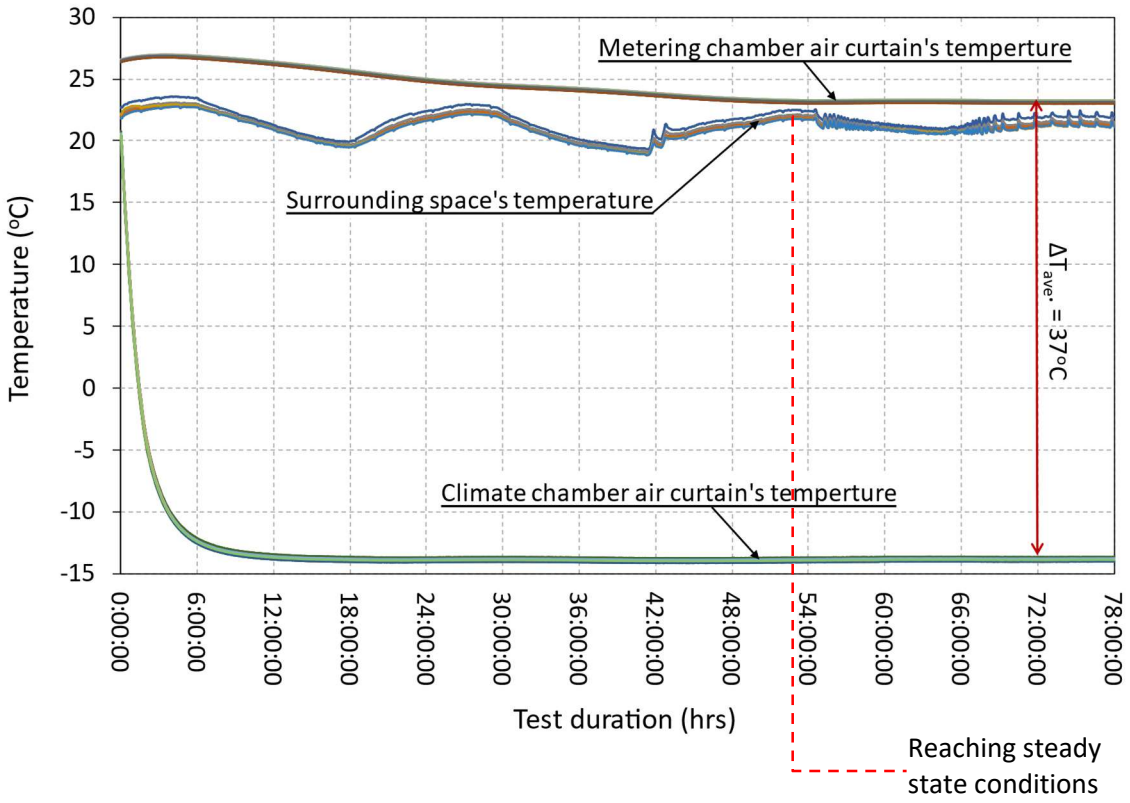

Figure 4.7. Sample of measured data.

4.6.4 Computation procedure

First, the net amount of heat transfer through the specimen (Q_s) was estimated by subtracting the total heat loss from the net amount of heat supplied into the metering chamber. The net amount of heat supply was presented as the heat dissipated by the heater (Q_{in}) and air circulation system (fans) (Q_f). The electric power consumed by the heater and fans was metered and considered to be fully converted into heat. The net amount of heat loss, which includes the metering wall loss (Q_{mw}) and flanking loss (Q_{fl}), was estimated as discussed above.

$$Q_s = [Q_{in} + Q_f] - [Q_{mw} + Q_{fl}] \quad (4.2)$$

Second, the time averages of temperature in both the hot and cold chambers ($T_{h,air}$) and ($T_{c,air}$), which were experimentally obtained as presented in Table 4.3, were incorporated in equations (4.1-4.3) to compute the overall thermal resistance (R) and thermal transmittance (U).

$$R = \frac{A_s * \left(T_{h,air} - T_{c,air}\right)}{Q_s} \quad (4.3)$$

$$U = \frac{1}{R} \quad (4.4)$$

where: A_s is the area of the tested specimen in m^2.

Based on the explanation in Subsection 4.6.2.2, the correlation and assumption were employed to estimate the amounts of associated losses as presented in Table 4.4. The heat amounts presented in the table are calculated based on the temperatures in Table 4.3. Notice that no values of metering wall loss the numerical simulation in the table because the simulation was only run for the section that included the tested specimen and the specimen frame, as presented in Figure 4.8.

Table 4.4. Heat loss amounts associated with numerical simulations and experimental measurements.

Specimen	**Round of testing**	**Numerical simulations**			**Experimental measurements**		
		Total heat*	**Flanking loss**		**Total heat****	**Metering wall loss**	**Flanking loss*****
	#	(W)	(W)	(%)	(W)	(W)	(W)
Reference case	1st	8.16	2.30	28.19	8.55	0.42	2.29
	2nd	9.37	2.64	28.18	10.65	1.32	2.63
	3rd	10.90	3.07	28.17	12.09	1.23	3.06
	4th	12.40	3.50	28.23	14.55	2.20	3.49
Configuration I	1st	9.34	2.35	25.16	11.35	2.08	2.33
	2nd	10.60	2.66	25.09	11.38	0.87	2.64
	3rd	12.76	3.21	25.16	14.55	1.86	3.19
	4th	14.30	3.59	25.10	17.05	2.85	3.57

Configuration II	1st	8.39	2.29	27.29	9.85	1.32	2.33
	2nd	10.01	2.73	27.27	11.35	1.20	2.77
	3rd	11.86	3.24	27.32	14.55	2.49	3.29
	4th	13.73	3.75	27.31	17.05	3.11	3.81
Configuration III	1st	10.95	2.09	19.09	11.35	0.46	2.08
	2nd	12.99	2.48	19.09	13.05	0.1	2.47
	3rd	15.14	2.89	19.09	15.10	0.05	2.87
	4th	17.07	3.26	19.10	17.05	0.08	3.24
Configuration IV	1st	10.40	2.20	21.15	11.35	0.91	2.21
	2nd	12.22	2.59	21.19	13.05	0.75	2.61
	3rd	13.98	2.96	21.17	14.95	0.90	2.97
	4th	15.90	3.36	21.13	17.05	1.09	3.37
Configuration V	1st	11.07	2.12	19.15	12.26	0.77	2.20
	2nd	13.04	2.50	19.17	14.07	0.59	2.58
	3rd	14.97	2.87	19.17	16.61	1.07	2.98
	4th	16.25	3.10	19.08	17.90	0.98	3.23

* Total heat transferred from metering chamber to climate chamber computed numerically.
** Total heat supplied into metering chamber measured in the laboratory.
*** Assuming flanking loss observed in experimental measurements corresponds to the flanking loss percentages encountered in numerical simulations.

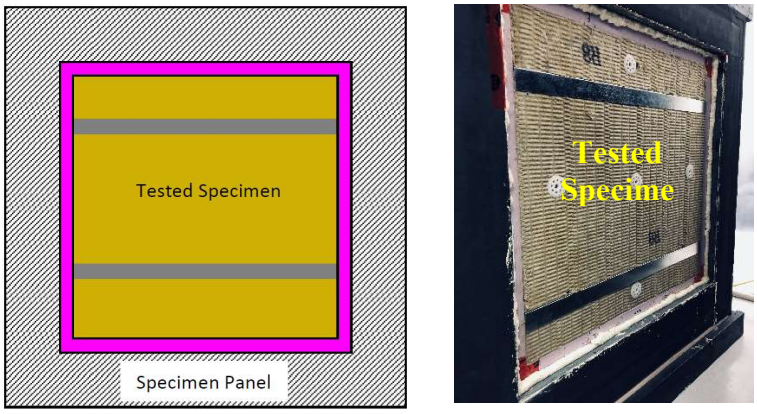

(a) (b)

Figure 4.8. Metered sample mounted inside the specimen frame: (a) Sketch; (b) Real.

The testing procedure can be summarized in the following steps:

- Prepare the wall sample and get all components affixed together.

- Install the sample into the specimen frame securely by spraying some foam at the interface with the specimen frame.
- Attach all temperature sensors in the proper positions about 150 mm apart from the sample faces.
- Close the box by moving both chambers toward the specimen frame and fasten them securely to minimize any heat or air transfer with the surrounding.
- Run the cooling system and set the temperature at 5 ^{o}C below the desired temperature inside the cold chamber. Also, the fans need to be operated to ensure uniform temperature.
- Operate the heating and air circulation systems of the metering chamber. The heat was provided at a constant rate in the metering chamber. DC voltage regulators were used to monitor and adjust the heat amount and fan speed.
- Run the test for a period of time while monitoring the temperature inside both chambers until reaching a steady state.
- The data used for thermal calculation were collected for a minimum period of six hours after reaching the steady state conditions.
- Re-run the test under different temperatures to ensure consistency of obtained results.

4.7 Results and discussion

This section presents the variation in thermal performance of a wall specimen by means of increasing the level of structural complexity. The sample represents an exterior insulated steel-framed wall assembly as described above.

For each tested wall configuration, relations between the temperature differences and amount of heat crosses the specimen were developed in Figure 4.9. Likewise, relations were established between the mean temperature and the overall thermal transmittance,

as shown in Figure 4.10. The results of heat flow and thermal transmittance presented in Table 4.5 are obtained based on the collected and computed data listed in Table 4.3 and Table 4.4.

Table 4.5. Obtained results of tested wall configurations.

Specimen	Round of testing	Temp. difference	Mean temp.	Heat flow via tested specimen		Overall thermal transmittance *		Difference
				Num.	Exp.	Num.	Exp.	
	#	(°C)	(°C)	(W)		(W/(m² K))		%
Reference case	1st	23.94	10.34	5.86	5.84	0.302	0.301	0.3
	2nd	27.49	8.99	6.73	6.70	0.302	0.301	0.3
	3rd	31.98	6.69	7.83	7.80	0.302	0.301	0.3
	4th	36.97	4.64	8.90	8.87	0.297	0.296	0.3
Configuration I	1st	25.10	10.76	6.99	6.94	0.344	0.341	0.9
	2nd	28.47	7.88	7.94	7.87	0.344	0.341	0.9
	3rd	34.27	6.42	9.55	9.50	0.344	0.342	0.6
	4th	38.42	4.41	10.71	10.64	0.344	0.342	0.6
Configuration II	1st	24.02	10.20	6.10	6.20	0.314	0.319	-1.6
	2nd	28.66	8.27	7.28	7.38	0.314	0.318	-1.3
	3rd	33.94	6.62	8.62	8.77	0.314	0.319	-1.6
	4th	39.30	4.91	9.98	10.13	0.314	0.318	-1.3
Configuration III	1st	23.62	10.07	8.86	8.81	0.463	0.461	0.4
	2nd	28.03	7.74	10.51	10.48	0.463	0.462	0.2
	3rd	32.67	5.63	12.25	12.17	0.463	0.460	0.7
	4th	36.83	3.46	13.81	13.73	0.463	0.460	0.7
Configuration IV	1st	24.25	10.37	8.20	8.23	0.417	0.419	-0.5
	2nd	28.48	8.15	9.63	9.69	0.417	0.420	-0.7
	3rd	32.58	5.79	11.02	11.07	0.418	0.420	-0.5
	4th	37.06	3.72	12.54	12.59	0.418	0.419	-0.2
Configuration V	1st	24.31	10.46	8.95	9.29	0.455	0.472	-3.7
	2nd	28.63	8.03	10.54	10.90	0.455	0.470	-3.2
	3rd	32.87	5.65	12.10	12.56	0.454	0.472	-3.9
	4th	35.69	4.36	13.15	13.69	0.455	0.474	-4.1

* The overall thermal transmittance values include the impact of the surface film coefficients.

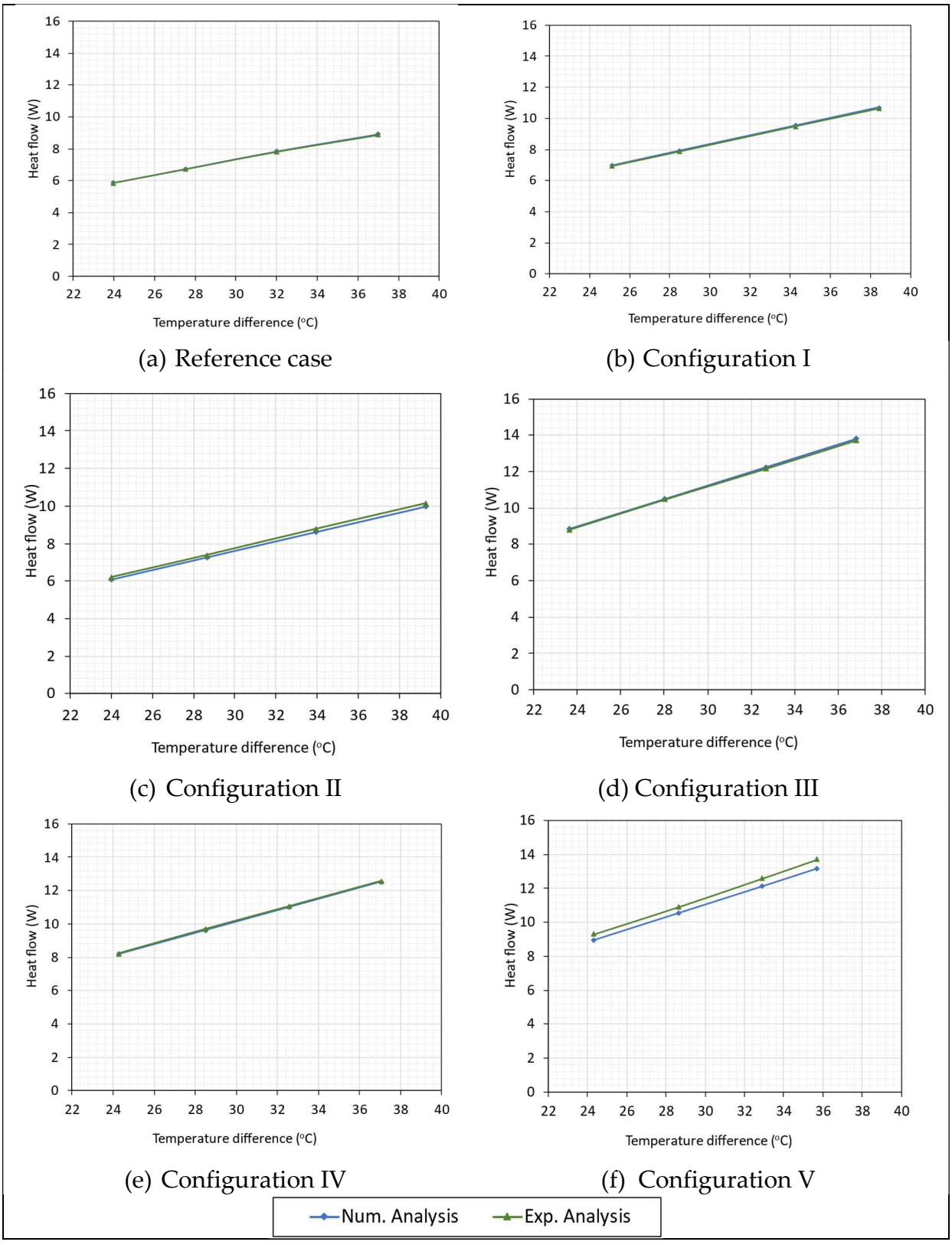

Figure 4.9. Relation between the temperature differences and amount of heat flows.

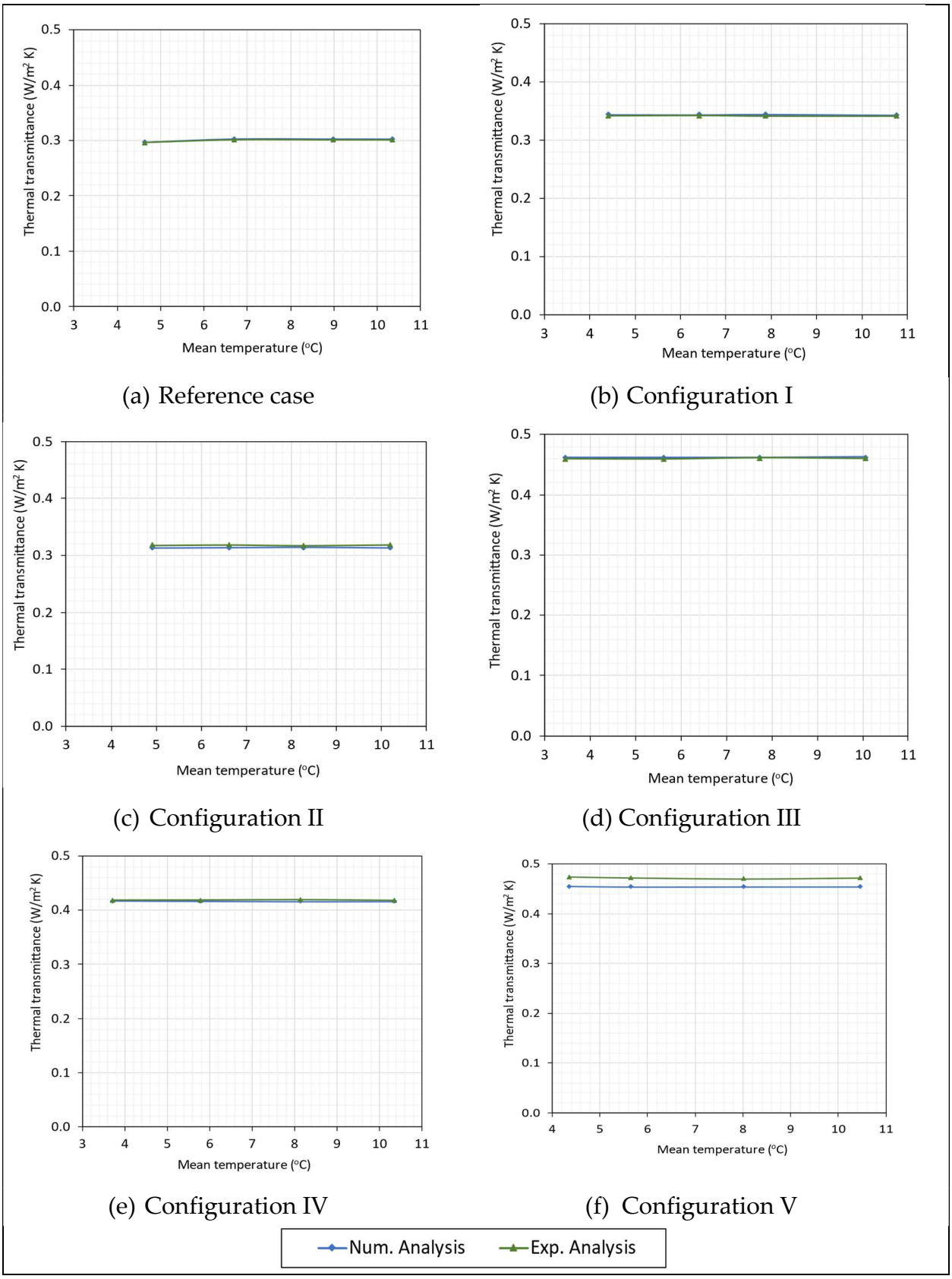

Figure 4.10. Relation between the mean temperatures and thermal transmittances.

In the current study, the influence of thermal bridges created by secondary structural components of the steel-framed wall assembly on the thermal performance of the building envelope was investigated. Various configurations were investigated numerically and validated experimentally. The consistency between the numerical and experimental results was noticeable. Table 4.5 presents the variation in the amounts of heat flow through the tested specimen and thermal transmittance of the tested wall configurations as the structure details increase in complexity. Each wall configuration was investigated under different temperatures within the adjacent environments. The amounts of heat transfers via specimen were presented as a function of the temperature difference Figure 4.9. The thermal transmittances were presented as a function of the mean temperature Figure 4.10. Furthermore, the deviations between measured and simulated amounts of heat flow via the specimen were obtained. These differences were as percentages (always below 4.0%).

Among the different wall configurations we tested, the first configuration stands out as the only one with an insulation layer completely free from any penetration by highly thermally conductive materials (cladding attachments). To gauge the impact, we measured the percentage change in thermal transmittance (U-value) for each tested wall configuration in comparison to this initial reference case.

In the second wall configuration, the insulation layer experiences complete penetration by T-Brackets. As a result, this leads to an observed increase of approximately 14.0% in the experimentally measured thermal transmittance values. However, when we substituted the longer T-Brackets (4") with shorter ones (3"), the measured thermal transmittance increased by only about 6.0% in comparison to the reference case.

Subsequently, upon adding L-Rails to the wall specimen, we noted a significant 53.5% increase in the measured thermal transmittance relative to the reference case. To mitigate

this, introducing foam spacers (thermal breaks) at the interface regions between the T-Brackets and L-Rails helped curtail the rise in thermal transmittance to around 40% compared to the reference case.

Furthermore, we examined the effect of removing all neoprene spacers, situated at the interfaces of the T-Brackets and L-Rails, as well as between the T-Brackets and sheathing. This removal led to a substantial 57% increase in the measured thermal transmittance, representing the most pronounced impact within our study. For a visual representation, please refer to Figure 4.11.

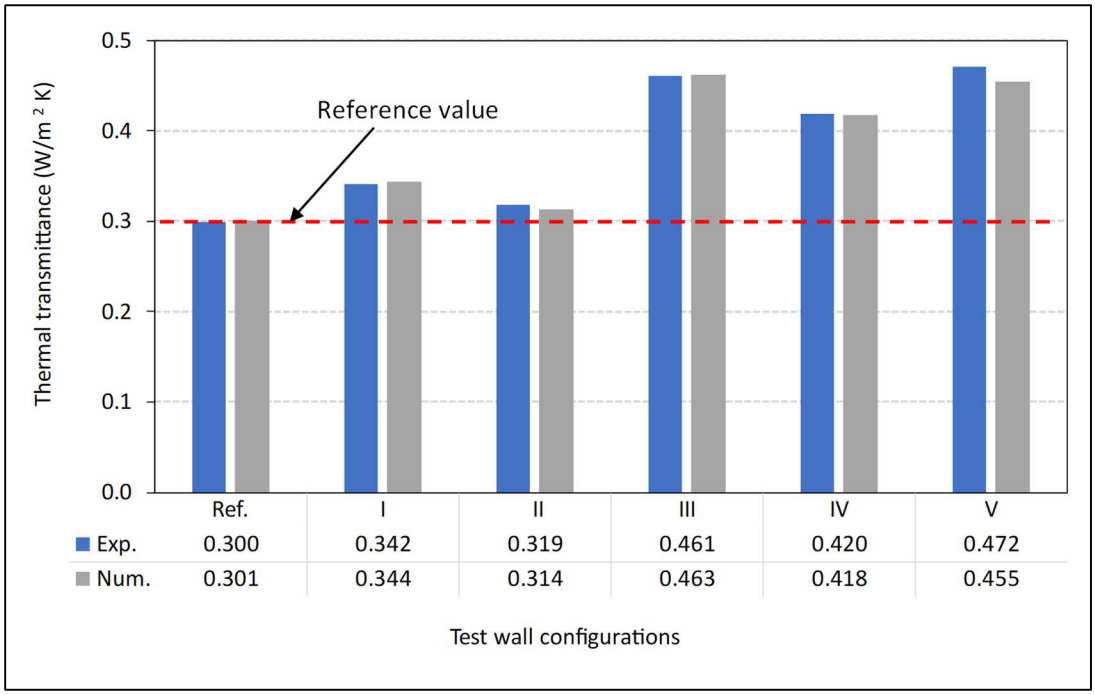

Figure 4.11. Thermal transmittance of tested wall configurations obtained numerically and experimentally.

4.8 Conclusions

In this study, the thermal characteristics of different exterior insulated steel-framed wall assembly configurations were evaluated numerically and experimentally. The analyzed wall configurations have different levels of structural complexity regarding the cladding

attachment system, which connects the cladding layer to the backup wall. The primary objectives were to: (1) assess the influence of each element of the cladding attachments on the heat transfer characteristics of the steel-framed wall, and (2) compare between measured and simulated results. The numerical analyses were performed using 3D FEM-based simulation software (HEAT3). Experiments were conducted using a calibrated hot box apparatus. A total of six wall configurations were investigated. The major conclusions are listed below. It is to be noted that the percentages presented below have been calculated relative to the reference case, which is free of any cladding attachment elements.

- The differences between numerically simulated and measured thermal properties are always less than 4% with an average of 0.5%.
- The completely penetration of T-Brackets through the insulation layer (Configuration I) caused an increase in the U-value of about +14% (in both numerical and experimental analyses). Whereas the partial penetration of T-Brackets (Configuration II) caused an increase in the U-value of about only +4% (numerical simulations) and +6% (experimental measurements).
- Numerical analyses and experimental observations show that adding the L-Rails to the exterior insulated wall assembly (Configuration III) caused an increase in the U-value of about +53%, which is about 45% increase in U-value comparing to the Config. II.
- Neoprene spacers placed at the interfaces of T-Brackets and L-Rails (Configuration IV) improved the thermal performance of the insulated steel-framed wall assembly, reducing the U-value by 9% compared to the case without spacers (Configuration III).
- Eliminating all neoprene spacers (Configuration V), including those at the interfaces of T-Brackets and L-Rails, as well as those at the interfaces of T-Brackets and

sheathing layer, resulted in a significant increase in U-value, with a 57% increase in experimental measurements and a 51% increase in numerical simulations. This increase represented about 13% compared to the case with neoprene spacers at all interfaces.

Chapter 5: Conclusions and Outlook.

5.1 Conclusions

This dissertation represents a comprehensive investigation of the challenges that are caused by heat loss through thermal bridges in building envelopes and provides strategies to mitigate heat loss and enhance the energy efficiency of buildings.

The research begins (Chapter 1) with a critical review of the existing literature, revealing a persistent need for further research and development initiatives in this field. Most prior studies heavily rely on numerical simulations, which may result in differences between numerical predictions and actual building performance. In response to this potential disparity, this research introduces an experimental methodology in conjunction with numerical analysis. Numerical assessments were performed by employing a three-dimensional finite element simulation software (HEAT3), and laboratory experiments were conducted with a calibrated hot box apparatus.

The first task of the experimental work (Chapter 2) presented in this dissertation is the development of a hot box apparatus that can maintain the required temperature stability. The structure of the hot box apparatus includes vacuum insulation panels (VIPs) sandwiched between extruded polystyrene (XPS) boards, resulting in exceptionally high thermal resistance (R-52). During the calibration process, it was evident that the experimental outcomes closely matched both numerical and theoretical predictions, with a difference of less than 3.0%. This apparatus is designed for assessing the thermal performance of building envelope components and assemblies. The metering dimensions of this apparatus are 1.0 meter in height and 1.0 meter in width.

A significant portion of this research initiative (Chapter 3) is focused on the experimental and numerical evaluation of the impact of the balcony thermal bridges and the

assessment of various mitigation strategies. The investigation involved testing five balcony specimens, including a conventional slab, a slab with a commercial thermal break, a slab with the GFRP rebars, and a slab with aerogel-concrete layers at the top and bottom surfaces. The observations demonstrate agreement between the experimental and numerical findings, highlighting the dependability of numerical simulation techniques. To quantify the heat loss through thermal bridges in balcony slabs, linear thermal transmittance values were computed and presented. The reduction in heat loss diminishes the temperature differential between the slab surfaces and the ambient air within the metering chamber. Consequently, it lowers the risk of condensation on interior surfaces, which is a crucial consideration for effective moisture management in building enclosures.

Finally, this dissertation centers on assessing the thermal properties of an exterior insulated lightweight steel framed (LSF) wall system (Chapter 4) through both experimental and numerical investigations. Specifically, the research delves into studying how the cladding attachment elements of the LSF wall impact its thermal performance. The investigation covers various configurations with differing levels of structural complexity concerning cladding attachment systems. The results emphasize the substantial influence of the cladding attachment components such as T-Brackets and L-Rails and offer valuable insights into how they affect the U-value of the assembly. The study also assessed the importance of incorporating neoprene spacers to improve thermal performance.

In summary, this dissertation offers a comprehensive approach to tackle the challenges of thermal bridging in building envelopes. The use of a state-of-the-art hot box apparatus to perform the experimental analysis, alongside numerical simulations, provides robust solutions to enhance the energy efficiency of buildings. The findings from balcony and lightweight steel framing investigations offer practical insights for architects, engineers,

and builders to optimize building envelope components and cladding attachment systems, ultimately contributing to more energy-efficient and sustainable construction practices. This research bridges the gap between theoretical predictions and real-world performance, advancing the field of building science and thermal engineering.

From the perspective of a researcher, conducting this research was a significant and demanding challenge that necessitated extensive problem-solving and continuous learning, leading to substantial personal growth and the gain of valuable knowledge.

5.2 Outlook on future work

This research presents a first step towards (i) designing, constructing, and calibrating a state-of-the-art hot box apparatus; and (ii) performing experimental measurements alongside numerical simulations to ensure the reliability of the obtained results. However, there remains room for further progress as outlined below.

- This research marks the initial step taken by the building science laboratory at the University of Victoria in establishing a large-scale testing facility for examining larger specimens. Additionally, the current calibrated hot box testing facility can be adapted into a guarded hot box type, potentially reducing the time required to achieve temperature stability.
- Building envelope constructions have various types of thermal bridges, including balconies, steel studs, cladding attachment elements, window-wall interfaces, and floor/roof parapets, among others. While this research focuses on two specific types of thermal bridges, there is a need for in-depth investigation into other thermal bridge types.
- This research primarily concentrates on the thermal investigation of balcony thermal bridges and introduces new approaches, such as the integration of GFRP rebars and

aerogel concrete in balcony constructions. It is imperative to assess the structural performance of these new technologies to ensure their safety and effectiveness.

Bibliography

[1] "IEA – International Energy Agency," IEA. Accessed: Oct. 17, 2023. [Online]. Available: https://www.iea.org

[2] K. Amasyali and N. M. El-Gohary, "A review of data-driven building energy consumption prediction studies," *Renewable and Sustainable Energy Reviews*, vol. 81, pp. 1192–1205, Jan. 2018, doi: 10.1016/j.rser.2017.04.095.

[3] Becerik-Gerber Burcin *et al.*, "Civil Engineering Grand Challenges: Opportunities for Data Sensing, Information Analysis, and Knowledge Discovery," *Journal of Computing in Civil Engineering*, vol. 28, no. 4, p. 04014013, Jul. 2014, doi: 10.1061/(ASCE)CP.1943-5487.0000290.

[4] "Energy Efficiency Trends in Canada 1990 to 2013." Accessed: Aug. 22, 2017. [Online]. Available: http://www.nrcan.gc.ca/energy/publications/19030

[5] N. R. Canada, "Energy Efficiency Trends in Canada 1990 to 2013." [Online]. Available: https://www.nrcan.gc.ca/energy/publications/19030

[6] T. G. Theodosiou and A. M. Papadopoulos, "The impact of thermal bridges on the energy demand of buildings with double brick wall constructions," *Energy and Buildings*, vol. 40, no. 11, pp. 2083–2089, Jan. 2008, doi: 10.1016/j.enbuild.2008.06.006.

[7] J. Šadauskienė, J. Ramanauskas, L. Šeduikytė, M. Daukšys, and A. Vasylius, "A simplified methodology for evaluating the impact of point thermal bridges on the high-energy performance of a passive house," *Sustainability*, vol. 7, no. 12, pp. 16687–16702, 2015.

[8] C. Carbonaro, Y. Cascone, S. Fantucci, V. Serra, M. Perino, and M. Dutto, *Energy Assessment of A Pcm–Embedded Plaster: Embodied Energy Versus Operational Energy*, vol. 78. 2015. doi: 10.1016/j.egypro.2015.11.782.

[9] "RDH Building Science | Making Buildings Better™," RDH Building Science. Accessed: Aug. 22, 2017. [Online]. Available: http://www.rdh.com/

[10] E. Roque and P. Santos, "The Effectiveness of Thermal Insulation in Lightweight Steel-Framed Walls with Respect to Its Position," *Buildings*, vol. 7, no. 1, p. 13, Feb. 2017, doi: 10.3390/buildings7010013.

[11] "Building envelope thermal bridging guide released." Accessed: Aug. 22, 2017. [Online]. Available: https://www.bchydro.com/news/conservation/2014/building-envelope-thermal-bridging.html

[12] A. B. Larbi, "Statistical modelling of heat transfer for thermal bridges of buildings," *Energy and Buildings*, vol. 37, no. 9, pp. 945–951, Sep. 2005, doi: 10.1016/j.enbuild.2004.12.013.

[13] F. Ascione, N. Bianco, F. de' Rossi, G. Turni, and G. P. Vanoli, "Different methods for the modelling of thermal bridges into energy simulation programs: Comparisons of accuracy for flat heterogeneous roofs in Italian climates," *Applied Energy*, vol. 97, pp. 405–418, Sep. 2012, doi: 10.1016/j.apenergy.2012.01.022.

[14] J. Kośny, C. Curcija, A. D. Fontanini, H. Liu, and E. Kossecka, "A New Approach for Analysis of Complex Building Envelopes in Whole Building Energy Simulations".

[15] P. E. Totten, S. M. O'Brien, and M. Pazera, "The effects of thermal bridging at interface conditions," *Building Enclosure Science & Technology*, vol. 1, 2008, Accessed: Aug. 22, 2017. [Online]. Available: http://www.nibs.org/resource/resmgr/BEST/BEST1_034.pdf

[16] L. Olsen and N. Radisch, *Thermal bridges in residential buildings in Denmark*. KEA energetická agentura, 2002.

[17] K. Martin, A. Erkoreka, I. Flores, M. Odriozola, and J. M. Sala, "Problems in the calculation of thermal bridges in dynamic conditions," *Energy and Buildings*, vol. 43, no. 2, pp. 529–535, Feb. 2011, doi: 10.1016/j.enbuild.2010.10.018.

[18] H. Erhorn-Kluttig and H. Erhorn, "Impact of thermal bridges on the energy performance of buildings," *Information Paper P148 of the EPBD Buildings Platform*, 2009, Accessed: Aug. 22, 2017. [Online]. Available: http://www.buildup.eu/sites/default/files/content/P_148_EN_ASIEPI_WP4_IP2.pdf

[19] M. Ibrahim, P. H. Biwole, E. Wurtz, and P. Achard, "Limiting windows offset thermal bridge losses using a new insulating coating," *Applied Energy*, vol. 123, pp. 220–231, Jun. 2014, doi: 10.1016/j.apenergy.2014.02.043.

[20] J. W. Lstiburek, "A bridge too far: thermal bridges--steel studs, structural frames, relieving angles and balconies," *ASHRAE Journal*, vol. 49, no. 10, p. 64, 2007.

[21] J. Kosny and J. E. Christian, "Thermal evaluation of several configurations of insulation and structural materials for some metal stud walls," *Energy and Buildings*, vol. 22, no. 2, pp. 157–163, Jan. 1995, doi: 10.1016/0378-7788(94)00913-5.

[22] K. Ghazi Wakili, H. Simmler, and T. Frank, "Experimental and numerical thermal analysis of a balcony board with integrated glass fibre reinforced polymer GFRP elements," *Energy and Buildings*, vol. 39, no. 1, pp. 76–81, Jan. 2007, doi: 10.1016/j.enbuild.2006.05.002.

[23] "TRISCO." Accessed: Feb. 27, 2018. [Online]. Available: http://www.physibel.be/v0n2tr.htm

[24] K. Karabulut, E. Buyruk, and A. Fertelli, "Numerical Investigation of Heat Transfer for Thermal Bridges Taking into Consideration Location of Thermal Insulation with Different Geometries," *Strojarstvo : časopis za teoriju i praksu u strojarstvu*, vol. 51, no. 5, pp. 431–439, Oct. 2009.

[25] "ANSYS Fluent Software: CFD Simulation." Accessed: Mar. 08, 2018. [Online]. Available: //www.ansys.com/products/fluids/ansys-fluent

[26] K. Karabulut, E. Buyruk, and A. Fertelli, "Numerical investigation of the effect of insulation on heat transfer of thermal bridges with different types," *Thermal Science*, vol. 20, no. 1, pp. 185–195, 2016.

[27] "Examples of Structural Thermal Bridges in Buildings - Schöck USA Inc." Accessed: Aug. 24, 2017. [Online]. Available: http://www.schock-us.com/en_us/examples-of-structural-thermal-bridges-in-buildings

[28] "HEAT3." Accessed: Mar. 09, 2018. [Online]. Available: http://www.buildingphysics.com/index-filer/Page691.htm

[29] H. Ge, V. R. McClung, and S. Zhang, "Impact of balcony thermal bridges on the overall thermal performance of multi-unit residential buildings: A case study," *Energy and Buildings*, vol. 60, pp. 163–173, May 2013, doi: 10.1016/j.enbuild.2013.01.004.

[30] "THERM | Windows and Daylighting." Accessed: Mar. 09, 2018. [Online]. Available: https://windows.lbl.gov/software/therm

[31] "eQUEST." [Online]. Available: http://www.doe2.com/equest/

[32] I. Susorova and B. Skelton, "THE EFFECT OF BALCONY THERMAL BREAKS ON BUILDING THERMAL AND ENERGY PERFORMANCE," *IBPSA-USA Journal*, vol. 6, no. 1, 2016, Accessed: Aug. 22, 2017. [Online]. Available: http://ibpsa-usa.org/index.php/ibpusa/article/download/370/356

[33] K. Goulouti, J. de Castro, A. P. Vassilopoulos, and T. Keller, "Thermal performance evaluation of fiber-reinforced polymer thermal breaks for balcony connections," *Energy and Buildings*, vol. 70, pp. 365–371, Feb. 2014, doi: 10.1016/j.enbuild.2013.11.070.

[34] K. Goulouti, J. de Castro, and T. Keller, "Aramid/glass fiber-reinforced thermal break – thermal and structural performance," *Composite Structures*, vol. 136, pp. 113–123, Feb. 2016, doi: 10.1016/j.compstruct.2015.10.001.

[35] C. Murad, H. Doshi, and R. Ramakrishnan, "Impact of Insulated Concrete Curb on Concrete Balcony Slab," *Procedia Engineering*, vol. 118, pp. 1030–1037, Jan. 2015, doi: 10.1016/j.proeng.2015.08.545.

[36] H. Ge and F. Baba, "Dynamic effect of thermal bridges on the energy performance of a low-rise residential building," *Energy and Buildings*, vol. 105, pp. 106–118, Oct. 2015, doi: 10.1016/j.enbuild.2015.07.023.

[37] "WUFI® Plus | WUFI (en)." Accessed: Mar. 08, 2018. [Online]. Available: https://wufi.de/en/software/wufi-plus/

[38] F. Baba and H. Ge, "Dynamic effect of balcony thermal bridges on the energy performance of a high-rise residential building in Canada," *Energy and Buildings*, vol. 116, pp. 78–88, Mar. 2016, doi: 10.1016/j.enbuild.2015.12.044.

[39] K. Dikarev, A. Berezyuk, O. Kuzmenko, and A. Skokova, "Experimental and Numerical Thermal Analysis of Joint Connection «Floor Slab – Balcony Slabe» with Integrated Thermal Break," *Energy Procedia*, vol. 85, pp. 184–192, Jan. 2016, doi: 10.1016/j.egypro.2015.12.325.

[40] S. Real, M. G. Gomes, A. Moret Rodrigues, and J. A. Bogas, "Contribution of structural lightweight aggregate concrete to the reduction of thermal bridging effect in buildings," *Construction and Building Materials*, vol. 121, pp. 460–470, Sep. 2016, doi: 10.1016/j.conbuildmat.2016.06.018.

[41] "EnergyPlus | EnergyPlus." Accessed: Mar. 09, 2018. [Online]. Available: https://energyplus.net/

[42] A. Ben Larbi, M. Couchaux, and A. Bouchair, "Thermal and mechanical analysis of thermal break with end-plate for attached steel structures," *Engineering Structures*, vol. 131, pp. 362–379, Jan. 2017, doi: 10.1016/j.engstruct.2016.10.049.

[43] X. Zhang, G.-J. Jung, and K.-N. Rhee, "Performance Evaluation of Thermal Bridge Reduction Method for Balcony in Apartment Buildings," *Buildings*, vol. 12, no. 1, Art. no. 1, Jan. 2022, doi: 10.3390/buildings12010063.

[44] D. Borelli, P. Cavalletti, A. Marchitto, and C. Schenone, "A comprehensive study devoted to determine linear thermal bridges transmittance in existing buildings," *Energy and Buildings*, vol. 224, p. 110136, Oct. 2020, doi: 10.1016/j.enbuild.2020.110136.

[45] S. Aghasizadeh, B. M. Kari, and R. Fayaz, "Thermal performance of balcony thermal bridge solutions in reinforced concrete and steel frame structures," *Journal of Building Engineering*, vol. 48, p. 103984, May 2022, doi: 10.1016/j.jobe.2021.103984.

[46] M. J. Romero, F. Aguilar, and P. G. Vicente, "Analysis of design improvements for thermal bridges formed by double-brick façades and intermediate slabs for nZEB residential buildings in Spain," *Journal of Building Engineering*, vol. 44, p. 103270, Dec. 2021, doi: 10.1016/j.jobe.2021.103270.

[47] D. Borelli, P. Cavalletti, A. Marchitto, and C. Schenone, "A comprehensive study devoted to determine linear thermal bridges transmittance in existing buildings," *Energy and Buildings*, vol. 224, p. 110136, Oct. 2020, doi: 10.1016/j.enbuild.2020.110136.

[48] A. E. Saied, C. Maalouf, T. Bejat, and E. Wurtz, "Slab-on-grade thermal bridges: A thermal behavior and solution review," *Energy and Buildings*, vol. 257, p. 111770, Feb. 2022, doi: 10.1016/j.enbuild.2021.111770.

[49] L. Pérez-Lombard, J. Ortiz, and C. Pout, "A review on buildings energy consumption information," *Energy and Buildings*, vol. 40, no. 3, pp. 394–398, Jan. 2008, doi: 10.1016/j.enbuild.2007.03.007.

[50] F. Asdrubali, M. Bonaut, M. Battisti, and M. Venegas, "Comparative study of energy regulations for buildings in Italy and Spain," *Energy and Buildings*, vol. 40, no. 10, pp. 1805–1815, Jan. 2008, doi: 10.1016/j.enbuild.2008.03.007.

[51] "Test Method for Steady-State Heat Flux Measurements and Thermal Transmission Properties by Means of the Guarded-Hot-Plate Apparatus," ASTM International. doi: 10.1520/C0177-19.

[52] "Test Method for Steady-State Thermal Transmission Properties by Means of the Heat Flow Meter Apparatus," ASTM International. doi: 10.1520/C0518-17.

[53] R. R. Zarr, "A history of testing heat insulators at the national institute of standards and technology," *Ashrae Transactions*, vol. 107, p. 661, 2001.

[54] M. S. Van Dusen and J. L. Finck, "Heat transfer through building walls," *Bur. Stand. J. Res*, vol. 6, no. 3, p. 493, 1931.

[55] T. de Rubeis, M. Muttillo, I. Nardi, L. Pantoli, V. Stornelli, and D. Ambrosini, "Integrated Measuring and Control System for Thermal Analysis of Buildings Components in Hot Box Experiments," *Energies*, vol. 12, no. 11, Art. no. 11, Jan. 2019, doi: 10.3390/en12112053.

[56] J. H. Klems, "A CALIBRATED HOTBOX FOR TESTING WINDOW SYSTEMS? CONSTRUCTION, CALIBRATION, AND MEASUREMENTS ON PROTOTYPE HIGH-PERFORMANCE WINDOWS," 1979.

[57] X. De Fang, "A study of the U-factor of the window with a high-reflectivity venetian blind," *Solar Energy*, vol. 68, no. 2, pp. 207–214, 2000.

[58] K. G. Wakili and C. Tanner, "U-value of a dried wall made of perforated porous clay bricks: Hot box measurement versus numerical analysis," *Energy and Buildings*, vol. 35, no. 7, pp. 675–680, 2003.

[59] J. R. Mumaw, "Calibrated Hot Box: An Effective Means for Measuring Thermal Conductance in Large Wall Sections," *Heat Transmission Measurements in Thermal Insulations*, Jan. 1974, doi: 10.1520/STP34779S.

[60] D. M. Burch, R. R. Zarr, and B. A. Licitra, "A dynamic test method for determining transfer function coefficients for a wall specimen using a calibrated hot box," in *Insulation Materials, Testing and Applications*, ASTM International, 1990.

[61] H. J. Sabine, M. B. Lacher, D. R. Flynn, and T. L. Quindry, "Acoustical and thermal performance of exterior residential walls, doors, and windows," National Bureau of Standards, Washington, DC (USA); US Dept. of Commerce …, 1975.

[62] R. G. Miller, E. L. Perrine, and P. W. Linehan, "A calibrated/guarded hot-box test facility," in *Thermal Transmission Measurements of Insulation*, ASTM International, 1978.

[63] J. R. Mumaw, "Thermal research facility—A large calibrated hot box for horizontal building elements," in *Thermal insulation performance*, ASTM International, 1980.

[64] P. R. Achenbach, "Design of a calibrated hot-box for measuring the heat, air, and moisture transfer of composite building walls," *Thermal performance of the exterior envelopes of buildings, Proceedings-1*, pp. 308–324, 1981.

[65] A. E. Fiorato, "Laboratory tests of thermal performance of exterior walls," *Therm. Perform. Exter. Envel. Build., American Society of Heating Refrigerating and Air-conditioning Engineers and US. Department of Energy Office of Energy Conservation and solar Energy Buildings and Community Systems Division, Kissimmee, Florida, USA*, pp. 221–236, 1979.

[66] E. L. Perrine, P. W. Linehan, J. W. Howanski, and L. S. Shu, "The Design and Construction of a Calibrated/Guarded Hot Box Facility," *Thermal Performance of the Exterior Envelopes of Buildings; ASHRAE SP28; American Society of Heating, Refrigerating, and Air-Conditioning Engineers, Inc.: New York, NY, USA*, pp. 299–307, 1981.

[67] J. L. Rucker and J. R. Mumaw, "Calibration procedures and results for a large calibrated hot box," *Thermal Performance of the Exterior Envelopes of Buildings, ASHRAE SP*, vol. 28, pp. 237–249, 1981.

[68] F. J. Powell and E. L. Bales, "Design of Round-Robin Tests with Guarded/Calibrated Hot Boxes, Guarded Hot Plates, and Heat Flow Meters," in

Thermal Insulation, Materials, and Systems for Energy Conservation in the'80s, ASTM International, 1983.

[69] T. B. Broderick, "Design and calibration of a guard added to an existing hot box," *Journal of testing and evaluation*, vol. 15, no. 3, pp. 145–152, 1987.

[70] R. R. Zarr, D. M. Burch, T. K. Faison, C. E. Arnold, and M. E. O'Connell, "Calibration of the NBS calibrated hot box," *Journal of testing and evaluation*, vol. 15, no. 3, pp. 167–177, 1987.

[71] "Standard Test Method for Thermal Performance of Building Materials and Envelope Assemblies by Means of a Hot Box Apparatus." Accessed: Jan. 24, 2022. [Online]. Available: http://www.astm.org/c1363-05.html

[72] E. Standards, "BS EN ISO 8990:1996 Thermal insulation. Determination of steady-state thermal transmission properties. Calibrated and guarded hot box," https://www.en-standard.eu. Accessed: Jun. 16, 2021. [Online]. Available: https://www.en-standard.eu/bs-en-iso-8990-1996-thermal-insulation-determination-of-steady-state-thermal-transmission-properties-calibrated-and-guarded-hot-box/

[73] "Annual Reports," ClimateWorks Foundation. [Online]. Available: https://www.climateworks.org/report/annual-reports/

[74] K. Martin, A. Campos-Celador, C. Escudero, I. Gómez, and J. M. Sala, "Analysis of a thermal bridge in a guarded hot box testing facility," *Energy and Buildings*, vol. 50, pp. 139–149, Jul. 2012, doi: 10.1016/j.enbuild.2012.03.028.

[75] H. Kus, E. Özkan, Ö. Göcer, and E. Edis, "Hot box measurements of pumice aggregate concrete hollow block walls," *Construction and Building Materials*, vol. 38, pp. 837–845, Jan. 2013, doi: 10.1016/j.conbuildmat.2012.09.053.

[76] F. Chen and S. K. Wittkopf, "Summer condition thermal transmittance measurement of fenestration systems using calorimetric hot box," *Energy and Buildings*, vol. 53, pp. 47–56, Oct. 2012, doi: 10.1016/j.enbuild.2012.07.005.

[77] C. J. Schumacher, J. F. Straube, D. G. Ober, and A. P. Grin, "Development of a New Hot Box Apparatus to Measure Building Enclosure Thermal Performance," p. 19.

[78] F. Asdrubali and G. Baldinelli, "Thermal transmittance measurements with the hot box method: Calibration, experimental procedures, and uncertainty analyses of three different approaches," *Energy and Buildings*, vol. 43, no. 7, pp. 1618–1626, Jul. 2011, doi: 10.1016/j.enbuild.2011.03.005.

[79] P. Ricciardi, E. Belloni, and F. Cotana, "Innovative panels with recycled materials: Thermal and acoustic performance and Life Cycle Assessment," *Applied Energy*, vol. 134, pp. 150–162, Dec. 2014, doi: 10.1016/j.apenergy.2014.07.112.

[80] S. Seitz and C. MacDougall, "Design of an Affordable Hot Box Testing Apparatus," *NOCMAT 2015-Construction for Sustainability-Green Materials & Technologies*, 2015.

[81] C. Buratti, E. Belloni, L. Lunghi, A. Borri, G. Castori, and M. Corradi, "Mechanical characterization and thermal conductivity measurements using of a new 'small hot-box' apparatus: innovative insulating reinforced coatings analysis," *Journal of Building Engineering*, vol. 7, pp. 63–70, Sep. 2016, doi: 10.1016/j.jobe.2016.05.005.

[82] C. Buratti, E. Belloni, L. Lunghi, and M. Barbanera, "Thermal Conductivity Measurements By Means of a New 'Small Hot-Box' Apparatus: Manufacturing, Calibration and Preliminary Experimental Tests on Different Materials," *Int J Thermophys*, vol. 37, no. 5, p. 47, Mar. 2016, doi: 10.1007/s10765-016-2052-2.

[83] A. Alongi, A. Angelotti, and L. Mazzarella, "Experimental investigation of the steady state behaviour of Breathing Walls by means of a novel laboratory apparatus," *Building and Environment*, vol. 123, pp. 415–426, Oct. 2017, doi: 10.1016/j.buildenv.2017.07.013.

[84] D. Chowdhury and S. Neogi, "Thermal performance evaluation of traditional walls and roof used in tropical climate using guarded hot box," *Construction and Building Materials*, vol. 218, pp. 73–89, Sep. 2019, doi: 10.1016/j.conbuildmat.2019.05.032.

[85] A. Barbaresi, M. Bovo, E. Santolini, L. Barbaresi, D. Torreggiani, and P. Tassinari, "Development of a low-cost movable hot box for a preliminary definition of the thermal conductance of building envelopes," *Building and Environment*, vol. 180, p. 107034, Aug. 2020, doi: 10.1016/j.buildenv.2020.107034.

[86] Z. Shen, A. L. Brooks, Y. He, S. S. Shrestha, and H. Zhou, "Evaluating dynamic thermal performance of building envelope components using small-scale calibrated hot box tests," *Energy and Buildings*, vol. 251, p. 111342, 2021, doi: https://doi.org/10.1016/j.enbuild.2021.111342.

[87] R. Tejeda-Vázquez, E. V. Macias-Melo, I. Hernández-Pérez, K. M. Aguilar-Castro, and J. Serrano-Arellano, "Empirical model of hygrothermal behavior of masonry wall under different climatic conditions using a hot box," *Energy and Buildings*, vol. 249, p. 111209, Oct. 2021, doi: 10.1016/j.enbuild.2021.111209.

[88] F. Boukhelf, A. Trabelsi, R. Belarbi, and M. Bachir Bouiadjra, "Experimental and numerical modelling of hygrothermal transfer: Application on building energy performance," *Energy and Buildings*, vol. 254, p. 111633, Jan. 2022, doi: 10.1016/j.enbuild.2021.111633.

[89] "Thermal Insulation." Accessed: Mar. 02, 2021. [Online]. Available: https://d8-na.industrial.panasonic.com/node/956

[90] M. K. Kumaran and M. K. Kumaran, *Material properties*. in International Energy Agency energy conservation in buildings and community systems programme Heat, air and moisture transfer through new and retrofitted insulated envelope parts, no. [IEA-ECB&CS] ; Annex 24 : (Hamtie) ; Task 3/Final report. Leuven: Laboratorium Bouwfysica, Dep. Burgerlijke Bouwkunde, K.U.-Leuven, 1996.

[91] "Standard Specification for Rubber Cellular Cushion Used for Carpet or Rug Underlay."

[92] "Plywood." Accessed: Mar. 02, 2021. [Online]. Available: http://www.matweb.com/search/datasheet_print.aspx?matguid=bd6620450973496ea2578c283e9fb807

[93] H. Simmler *et al.*, "Vacuum Insulation Panels-Study on VIP-components and panels for service life prediction of VIP in building applications (Subtask A)," 2005.

[94] "Standard Test Method for Thermal Performance of Building Materials and Envelope Assemblies by Means of a Hot Box Apparatus."

[95] "HEAT3 – Heat transfer in three dimensions – Buildingphysics.com." Accessed: Jan. 29, 2019. [Online]. Available: https://buildingphysics.com/heat3-3/

[96] A. G. Lavine, J. L. Rucker, and K. E. Wilkes, "Flanking loss calibration for a calibrated hot box," in *Thermal Insulation, Materials, and Systems for Energy Conservation in the'80s*, ASTM International, 1983.

[97] "2020 Global Status Report for Buildings and Construction | Globalabc." Accessed: Aug. 04, 2022. [Online]. Available: https://globalabc.org/resources/publications/2020-global-status-report-buildings-and-construction

[98] "Global Status Report for Buildings and Construction 2019 – Analysis," IEA. Accessed: Aug. 04, 2022. [Online]. Available: https://www.iea.org/reports/global-status-report-for-buildings-and-construction-2019

[99] H. Ge and F. Baba, "Dynamic effect of thermal bridges on the energy performance of a low-rise residential building," *Energy and Buildings*, vol. 105, pp. 106–118, Oct. 2015, doi: 10.1016/j.enbuild.2015.07.023.

[100] J. Ge, Y. Xue, and Y. Fan, "Methods for evaluating and improving thermal performance of wall-to-floor thermal bridges," *Energy and Buildings*, vol. 231, p. 110565, Jan. 2021, doi: 10.1016/j.enbuild.2020.110565.

[101] T. G. Theodosiou and A. M. Papadopoulos, "The impact of thermal bridges on the energy demand of buildings with double brick wall constructions," *Energy and Buildings*, vol. 40, no. 11, pp. 2083–2089, Jan. 2008, doi: 10.1016/j.enbuild.2008.06.006.

[102] J. Kośny, C. Curcija, A. D. Fontanini, H. Liu, and E. Kossecka, "A New Approach for Analysis of Complex Building Envelopes in Whole Building Energy Simulations".

[103] G. Finch, J. Higgins, and B. Hanam, "The importance of balcony and slab edge thermal bridges in concrete construction,"

[104] T. Theodosiou, K. Tsikaloudaki, K. Kontoleon, and C. Giarma, "Assessing the accuracy of predictive thermal bridge heat flow methodologies," *Renewable and Sustainable Energy Reviews*, vol. 136, p. 110437, Feb. 2021, doi: 10.1016/j.rser.2020.110437.

[105] H. Ge, V. R. McClung, and S. Zhang, "Impact of balcony thermal bridges on the overall thermal performance of multi-unit residential buildings: A case study," *Energy and Buildings*, vol. 60, pp. 163–173, May 2013, doi: 10.1016/j.enbuild.2013.01.004.

[106] "Structural Thermal Breaks – Schöck North America." [Online]. Available: http://www.schock-na.com/en-us/home

[107] "RDH Building Science | Making Buildings Better™," RDH Building Science. [Online]. Available: https://www.rdh.com/

[108] K. Ghazi Wakili, H. Simmler, and T. Frank, "Experimental and numerical thermal analysis of a balcony board with integrated glass fibre reinforced polymer GFRP elements," *Energy and Buildings*, vol. 39, no. 1, pp. 76–81, Jan. 2007, doi: 10.1016/j.enbuild.2006.05.002.

[109] K. Goulouti, J. de Castro, A. P. Vassilopoulos, and T. Keller, "Thermal performance evaluation of fiber-reinforced polymer thermal breaks for balcony connections," *Energy and Buildings*, vol. 70, pp. 365–371, Feb. 2014, doi: 10.1016/j.enbuild.2013.11.070.

[110] K. Goulouti, J. de Castro, and T. Keller, "Aramid/glass fiber-reinforced thermal break – thermal and structural performance," *Composite Structures*, vol. 136, pp. 113–123, Feb. 2016, doi: 10.1016/j.compstruct.2015.10.001.

[111] "ISO 10211:2017 - Thermal bridges in building construction -- Heat flows and surface temperatures -- Detailed calculations." [Online]. Available: https://www.iso.org/standard/65710.html

[112] F. Aguilar, J. P. Solano, and P. G. Vicente, "Transient modeling of high-inertial thermal bridges in buildings using the equivalent thermal wall method," *Applied Thermal Engineering*, vol. 67, no. 1, pp. 370–377, Jun. 2014, doi: 10.1016/j.applthermaleng.2014.03.058.

[113] T. G. Theodosiou, A. G. Tsikaloudaki, K. J. Kontoleon, and D. K. Bikas, "Thermal bridging analysis on cladding systems for building facades," *Energy and Buildings*, vol. 109, pp. 377–384, Dec. 2015, doi: 10.1016/j.enbuild.2015.10.037.

[114] S. A. Jabbar and S. B. H. Farid, "Replacement of steel rebars by GFRP rebars in the concrete structures," *Karbala International Journal of Modern Science*, vol. 4, no. 2, pp. 216–227, Jun. 2018, doi: 10.1016/j.kijoms.2018.02.002.

[115] T. Gao, B. P. Jelle, A. Gustavsen, and S. Jacobsen, "Aerogel-incorporated concrete: An experimental study," *Construction and Building Materials*, vol. 52, pp. 130–136, Feb. 2014, doi: 10.1016/j.conbuildmat.2013.10.100.

[116] S. Ng, B. P. Jelle, L. I. C. Sandberg, T. Gao, and Ó. H. Wallevik, "Experimental investigations of aerogel-incorporated ultra-high performance concrete," *Construction and Building Materials*, vol. 77, pp. 307–316, Feb. 2015, doi: 10.1016/j.conbuildmat.2014.12.064.

[117] S. Fickler, B. Milow, L. Ratke, M. Schnellenbach-Held, and T. Welsch, "Development of High Performance Aerogel Concrete," *Energy Procedia*, vol. 78, pp. 406–411, Nov. 2015, doi: 10.1016/j.egypro.2015.11.684.

[118] U. Berardi, "The benefits of using aerogel-enhanced systems in building retrofits," *Energy Procedia*, vol. 134, pp. 626–635, Oct. 2017, doi: 10.1016/j.egypro.2017.09.576.

[119] S. Liu, K. Zhu, S. Cui, X. Shen, and G. Tan, "A novel building material with low thermal conductivity: Rapid synthesis of foam concrete reinforced silica aerogel and energy performance simulation," *Energy and Buildings*, vol. 177, pp. 385–393, Oct. 2018, doi: 10.1016/j.enbuild.2018.08.014.

[120] T. Welsch and M. Schnellenbach-Held, "High Performance Aerogel Concrete," in *High Tech Concrete: Where Technology and Engineering Meet*, D. A. Hordijk and M. Luković, Eds., Springer International Publishing, 2018, pp. 117–124.

[121] "HEAT3 – Heat transfer in three dimensions – Buildingphysics.com." Accessed: Oct. 12, 2022. [Online]. Available: https://buildingphysics.com/heat3-3/

[122] "Structural Thermal Breaks – Schöck North America." Accessed: Oct. 17, 2022. [Online]. Available: http://www.schoeck.com/en-us/home

[123] "High temperature insulation board - up to 1600 C." Accessed: Jul. 05, 2022. [Online]. Available: https://www.gteek.com/high-temperature-insulation-board-1500-1600

[124] A. Alhawari and P. Mukhopadhyaya, "Construction and Calibration of a Unique Hot Box Apparatus," *Energies*, vol. 15, no. 13, Art. no. 13, Jan. 2022, doi: 10.3390/en15134677.

[125] P. K. Mallick, *Fiber-reinforced composites: materials, manufacturing, and design*. CRC press, 2007.

[126] H. Ritchie and M. Roser, "Energy," *Our World in Data*, Nov. 2020, Accessed: Nov. 29, 2021. [Online]. Available: https://ourworldindata.org/energy-mix

[127] X.-C. Wang *et al.*, "Air pollution terrain nexus: A review considering energy generation and consumption," *Renewable and Sustainable Energy Reviews*, vol. 105, pp. 71–85, May 2019, doi: 10.1016/j.rser.2019.01.049.

[128] A. Allouhi, Y. El Fouih, T. Kousksou, A. Jamil, Y. Zeraouli, and Y. Mourad, "Energy consumption and efficiency in buildings: current status and future trends," *Journal of Cleaner Production*, vol. 109, pp. 118–130, Dec. 2015, doi: 10.1016/j.jclepro.2015.05.139.

[129] W. Wang, T. Hong, X. Xu, J. Chen, Z. Liu, and N. Xu, "Forecasting district-scale energy dynamics through integrating building network and long short-term memory learning algorithm," *Applied Energy*, vol. 248, pp. 217–230, Aug. 2019, doi: 10.1016/j.apenergy.2019.04.085.

[130] H. Rajanayagam *et al.*, "Thermal Performance of LSF Wall Systems with Vacuum Insulation Panels," *Buildings*, vol. 11, no. 12, Art. no. 12, Dec. 2021, doi: 10.3390/buildings11120621.

[131] V. Murtinho, H. Ferreira, A. Correia, L. Simões da Silva, C. Rebelo, and P. Santos, "Affordable houses: architectural concept of light steel residential house," in *ICSA2010–International conference on structures and architecture*, 2010, pp. 1291–1297.

[132] P. Santos, C. Martins, and L. S. da Silva, "Thermal performance of lightweight steel-framed construction systems," *Metallurgical Research & Technology*, vol. 111, no. 6, pp. 329–338, 2014.

[133] C. Kendrick, R. Ogden, X. Wang, and B. Baiche, "Thermal mass in new build UK housing: A comparison of structural systems in a future weather scenario," *Energy and Buildings*, vol. 48, pp. 40–49, May 2012, doi: 10.1016/j.enbuild.2012.01.009.

[134] L. T. Rodrigues, M. Gillott, and D. Tetlow, "Summer overheating potential in a low-energy steel frame house in future climate scenarios," *Sustainable Cities and Society*, vol. 7, pp. 1–15, Jul. 2013, doi: 10.1016/j.scs.2012.03.004.

[135] P. Santos, M. Gonçalves, C. Martins, N. Soares, and J. J. Costa, "Thermal transmittance of lightweight steel framed walls: Experimental versus numerical and analytical approaches," *Journal of Building Engineering*, vol. 25, p. 100776, Sep. 2019, doi: 10.1016/j.jobe.2019.100776.

[136] A. Alhawari and P. Mukhopadhyaya, "Thermal bridges in building envelopes – An overview of impacts and solutions," *International Review of Applied Sciences and Engineering*, vol. 9, no. 1, pp. 31–40, Jun. 2018, doi: 10.1556/1848.2018.9.1.5.

[137] "Thermal Envelope." Accessed: Jul. 21, 2023. [Online]. Available: https://thermalenvelope.ca/catalogue/5.1.57/

[138] C. Martins, P. Santos, and L. S. da Silva, "Lightweight steel-framed thermal bridges mitigation strategies: A parametric study," *Journal of Building Physics*, vol. 39, no. 4, pp. 342–372, Jan. 2016, doi: 10.1177/1744259115572130.

[139] T. Höglund and H. Burstrand, "Slotted steel studs to reduce thermal bridges in insulated walls," *Thin-Walled Structures*, vol. 32, no. 1, pp. 81–109, Sep. 1998, doi: 10.1016/S0263-8231(98)00028-7.

[140] T. R. Blomberg and J. Claesson, "Heat transmission through walls with slotted steel studs," in *Conference proceedings by ASHRAE. In: Thermal envelopes VII, Clearwater, FL*, 1998, pp. 6–10.

[141] D. A. Kontogeorgos, I. A. Atsonios, I. D. Mandilaras, and M. A. Founti, "Numerical investigation of the effect of vacuum insulation panels on the thermal bridges of a lightweight drywall envelope," *Journal of Facade Design and Engineering*, vol. 4, no. 1–2, pp. 3–18, Jan. 2016, doi: 10.3233/FDE-160047.

[142] J. Rose and S. Svendsen, "Validating Numerical Calculations against Guarded Hot Box Measurements," *Nordic Journal of Building Physics*, vol. 4, p. 9, 2004.

[143] "Thermal Performance of Building Envelope Details for Mid and High-rise Buildings (ASHRAE RP-1365)," Morrison Hershfield. Accessed: Sep. 19, 2022. [Online]. Available: https://morrisonhershfield.com/bpa_library/thermal-performance-of-building-envelope-details-for-mid-and-high-rise-buildings/

[144] M. Hershfield, "Building Envelope Thermal Bridging Guide—Analysis, Applications and Insights," *BC Hydro Power Smart. Atlanta: Morrison Hershfield*, 2014.

[145] "IEA Annex 24 Task 3 Catalogue (extract).pdf." Accessed: Mar. 02, 2021. [Online]. Available: https://bwk.kuleuven.be/bwf/projects/annex41/protected/Common_Exercises/CE1/CE1/IEA%20Annex%2024%20Task%203%20Catalogue%20(extract).pdf

[146] I. organization for standardization, "ISO 6946: 2017-Building components and building elements-Thermal resistance and thermal transmittance," *Int. Organ. Stand. Geneva, Switz.*, 2017.

[147] "2021 ASHRAE Handbook -- Fundamentals (SI) | ASHRAE Store." Accessed: Aug. 27, 2023. [Online]. Available: https://www.techstreet.com/ashrae/standards/2021-ashrae-handbook-fundamentals-si?gateway_code=ashrae&product_id=2224992

[148] "Test Method for Thermal Performance of Building Materials and Envelope Assemblies by Means of a Hot Box Apparatus," ASTM International. doi: 10.1520/C1363-19.

[149] "Temperature Sensor," smtresearch. Accessed: Aug. 26, 2023. [Online]. Available: https://www.smtresearch.ca/product-page/temperature-sensor